Multimodal Microscopy of Focal Adhesions

Karin Legerstee

Multimodal Microscopy of Focal Adhesions

Karin Legerstee

Multimodal Microscopy of Focal Adhesions

Multimodale microscopie van focal adhesions

proefschrift

ter verkrijging van de graad van doctor aan de
Erasmus Universiteit Rotterdam
op gezag van de rector magnificus

Prof. dr. R.C.M.E. Engels

en volgens besluit van het College voor Promoties.

De openbare verdediging zal plaatsvinden op
dinsdag 29 september 2020 om 15.30 uur.

door

Karin Legerstee
geboren te Utrecht

Erasmus University Rotterdam

Promotiecommissie

Promotor: Prof. dr. A.B. Houtsmuller

Overige leden: Prof. dr. N.J. Galjart
                       Prof. dr. A. Cambi
                       Prof. dr. L.F.A. Wessels

Copromotor: dr. W.A. van Cappellen

Table of contents

Scope of this thesis

The aim of the research described in this thesis is to increase knowledge of the structure and behaviour of focal adhesions and focal adhesion proteins through the application of a range of advanced light microscopy techniques. To increase the level of complementariness of the information gained from the different techniques, cell type (U2OS bone cancer cells) and ECM coating (collagen type I) were kept consistent in the research presented in this thesis. Additionally, focal adhesions in U2OS cells were consistently monitored by expressing one or two fluorescently tagged proteins selected from four hallmark focal adhesion proteins, paxillin, vinculin, zyxin and VASP. These proteins form functionally related pairs. Paxillin and vinculin are both large scaffold proteins while zyxin and VASP are both closely linked to the actin associated with focal adhesions.

Chapter 1 provides a general introduction to focal adhesions, including their importance in health and disease and to cell migration in vitro and in vivo. This is followed by an overview of their molecular composition with special emphasis on paxillin, vinculin, zyxin and VASP. Additionally, advanced light microscopy techniques are introduced, with a focus on those applied in this thesis

In **chapter 2** we used total internal reflection (TIRF) microscopy in combination with Fluorescence Recovery After Photobleaching (FRAP) to examine and quantify the binding dynamics of the four selected focal adhesion proteins. We show that the stably bound fraction of paxillin and vinculin is surprisingly large and consistent across two different cell types from different species. Of the paxillin and vinculin proteins associated with focal adhesions, nearly half remains stably associated for times comparable to the average focal adhesion lifetime. Zyxin and VASP predominantly displayed more transient interactions. We also reveal a connection between focal adhesion protein binding dynamics and focal adhesion location and orientation, a connection which is particularly strong for zyxin and VASP.

In **chapter 3** we present a dedicated photoconversion assay using a FRAP set-up on a confocal microscope. Traditional FRAP can provide accurate estimates of the size of the stably bound fraction, the novel assay is used to specifically visualise the proteins of this fraction within a macromolecular complex, distinguishing it from its dynamically exchanging counterpart. We applied this assay to further investigate the particularly large stably bound fractions of paxillin and vinculin as seen in the FRAP experiments described in chapter 2. The assay revealed that the stably bound fractions of paxillin and vinculin form small clusters within focal adhesions. These clusters were predominantly observed at the half of the adhesion pointing towards the centre of the cell. Furthermore, the paxillin clus-

ters were markedly smaller than the vinculin clusters. This means the paxillin clusters are more concentrated than the vinculin clusters since the photobleaching data showed their stably bound fractions are of nearly equal size. Although in this thesis the developed technique was applied to focal adhesions, it can easily be applied to many different macromolecular complexes to specifically visualise the stably bound proteins within them.

In **chapter 4** we applied structured illumination microscopy to examine the distribution of paxillin, vinculin, zyxin and VASP along focal adhesions at superresolution level. We show that at the focal adhesion ends pointing towards the adherent membrane edge (heads), paxillin protrudes slightly further than the other proteins. At the opposite adhesion ends (tails) the other three proteins protrude further than paxillin, while at tail tips vinculin extended further than any of the other proteins. We also show scattering, which increases the random migration of cells, alters head and tail compositions. Furthermore, focal adhesions at protruding or retracting membrane edges had longer paxillin heads than focal adhesions at static edges.

In **chapter 5** we examine focal adhesions at an even higher resolution by using correlative light and electron microscopy, an imaging technique combining light microscopy with electron microscopy. We discovered a highly abundant distinct nanostructure around the actin fibre entry side formed by an area with increased protein density and possibly also with increased phosphorylation levels. In nearly three-quarters of focal adhesions, these nanostructures had a fork shape, with the actin forming the stem and the high density nanostructure within the focal adhesion the fork.

In conclusion, in this thesis a coherent set of experiments is described in which multiple advanced light microscopy methods and image analysis protocols were applied to increase insight in the dynamic composition of focal adhesions. This multimodal approach was chosen because each of the applied microscopy techniques has its own set of advantages and disadvantages. For this reason, the information gained was often complementary and sometimes synergistic, especially when the data was analysed quantitatively. A good example of this is that by combining the data described in chapters two and three, we were able to conclude that stably bound paxillin patches are more concentrated than stably bound vinculin. We also showed that the location and orientation of focal adhesions correlate with the dynamics of their intracellular proteins. Furthermore, the data described in the different chapters highlight that focal adhesions are non-uniform structures with two distinct tips which differ from each other in many aspects including in their protein dynamics, composition and density.

Chapter 1

General introduction

A brief introduction to focal adhesions

In their simplest form, eukaryotic cells are sacs of plasma membrane filled with cytoplasm, with a second set of membranes surrounding their DNA, the nucleus. Proteins are present throughout cells and form the majority of the cellular machinery. Structural support is provided by what is collectively termed the cytoskeleton, long filamentous proteins forming a network within the cytoplasm. In multicellular organisms, multiple cells group together in an organised fashion to form tissue. The extracellular matrix (ECM), a large three-dimensional macromolecular network surrounding the cells, adds further structure to the tissue. To maintain tissue integrity it is important that most cells remain fixed in place. For this purpose cells adhere both to each other as well as to the ECM.
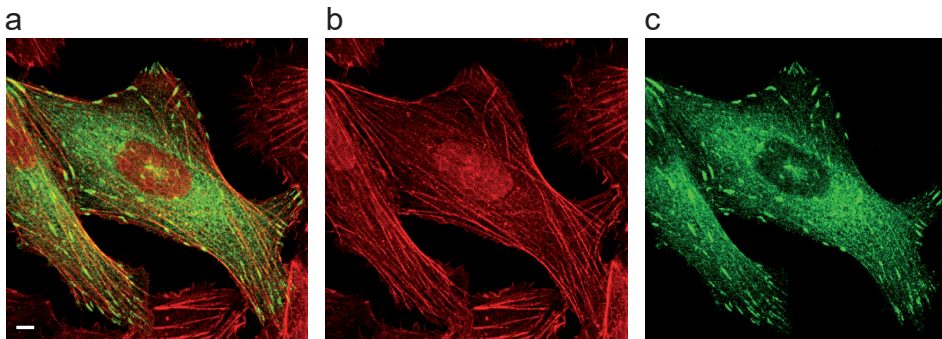

Figure 1. Focal adhesions and F-actin stress fibres.
(a) Overlay of the maximum projection of the confocal image of a U2OS cell stably expressing the intracellular FA protein paxillin-GFP (green) and stained with phalloidin-CF405 (pseudocolour red), a toxin that specifically binds to F-actin such as the stress fibres connecting to focal adhesions. Scale bar: 5 μm **(b)** Pseudo coloured red channel of the data shown in a. **(c)** Green channel of the data shown in a.

Cellular adhesion to the ECM is facilitated by focal adhesions (FAs), flat elongated structures 1-5 μm long, 300-500 nm wide and up to 50 nm thick[1-4] (Fig. 1a). They are macromolecular multiprotein assemblies that link the intracellular cytoskeleton to the extracellular matrix. Their linkage to the ECM is mainly mediated by integrins, transmembrane receptors that are part of the FA complex and directly bind to the ECM. Connection to the cytoskeleton takes place through stress-fibres, a specialised form of F-actin or filamentous actin, associated with contractile myosin II[5] (Fig. 1b). As protein complexes linking two constantly remodelling networks, the ECM and the cytoskeleton, FAs are continuously exposed to force. The force experienced by FAs depends on the combination of myosin-II contractility, which determines the force exerted on the FA by the stress fibres, and on the stiffness of the ECM. FAs are the points of force transmission from the cytoskeleton to the ECM and they change in number, size and

composition in response to the level of force experienced[6-14].

Focal adhesions in health and disease

Because of their importance in cell adhesion and for the transmission of force, FAs are crucial to most types of cell migration, including in vitro over a two-dimensional surface[15]. Since cell migration and adhesion are important in many physiological processes, FAs also play major roles in many physiological processes. Of note, FAs are vital to embryonic development, where they coordinate stem cell differentiation in response to ECM stiffness and are key to organogenesis and morphogenesis[16-18]. The importance of FAs is not limited to foetal physiological processes however, they are also pivotal to the normal functioning of the immune system and to wound healing[19]. Considering their importance to embryonic development and the immune system, it is unsurprising that FAs also have major roles in many developmental and immunological disorders[15,18,19]. Nevertheless, in pathology most FA research focusses on their role in cancer, where they are especially important during metastasis[20-22]. Integrins and other FA components are often upregulated in aggressive forms of cancer[23-25] and they are crucial to the Epithelial-Mesenchymal Transition (EMT)[26-30]. EMT is the process whereby epithelial cells, specialised cells that are arranged in layers and form most organs and tissue types, become more like mesenchymal cells, the less specialised typically highly motile cells that include stem cells and blood cells[31]. During EMT cells lose their cell-cell junctions, their dependency on cell adhesion and their apical-basal polarity. Cells also reorganise their cytoskeleton and activate different signalling and gene expression pathways during this process. Ultimately, EMT increases the motility and invasiveness of cells and therefore EMT is also an important step in tumour progression.

Focal adhesions on glass and in vivo

FAs are large macromolecular multiprotein assemblies that vary in their overall structure and protein composition and to which differences in posttranslational modifications add further complexity[32-34]. The ECM is also complex, it is a large three-dimensional network with hundreds of different proteins, proteoglycans and glycosaminoglycans as possible components that is constantly being reorganised by matrix degrading enzymes[35]. There is also a direct interplay between the ECM and FAs, *i.e.* both ECM chemical composition and its mechanical properties (e.g. stiffness) influence FA composition, size and structure[36,37]. Because of the combined complexity of FAs, the ECM and their interactions, a coating of a single type of ECM protein on glass is often used for mechanistic studies. This strongly simplifies the complexity of the extracellular environment.

1

Although reducing complexity is a clear advantage for mechanistic studies, concerns have been raised about the relevance of FAs observed on coated coverslips to cell adherence and migration under physiological conditions. The primary concern is the extreme stiffness of glass (over 50 GPa) compared to the stiffness encountered in the human body, which ranges from ~1 kPa for the brain and ~10 kPa for muscle to ~100kPa for bones. Substrate stiffness has a direct impact on FAs and FA components. For example, if cells are cultured on glass or other stiff substrates the formed FAs are larger and expression of numerous FA proteins including talin, paxillin and vinculin is increased[16,36]. However, when cells are plated on gels with stiffness comparable to *in vivo* conditions, FAs are still observed. These FAs are composed of the same elements as FAs formed on glass, although they are typically smaller. A second concern is that glass coated coverslips provide a two-dimensional environment for the cells to bind to, instead of the three-dimensional ECM typically encountered *in vivo*. Again, this concern has been addressed using gels. In three-dimensional gels FAs are observed, which are smaller than FAs formed on glass but composed of the same proteins[32,38]. Therefore, FAs are not artefacts only formed when cells are exposed to very stiff two-dimensional environments. Indeed, FAs have been observed *in vivo* and recent *in vivo* studies confirmed their importance for several developmental processes and wound healing[39-43].

The molecular composition of focal adhesions

FAs were first described more than 40 years ago in reports that visualised the movement of cells on ECM-coated coverslips using interference reflection microscopy[44-46]. A decade later vinculin was the first intracellular FA protein described[47,48]. Since then, it has become apparent that FAs are large and diverse macromolecular protein assemblies, with over two hundred different reported proteins[15,49]. These include (trans)membrane receptors, adaptor proteins and many different signalling proteins such as kinases, phosphatases and G-protein regulators, which through post-translational modifications add significantly to FA complexity. Moreover, currently, a few thousand more proteins are candidates to be added to this list based on mass spectrometry experiments[50,51]. Intracellular FA proteins are organised in a layered nanostructure. A seminal study revealed the presence of three different layers: at the bottom, closest to the adherent membrane (within ~10-20 nm), the so-called integrin signalling layer (ISL), at the top (~50-60 nm from the adherent membrane) the actin-regulatory layer (ARL) and in between the force transduction layer (FTL)[3]. Later studies, using different techniques, confirmed the layered nanostructure of FAs along the z-axis[52-54].
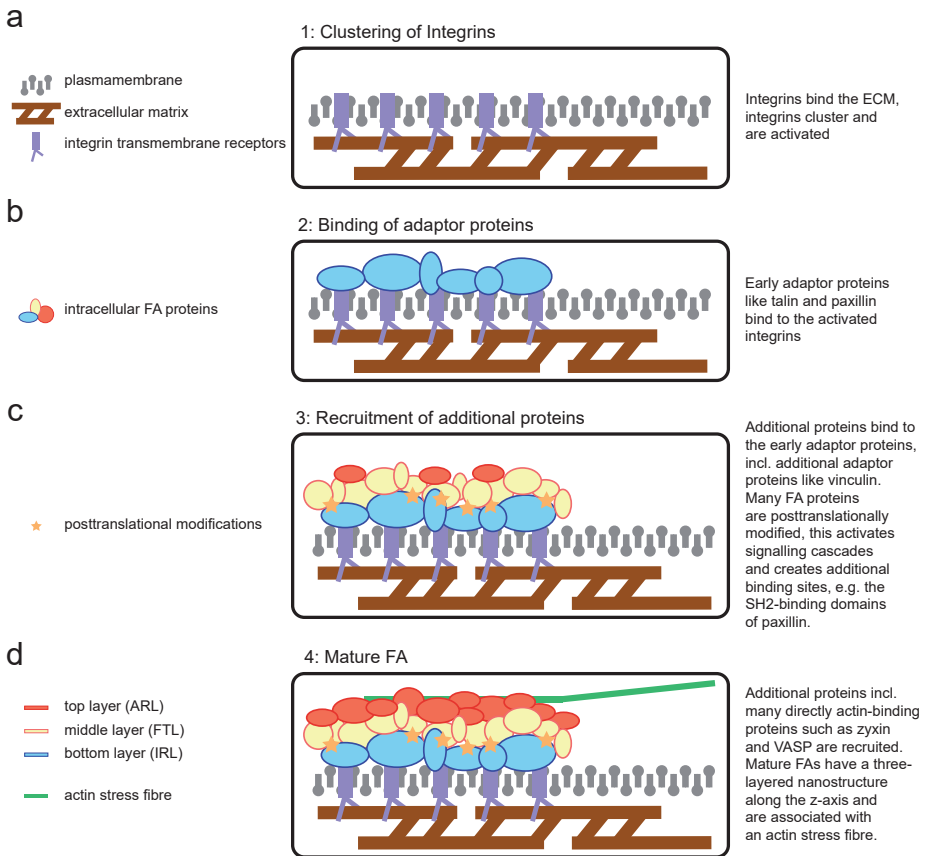
a

1: Clustering of Integrins

plasmamembrane

extracellular matrix

integrin transmembrane receptors

Integrins bind the ECM, integrins cluster and are activated

b

2: Binding of adaptor proteins

intracellular FA proteins

Early adaptor proteins like talin and paxillin bind to the activated integrins

c

3: Recruitment of additional proteins

posttranslational modifications

Additional proteins bind to the early adaptor proteins, incl. additional adaptor proteins like vinculin. Many FA proteins are posttranslationally modified, this activates signalling cascades and creates additional binding sites, e.g. the SH2-binding domains of paxillin.

d

4: Mature FA

top layer (ARL)

middle layer (FTL)

bottom layer (IRL)

actin stress fibre

Additional proteins incl. many directly actin-binding proteins such as zyxin and VASP are recruited. Mature FAs have a three-layered nanostructure along the z-axis and are associated with an actin stress fibre.

Figure 2. The formation of a focal adhesion complex through time.
(a-d) Simplified overview of the main steps involved in the formation of a focal adhesion complex. Steps shown in chronological order, from the initial clustering of integrin receptors (a) to the eventual formation of a mature three-layered focal adhesion with associated F-actin stress fibre (d). Not to scale.

The characteristics of individual FAs, including their molecular composition, varies greatly depending on the different inputs they receive from their local environments, both intracellularly and from the ECM. However, all FAs incorporate integrin transmembrane receptors and actin stress fibres. Integrins are heterodimers of α- and β-integrins, in mammalian cells 24 different heterodimers have been reported, all with their own ligand specificity for (sets of) ECM proteins[55]. There are two types of stress fibres associated with FAs: ventral stress fibres are associated with FAs at either end and typically transverse the whole cell[56]. Dorsal stress fibres are linked to FAs on one end, typically near the cell front, then stretch upwards to the nucleus and the dorsal cell surface.

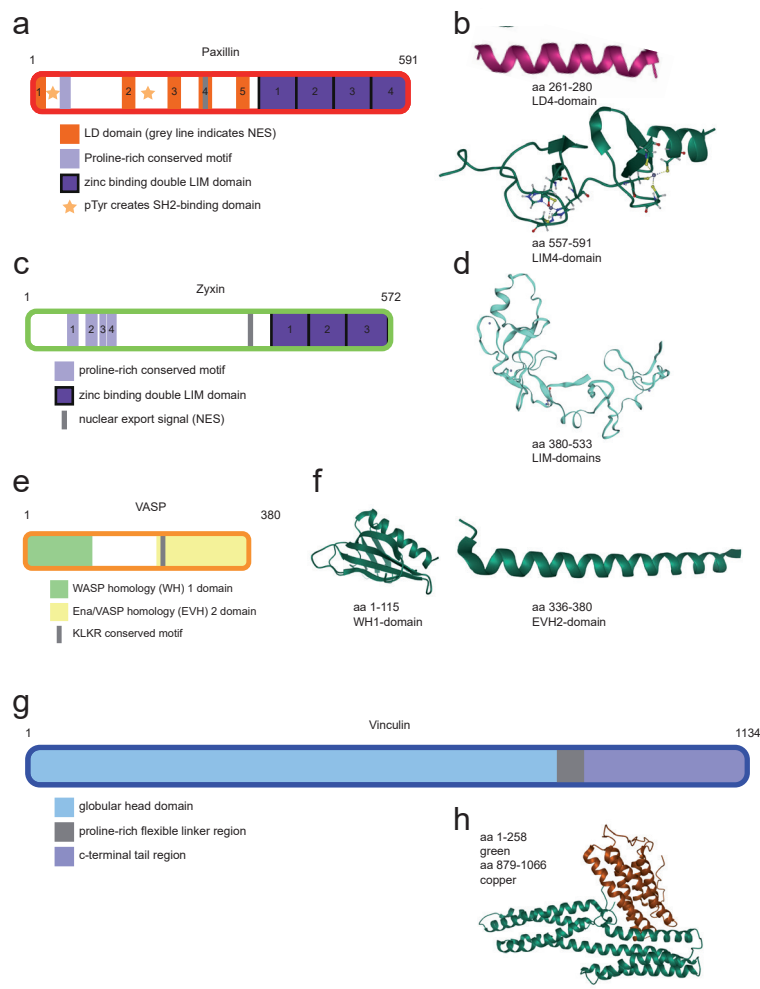The formation of new FA complexes involves several steps (Fig. 2). Firstly, in-

1

Figure 3. The structure of four intracellular FA proteins.

(a, c, e, g) Schematic representation of the paxillin (a), zyxin (c), VASP (e) and vinculin (g) proteins and their different domains, drawn to scale with respect to the amino acid backbone. Numbers indicate amino acid number along the protein backbone. **(b)** 3D structures of paxillin domains as visualised using the RCSB ProteinDataBank structure viewer Mol*[169]. Top: 3D structure of the LD-4 domain, which includes the paxillin nuclear export signal (NES). Based on X-ray diffraction data PDB ID: 6IUI[170]. Bottom: 3D structure of a large part of the paxillin LIM 4 domain based on Nuclear Magnetic Resonance (NMR) spectroscopy data PDB ID: 6U4M[171]. The blue spheres represent the two bound zinc-ions, amino acids interacting with these ions are visualised using the 'ball and stick' method. **(d)** Predicted 3D structure of a stretch spanning part of the first and all of the second and third zyxin LIM domains as predicted by the SWISS-MODEL database based on its homology with the LIM domains of the insulin gene enhancer protein ISL-2 with known 3D structure through X-ray diffraction data[172,173]. **(f)** 3D structures of VASP domains. Left: WH1-domain based on NMR spectroscopy data, PDB ID: 1EGX[174]. Right: structure of the last part (termed block C) of the EVH2-domain based on X-ray diffraction data, PDB ID: 1USE[175]. **(h)** 3D structure of the parts of the vinculin head and tail domains in complex when vinculin is in its closed conformation. Based on X-ray diffraction data, PDB ID: 1RKE[176].

tegrin transmembrane receptors bind to the extracellular matrix, which causes clustering of the integrins, leading to their activation with resultant conformational changes[8,57-59] (Fig. 2a). Secondly, intracellular adaptor proteins such as talin and paxillin are recruited[60,61] (Fig. 2b). These proteins in turn promote integrin activation, leading to the clustering of more integrins[62]. The adaptor proteins also provide a binding platform for the hundreds of other intracellular FA proteins which ultimately results in the recruitment of an actin stress fibre (Fig. 2c,d).

Paxillin

As an adaptor protein, paxillin is one of the proteins with the largest number of potential binding partners within FAs[49]. Paxillin is a direct integrin-binding protein present in the bottom (IRL) layer and it is among the first proteins to be recruited to newly forming FAs[3,60,61] (Fig. 2b).

The N-terminal domain of paxillin has two binding sites for Focal Adhesion Kinase (FAK), which can phosphorylate paxillin at Tyr-31 and Tyr-118[63,64] (Fig. 3a). This phosphorylation creates two SH2 binding sites, which are the main binding platforms for the other paxillin interactors, among which are many signalling proteins such as the kinase Src[65]. The phosphorylation process is mechanosensitive, *i.e.* it depends on the level of force experienced by the FA, where in this case, force increases phosphorylation levels[14]. Unsurprisingly, the creation of the SH2 binding domains through tyrosine phosphorylation of paxillin, is a key step during FA assembly[66]. It influences FA size, can be used as a measure of integrin signalling and is increased during EMT induced by transforming growth factor β (TGF-β) in various cell lines[29,30,67,68]. Incidentally, zyxin is required for efficient tyrosine phosphorylation of paxillin during TGF-β-induced EMT.

The C-terminal domain of paxillin contains four double zinc finger LIM domains, reminiscent of zinc finger transcription factors[64] (Fig. 2a,b). Indeed, paxillin is a functioning transcription factor, has a nuclear export signal and shuttles between FAs and the nucleus[69,70]. Furthermore, paxillin influences gene expression at the translational level by interacting with polyadenylate-binding protein 1 (PABP1), both at the endoplasmic reticulum and at FAs[71,72]. Aside from their critical role in transcription regulation the paxillin LIM domains are also required for its targeting to FAs, in particular the third LIM domain[64].

Consistent with paxillin being a key adaptor protein for FAs, paxillin knockout mice suffer from lethal heart and brain deficits during embryonic development[73]. Fibroblasts cultured from paxillin knockout mice display aberrant FAs, decreased migration and problems with cell spreading. This highlights the importance of paxillin to FAs and by extension to cell adherence and migration.

1

1

Zyxin and VASP

Zyxin and vasodilator-stimulated phosphoprotein (VASP) are binding partners that are recruited together to forming FA complexes at relatively late stages[74-76] (Fig. 2d). They are closely linked to the stress fibres associated with mature FAs and are found in the top (ARL) layer[3]. They accumulate at FAs and at actin-polymerisation complexes, which are periodically distributed along stress fibres[77-79]. Zyxin recruits VASP and α-actin to damaged stress fibres to coordinate their repair and maintenance[80]. VASP is part of the Ena/VASP protein family, a group of highly related proteins named for the drosophila protein enabled and its vertebrate homologue VASP.

The C-terminal domain of zyxin contains several double zinc finger LIM domains[81] (Fig. 3c,d). Zyxin is a functioning transcription factor, has a nuclear export signal and moves, particularly in response to force, from FAs to the nucleus where it promotes gene expression[69,82,83]. Nuclear zyxin is involved in the control of mitosis progression[79]. Since it is a direct polyadenylate-binding protein zyxin can influence protein expression at the translational level, next to its role at the transcriptional level[84]. Finally, the zyxin LIM-domains are responsible for its targetting to FAs, where zyxin is responsible for the mechanosensitive recruitment of VASP[75,85,86]. Note that this is similar to the role of the LIM domains in paxillin function.

The zyxin N-terminus is closely linked to actin regulation. It contains actin binding sites, but also binding sites for α-actinin, an actin-binding protein that is especially abundant on stress fibers[87,88]. Proline-rich stretches form binding sites for the Ena/VASP proteins[75,76] (Fig. 3c). These stretches are also binding sites for guanine exchange factors (GEFs) for the small GTPase Rho, through which zyxin, VASP and vinculin, in a co-dependent manner, stimulate actin polymerisation in response to mechanical stimuli[75,85,89-93].

In mammals the Ena/VASP family consist of three different proteins: VASP, mammalian protein enabled homolog (Mena) and Ena-VASP-like protein (Evl). These proteins are highly related and share the same functional domains (Fig. 3e). The N-terminus incorporates the WASP homology (WH) 1 domain, also known as the Ena/VASP homology (EVH) 1 domain (Fig. 3f). This is a protein interactor domain which binds to a specific proline-rich motif such as is present in zyxin and vinculin[94]. As discussed above, zyxin recruits VASP to FAs and consequently the WH 1 domain is also essential for the targeting of VASP to FAs.

The C-terminus of the Ena/VASP proteins contains the EVH 2 domain, which is closely linked to their actin regulatory functions (Fig. 3e). The EVH2 domain is

composed of three consecutive regions termed blocks A, B and C. The conserved KLKR motif within block A mediates the stimulation of actin polymerisation. Block B contains an F-actin binding site and block C terminates in a large alpha-helix (Fig. 3f). This alpha-helix mediates the tetramerization of the Ena/VASP proteins, which is required for their efficient functioning[95].

The study of VASP depleted or VASP knockout cells or mice is hampered by the presence of the other Ena/VASP family members. Nevertheless, a recent study using somatic gene disruptions of all three family members showed the Ena/VASP proteins positively contribute to cell adhesion and cell migration over two-dimensional stiff surfaces[96]. Zyxin knockout mice display no lethal embryological developmental problems or obvious histological abnormalities[69,97]. However, loss of zyxin, VASP or their interaction, results in an inability of cells to remodel their cytoskeleton in response to internal or external cues. Such cells are no longer able to thicken their stress fibres in response to mechanical stress or the actin stabilizer jasplakinolide[89,90,98]. This translates into an inflexibility of cellular behaviour. Fibroblasts cultured from zyxin knockout mice are unable to adjust their migratory speed or adhesiveness in response to cues from the ECM, although overall both migration and adhesiveness are enhanced in these cells compared to wild type.

The upregulation of zyxin is also a part of the TGF-β induced EMT response, where zyxin coordinates the remodelling of the actin cytoskeleton during EMT[29]. In line with this important role of zyxin in the EMT process, zyxin has been strongly linked to several types of cancer (progression), including bladder and breast cancer and Ewing's sarcoma where it acts as a tumour suppressor[99-101].

Vinculin

Vinculin is a large scaffold protein similar to paxillin and it is among the proteins with the most potential interaction partners within FAs[49]. Vinculin is among the earliest proteins recruited to newly forming FAs, although vinculin does not directly bind to the clustering integrins and consequently is recruited slightly later than paxillin[49,74] (Fig. 2c). Vinculin directly binds actin filaments and is involved in actin regulation at FAs[102]. It is found in the middle (FTL) layer of mature FAs[3].

Vinculin has a head and a tail domain with a flexible linker in between, allowing vinculin to adopt open and closed conformations[103] (Fig. 3g). In its closed, or inactive form, the head and tail domain interact (Fig. 3h). When vinculin opens to its active form several extra protein binding sites are revealed.

The vinculin head domain shares many important binding partners with paxillin, including talin[104]. Together with paxillin and talin, vinculin promotes integrin

1

activation and clustering[102]. The head domain also has a binding site for paxillin and paxillin is required for vinculin's recruitment to FAs in many, but not all, cell types[14,64,73,105,106]. This process is particularly well-studied in fibroblasts, where the paxillin-mediated recruitment of vinculin is force-dependent and as such is affected by both myosin-II contractility and matrix stiffness[14]. It requires tyrosine phosphorylation of paxillin, which is mediated by FAK in a mechanosensitive manner. The interaction between vinculin and paxillin also inhibits the translocation of paxillin to the nucleus[107].

The vinculin tail domain is closely linked to actin regulation. It contains actin binding sites but also binding sites for α-actinin and the Ena/VASP proteins[108-111]. Vinculin requires both zyxin and VASP to efficiently stimulate actin polymerisation at FAs[75,89-93].

Vinculin knockout mice, like the paxillin knockout mice, experience lethal heart and brain deficits during embryonic development[112]. Induced vinculin 'knockout' embryonic fibroblasts display problems with cell spreading, with adhesion to a variety of different substrates, with three-dimensional invasion, with FA maturation and with forming strong traction forces at FAs, although their random migration velocity is increased[113-116]. This shows that as another large adaptor protein vinculin, like paxillin, is of great importance to FAs and by extension to embryonic development.

The scattering response

A considerable part of the FA research field focuses on studying FAs during cell migration, mainly because of the importance of cell migration to embryonic development and metastasis. An often employed method to enhance cell migration is to stimulate cells with the Hepatocyte Growth Factor (HGF). HGF, also known as the scattering factor, induces a scattering response in epithelial cells[117-120]. During scattering the contact between cells is reduced and cells display increased motility and undirected migration.

The hepatocyte growth factor (HGF) and Met

HGF is an 80 kDa protein that was first discovered as the natural ligand for the tyrosine receptor encoded for by the proto-oncogene c-Met[121-123]. Both HGF and Met are glycosylated and cleaved by proteases from single-chain precursors into mature disulphide-linked heterodimers[124]. HGF is the only known natural ligand for Met and Met is the only known receptor for HGF. Upon HGF binding the kinase activity of Met is activated through autophosphorylation. Further phosphorylation creates docking sites for different intracellular signalling molecules that activate a host of signalling pathways with diverse biological effects[117].

HGF in health and disease

HGF/c-Met signalling is indispensable for organogenesis[125], during adulthood it is involved in the response to damage and in the maintenance of homeostasis of several organs[126]. In pathology, HGF signalling through c-Met is involved in the progression of several infectious diseases, but it is probably best known for its involvement in cancer, in particular for its promotion of metastasis[118,127-129]. As such, HGF/Met signalling is considered a promising target for the treatment of different cancer types[127,128,130-132]. The aberrant HFG/Met signalling seen in cancer (1) stimulates angiogenesis, (2) promotes survival of cells after detachment from the basal membrane by inhibiting apoptosis through a wide variety of mechanisms, (3) stimulates the excretion of proteases to allow cells to invade through the ECM and (4) strongly stimulates cell motility[127,128,133,134]. Taken together this explains the important role of HGF in metastasis.

Multimodal imaging of focal adhesions

Over the last few decades, the field of biology has greatly benefited from the development of different advanced light microscopy techniques. At their basis lie two important technological advances, the use of lasers as a light source and the development of genetically encoded fluorescent tags.

Lasers as a light source

Probably the most well-known microscopy form using lasers as a light source is confocal laser scanning microscopy[135,136]. This form of microscopy uses a laser to scan samples and pinholes to block out of focus light, which greatly improves image quality. Even without pinholes lasers offer significant improvements to light microscopy because of their ability to exclusively produce coherent light of a specific wavelength and because they are such powerful light sources, with more powerful lasers being developed all the time.

GFP and other genetically encoded fluorescent tags

Green Fluorescent Protein (GFP) is a small 27 kDa protein that was first isolated from the Aequorea victoria jellyfish in the sixties[137]. GFP became of key importance to cell biology with the realisation that it could be used to tag and follow proteins in live cells[138]. For this purpose, cells are transfected with engineered DNA constructs, in which the DNA encoding for GFP is added to the DNA encoding a protein of interest. As a result, fusion proteins of the protein of interest fused to GFP are produced by the DNA transcription machinery of the transfected cells. The GFP effectively functions as a 'build-in light' that turns on when it is excited by light of the appropriate wavelength, allowing the protein to be followed in

live cells. Since the first genetically encoded fluorescent tags, much research has led to the development of a significantly improved toolset. Brighter proteins are now available with emission wavelengths that span the entire colour spectrum and even beyond it into the ultraviolet and far-red wavelengths. The different colours do more than just create pretty images, they allow the visualisation of different fusion proteins at the same time because they can be distinguished through their colours.

Imaging fluorescent molecules

When GFP or other fluorescent molecules absorb photons with a specific amount of energy, their electrons change configuration to bring the molecules from the ground state to an excited state. Because this state is energetically unfavourable, the electrons quickly fall back to the ground state. During this process, the electrons release their excess energy in the form of a photon, which is known as fluorescence. Some energy is always lost during excitation, therefore the photons emitted by fluorescent molecules always have less energy than the photons they need to absorb for excitation. Consequently, the light emitted by fluorescent molecules always has a longer wavelength than the light they need to absorb for excitation since the wavelength of light is determined by the energy level of its photons and less energy means a longer wavelength. The emitted light also has a much lower intensity, typically the light used for excitation is approximately a thousandfold stronger than the light emitted. So, to make a clear image of the emitted light it needs to be filtered from the excitation light. Because of the different wavelengths, in fluorescence microscopes this can easily be achieved using chromatic filters which filter light of specific wavelengths.

Advanced light microscopy in the field of biology

The use of lasers as a light source and the development of genetically encoded tags opened up the road for the development of advanced light microscopy techniques and their application in the field of biology. As image quality improved with continuing development over time, light microscopy became one of the main research methods in cell biology. However, no matter how bright the lasers or how good the lenses, in principle the laws of physics place a limit on the resolution a light microscope can achieve. This was first recognised by the German scientist Ernst Karl Abbe (1840-1905) and is often referred to as Abbe's limit or simply the resolution limit. Ultimately, it means that the maximum resolution (the smallest distance at which two objects can still be resolved as being separate) a light microscope can ever achieve is approximately half the wavelength used for excitation. When using GFP this theoretical maximum resolution is approximately 250 nm. Since protein sizes range from about one to five nanometers, ide-

1

ally cells would be observed at considerably higher resolutions. Consequently, much of the modern advanced microscopy methods are focused on clever ways to break, or more accurately circumvent, the resolution limit. These include TIRF, SIM and single molecule imaging techniques such as PALM or STORM. Other advanced imaging techniques focus on using microscopy to obtain additional information from the images, information beyond the location of proteins. Examples of such techniques include FRAP, FCS and STICS, which focus on obtaining quantitative measurements related to the dynamic behaviour of proteins.
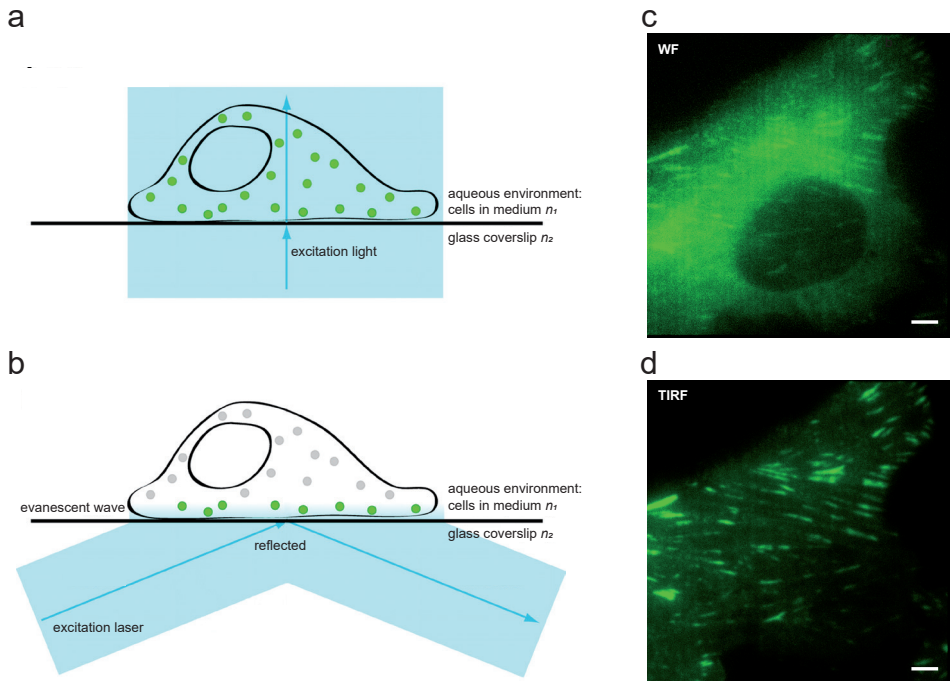

Figure 4. Widefield versus total internal reflection microscopy.
(a) Schematic overview of the light path during widefield or epifluorescence microscopy. The excitation laser shines straight through the sample, therefore fluorophores are excited throughout the cell (green circles). **(b)** Schematic overview of the light path during total internal reflection (TIRF) microscopy. The excitation laser exits the objective at such an angle that it is completely reflected at the glass-fluid interphase, formed by the glass coverslip and the aqueous environment of the cells in media, back into the objective. The reflecting laser light produces an electromagnetic field known as the evanescent wave, which declines exponentially. It is only powerful enough to excite fluorophores (green circles) in a thin layer 100-200 nm upwards from the coverslips, leaving fluorophores present at higher locations in the cell unexcited (grey circles). **(c, d)** The same area of a U2OS cell stably expressing paxillin-GFP imaged on the same microscope in widefield (c) or in TIRF (d) mode. In d the signal to background ratio is strongly improved for the focal adhesions.

Total internal reflection microscopy

Total internal reflection (TIRF) microscopy breaks the resolution limit in one direction by changing the angle of the excitation laser. It was first developed in the early eighties[139], then adapted for easy use in cell biology in the late eighties[140]. In

1

TIRF the excitation laser illuminates the sample at an angle. Consequently, the laser is reflected at the glass-fluid interphase because of the difference in refraction index between the glass coverslip and the aqueous solution (the cytoplasm or the culture medium) on top (Fig. 4b). The angle is adjusted to the precise angle where the entire laser beam is fully reflected back into the objective. This is known as total internal reflection and it is the same principle as is used for data transfer through fibre-optic cables. As implied by the 'total', in TIRF microscopy the entire laser beam is reflected at the glass-fluid interphase and its light is not directly used to excite fluorophores. The reflecting laser light produces an electromagnetic field, the evanescent wave. Because the wave declines exponentially, it is only strong enough to excite fluorophores up to a very small distance from the glass-fluid interphase, about 100-200 nm. In other words, only a thin layer one to two hundred nanometres upwards from the coverslip is visualised, breaking the resolution limit in this direction.

The thinness of the excitation layer limits the cellular objects that can be studied with TIRF to those found in, or very close to, the plasma membrane. Despite this limiting effect, the thinness is also the reason for the main advantage of TIRF, the strongly improved signal to background ratio. Any fluorophores further than two hundred nanometers from the adherent plasma membrane are not reached by the evanescent wave, for this reason, they are not excited and the potential background fluorescence is eliminated. When visualising FAs by fluorescently tagging intracellular FA proteins this effect is especially pronounced because these proteins are typically strongly expressed in the cytoplasm apart from their enrichment at FAs, increasing the potential for background fluorescence coming from the cytoplasm (Fig. 4c,d). Other advantages of the thin excitation layer are that almost no out-of-focus fluorescence is collected, also improving image quality, and cells are exposed to relatively little light, reducing phototoxicity.

Structured illumination microscopy

Structured Illumination Microscopy (SIM) also uses a specialised form of illumination to improve resolution. While in TIRF only the z-resolution is improved, SIM circumvents the resolution limit in all three directions[141]. In each direction, the resolution is improved approximately two-fold compared to a confocal microscope, in essence enabling the visualisation of three-dimensional objects eight (2^3) times as small[142].

The specialised illumination in SIM makes use of a grated pattern of light, which produces the Moiré effect. This phenomenon is a type of interference that occurs when two dense patterns are overlaid and it produces a third, larger pattern (Fig. 5a). In SIM, images are reconstructed through a complicated mathematical pro-
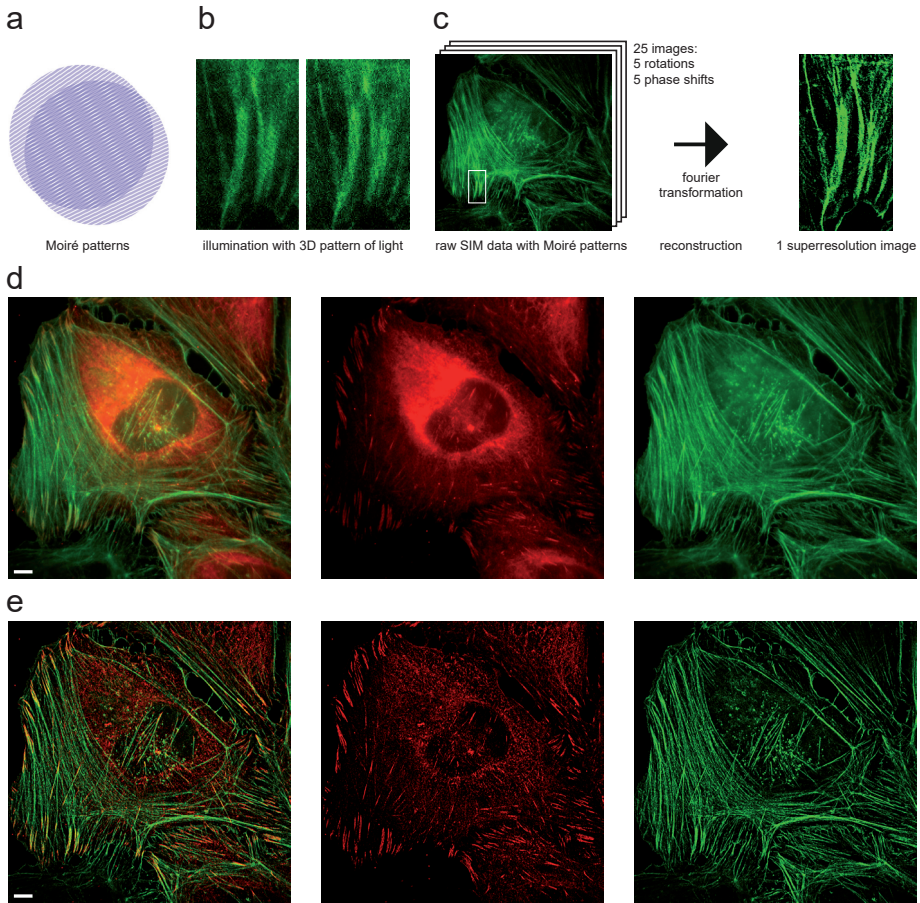
Figure 5. Structured Illumination Microscopy (SIM)
(a) Example of a Moiré pattern, an interference effect that occurs when two dense patterns are overlaid. Note that the formed Moiré pattern is always larger than the overlaid patterns. **(b, c)** An overview of SIM imaging. SIM uses a grated three dimensional pattern of light for illumination, meaning parts of the sample are not exposed to excitation light (black stripes in b). This form of illumination produces Moiré effects. Note that the black stripes in b change orientation, this is because the pattern of light is rotated to allow reliable reconstruction of the superresolution image based on the collected Moiré patterns (c). The illumination pattern is also shifted to allow data collection from the whole image. In total 25 raw data images are used to reconstruct 1 superresolution image. b is a magnification of the boxed area in c **(d, e)** Reconstruction of the widefield image (d) or the superresolution SIM image (e) of a U2OS cell stably expressing paxillin-mCherry (red) and stained with phalloidin-CF405 (pseudocolour green) to highlight the F-actin. Scalebar: 5 μm

cess involving Fourier transformations, on the basis of the (known) illumination pattern and the Moiré pattern observed in the raw data (Fig. 5b,c). This allows reconstruction of images beyond the resolution limit (Fig. 5e) because the Moiré patterns they are based on are always larger than the original overlaid patterns. In other words, in the Moiré patterns high frequency data is shifted to a lower, observable, frequency[143]. During the reconstruction process, this data is shifted

back to its high frequency position in Fourier space, then translated into a reconstructed high resolution image. To allow for reliable reconstruction the Moiré patterns need to be collected following 3 to 5 rotations of the illumination pattern. To make sure the whole image is covered by the illumination pattern it needs to be shifted as well. Accordingly, to create one reconstructed SIM image, 25 raw images need to be collected, slowing down the imaging process. Because SIM is a widefield technique, the whole image (or at least the whole image currently covered by the illumination pattern) is collected at once, hence SIM is still fast enough for live cell imaging despite the large number of raw images needed to reconstruct one superresolution image.

Correlative light and electron microscopy

A different approach to achieving a higher resolution is to couple light microscopy with electron microscopy. Electron microscopy (EM) uses an electron beam for visualisation purposes. Electron beams have wavelengths about a hundred thousand times smaller than light beams[142]. This means that even resolutions sufficient to visualise single molecules can easily be achieved without approaching Abbe's limit.

EM does not necessarily rely on tags for visualisation, where in fluorescence microscopy (FM) only the fluorescently tagged protein is visible, in EM all are visualised at the same time. This reveals the cellular context, but also makes it difficult to recognise specific structures or individual protein types, such as are easily identified in FM by their fluorescent tags. This problem is largely solved in Correlative or Correlated Light and Electron Microscopy (CLEM), which as the name suggests combines the two imaging modalities of light (typically fluorescence) microscopy and electron microscopy[144]. This allows the visualisation of a specific protein type, recognisable through FM, at high resolution and within the cellular context through EM.

Different types of EM can be used in CLEM. Since focal adhesions are dense structures found close to the cell surface they are particularly well suited to studying with scanning EM. In this technique images are formed by collecting electrons scattered by the sample surface, limiting imaging to a thin layer close to the sample surface. Density influences this scattering, making the dense FA complexes stand out from their surrounding environment. Using scanning EM eliminates the need for the complicated sample preparation required for transmission EM and simplifies the combination with FM.

In some forms of CLEM the FM is performed first followed by EM sample preparation and EM imaging, in others sample preparation is completed first followed

by both FM and EM imaging[145]. This second approach can improve the quality of the FM and EM overlay images. Firstly by avoiding the risk of EM sample preparation leading to distortions between the FM and EM images. Secondly, by allowing for both types of imaging to be performed on a single microscope, which makes it much easier to ascertain the exact same structure is imaged in both modalities. This approach of combining FM and EM in a single microscope was first achieved in the eighties[146]. It is termed integrated CLEM and currently microscopes using this approach are commercially available[145].

Fluorescence recovery after photobleaching

Fluorescence Recovery After Photobleaching (FRAP) is one of the advanced light microscopy techniques not aiming to enhance the resolution but focusing on obtaining quantitative parameters, specifically on the mobility and dynamics of proteins. FRAP was initially conceptualised and set-up at the end of the seventies[147-149]. When around the beginning of the millennium both laser-assisted microscopy and genetically encoded fluorescent tags became widely available, the rapidly expanding field of protein dynamics embraced FRAP as one of its principal tools of investigation[150-154].

FRAP takes advantage of the fact that when fluorescent tags are excited too strongly they irreversibly lose their fluorescent property, i.e. they are bleached. During a typical FRAP experiment, a small region of the cell is briefly illuminated with a powerful laser, bleaching the fluorescent tags of the fusion proteins exposed to this so-called bleach pulse. As a result, when this area of the cell is again illuminated by the excitation laser at its normal strength, the fluorescent light emitted is markedly reduced or even lost altogether. During a FRAP experiment, fluorescence levels are recorded and plotted against time in FRAP-curves. If the tagged proteins are able to move, over time the fluorescence levels will go up again, as the bleached proteins are replaced by fusion proteins with intact, unbleached, fluorescent tags moving into the bleached area.

From FRAP-curves a lot of information can be extracted about the mobility and binding dynamics of the studied proteins. For example, the steepness of the recovery curve is related to the mobility of the studied protein. The faster a protein moves the steeper the recovery of its FRAP-curve will be, since after the bleach pulse the unbleached molecules will move into the bleached area more quickly, resulting in a faster rise of fluorescence levels. If the final steady fluorescence level is much lower than the initial steady pre-bleach level, this reveals that a significant proportion of the proteins in the bleached area are stably bound and accordingly do not exchange for unbleached proteins within the time of the experiment. This means at the end of the experiment these bleached proteins are

still present within the bleached area, lowering the measured fluorescence levels. Of note, lower post-bleach fluorescence levels may also point to technical issues (such as monitor bleaching or bleaching of a too large proportion of the protein pool). These need to be ruled out through control experiments.

One of the key advantages of the FRAP technique is its swiftness: individual FRAP-experiments can often be conducted within a few minutes and neither the preparation nor the data analysis required to generate the FRAP-curves is particularly complicated or time consuming. This makes it especially well-suited to the extraction of reliable quantitative parameters by using the data from a high number of replicate experiments. Particularly if the experimentally-derived FRAP curves are further analysed by fitting them to curves generated by Monte Carlo based simulations[155]. This makes it possible to reliably extract from the FRAP curves many quantitative parameters, including the number of fractions with distinct dynamic parameters present within the protein pool, the sizes of these fractions and the associated k_{on}'s and k_{off}'s, while avoiding most of the simplification steps needed for the more traditional FRAP-curve analysis of mathematically solving differential equations[147,156].

Photoactivation and photoswitching

Besides brighter proteins with a diverse range of emission wavelengths, the continuing optimisation of fluorescent proteins also led to the development of proteins with altered emission characteristics in response to light of certain wavelengths, because of photochemical reactions or through conversions between chromophore stereoisomers[157]. These include the photoactivatable and the photoswitchable or photoconvertible fluorescent proteins[158].

Photoactivatable proteins require activation by illumination at a wavelength shorter than their excitation wavelength to become efficiently fluorescent. One of the first developed was photoactivatable GFP, a variant of GFP which after illumination with its activation wavelength (413 nm) becomes a hundred times more fluorescent at the wavelengths normal for enhanced GFP[159]. Continuing development has led to the engineering of a large number of photoactivatable fluorescent proteins with differing characteristics, for example in the emission spectrum, in the brightness and in the reversibility of the activation[160].

For the photoswitchable or photoconvertible fluorescent proteins irradiation with laser light of roughly four hundred nanometers results in a shift of their excitation and emission spectra. Again, continuing research has led to the development of a large number of photoconvertible fluorescent proteins together spanning a large emission spectrum with varying levels of brightness and revers-

ibility[160]. An example of a third generation optimised photoswitchable protein is mMaple3. It is a green fluorescent protein which after activation is converted to a red fluorescent protein. It is among the brightest and the most efficiently switched of the currently available photoswitchable proteins, yet it shows extremely low dimerization tendencies (a major concern for the other bright photoswitchable proteins)[161].

A common application of photoswitchable and photoactivatable proteins is in the superresolution techniques Photo Activated Location Microscopy (PALM) and Stochastic Optical Reconstruction Microscopy (STORM)[162-164]. In these forms of single molecule microscopy, low light intensities are used for photoswitching or photoactivation, making these processes slow enough to allow individual switched or activated fluorescent proteins to be sequentially detected, which in turn allows their localisation with increased precision.

Advances in data analysis

Large improvements in the employed data analysis methods also contributed strongly to the increased importance of light microscopy to modern biology, next to all the technological advances involving the light microscopes and flu-orophores. Most notably the single-molecule techniques of PALM and STORM depend entirely on post-acquisition data analysis techniques for the creation of their superresolution images. Raw PALM or STORM data resembles a long series of images with less than a hand full of activated or switched fluorophores in each separate image. Because of the optical limitations of the imaging system these fluorophores are imaged as larger spots than they actually are to form a diffraction-limited spot described by the point spread function. To generate superresolution images from this raw data extensive data analysis is required. Firstly, the point spread function is mathematically approximated with a 2D-gaussian distribution. This distribution is used to fit the spots imaged in the raw data to find their centres. These centres are used as an estimate of the location of the fluorophore underlying the diffraction-limited spot and are all overlayed in a single image, forming the reconstructed superresolution image. Similarly, raw SIM data is in essence composed of partial (because of the excitation with a 3D pattern of light rather than a continuous beam) widefield images overlaid with the even larger Moiré patterns that have a worse resolution than typical confocal images (Fig. 5b). Also here, elaborate data analysis is required, involving fourier transformations, the shifting of the information contained in the imaged Moiré patterns back into its original high frequency position and integration of multiple raw images, to reconstruct a single high resolution SIM image (Fig. 5c).

Because of the heavy reliance of PALM, STORM and SIM on data analysis tech-

1

niques, with the widespread implementation of these techniques, the widespread availability of advanced data analysis techniques also became necessary and the interest in advanced data analysis increased. With increased availability and interest, it is only natural that the image analysis of data acquired through other imaging techniques also improved, allowing more data to be extracted from these images too. A good example of this is the increased use of deconvolution software, where out of focus light is removed using image analysis software to create a three-dimensional image with improved contrast and resolution[165]. The increased availability and knowledge of data analysis techniques also allowed researchers to develop their own image processing or visualisation techniques. This process has been sped up by the availability of free open-source software such as ImageJ[166] and its framework Fiji[167], which allows researchers to focus on information within the image most relevant to their particular research question, by building with relative ease their own image analysis software, or adapt and build upon the image analysis methods developed by others. Especially by improving quantification, which increased the potential for reliable comparison between different conditions, this development has contributed strongly to many important scientific advances in the field of biology[168]. Therefore the contribution of image analysis software, including its free open-source versions, has contributed as much to the current importance of light microscopy to biology as the technological advances in light microscopes and fluorophores.

References

1   Yamada, K. M. & Geiger, B. Molecular interactions in cell adhesion complexes. *Current opinion in cell biology* 9, 76-85 (1997).

2   Geiger, B., Bershadsky, A., Pankov, R. & Yamada, K. M. Transmembrane crosstalk between the extracellular matrix--cytoskeleton crosstalk. *Nature reviews. Molecular cell biology* 2, 793-805, doi:10.1038/35099066 (2001).

3   Kanchanawong, P. *et al.* Nanoscale architecture of integrin-based cell adhesions. *Nature* 468, 580-584, doi:10.1038/nature09621 (2010).

4   Kim, D.-H. & Wirtz, D. Focal adhesion size uniquely predicts cell migration. *FASEB journal : official publication of the Federation of American Societies for Experimental Biology* 27, 1351-1361, doi:10.1096/fj.12-220160 (2013).

5   Burridge, K. & Guilluy, C. Focal adhesions, stress fibers and mechanical tension. *Experimental cell research* 343, 14-20, doi:10.1016/j.yexcr.2015.10.029 (2016).

6   Balaban, N. Q. *et al.* Force and focal adhesion assembly: a close relationship studied using elastic micropatterned substrates. *Nature cell biology* 3, 466-472, doi:10.1038/35074532 (2001).

7   Beningo, K. A., Dembo, M., Kaverina, I., Small, J. V. & Wang, Y. L. Nascent focal adhesions are responsible for the generation of strong propulsive forces in migrating fibroblasts. *The Journal of cell biology* 153, 881-888 (2001).

8   Tadokoro, S. *et al.* Talin binding to integrin beta tails: a final common step in integrin activation. *Science (New York, N.Y.)* 302, 103-106, doi:10.1126/science.1086652 (2003).

9   Chrzanowska-Wodnicka, M. & Burridge, K. Rho-stimulated contractility drives the forma-

1

tion of stress fibers and focal adhesions. *The Journal of cell biology* 133, 1403-1415 (1996).

10   Riveline, D. *et al.* Focal contacts as mechanosensors: externally applied local mechanical force induces growth of focal contacts by an mDia1-dependent and ROCK-independent mechanism. *The Journal of cell biology* 153, 1175-1186 (2001).

11   Wang, H. B., Dembo, M., Hanks, S. K. & Wang, Y. Focal adhesion kinase is involved in mechanosensing during fibroblast migration. *Proceedings of the National Academy of Sciences of the United States of America* 98, 11295-11300, doi:10.1073/pnas.201201198 (2001).

12   Galbraith, C. G., Yamada, K. M. & Sheetz, M. P. The relationship between force and focal complex development. *The Journal of cell biology* 159, 695-705, doi:10.1083/jcb.200204153 (2002).

13   Kaverina, I. *et al.* Tensile stress stimulates microtubule outgrowth in living cells. *Journal of cell science* 115, 2283-2291 (2002).

14   Pasapera, A. M., Schneider, I. C., Rericha, E., Schlaepfer, D. D. & Waterman, C. M. Myosin II activity regulates vinculin recruitment to focal adhesions through FAK-mediated paxillin phosphorylation. *The Journal of cell biology* 188, 877-890, doi:10.1083/jcb.200906012 (2010).

15   Winograd-Katz, S. E., Fassler, R., Geiger, B. & Legate, K. R. The integrin adhesome: from genes and proteins to human disease. *Nature reviews. Molecular cell biology* 15, 273-288, doi:10.1038/nrm3769 (2014).

16   Engler, A. J., Sen, S., Sweeney, H. L. & Discher, D. E. Matrix elasticity directs stem cell lineage specification. *Cell* 126, 677-689, doi:10.1016/j.cell.2006.06.044 (2006).

17   Thiery, J. P. Cell adhesion in development: a complex signaling network. *Curr Opin Genet Dev* 13, 365-371, doi:10.1016/s0959-437x(03)00088-1 (2003).

18   Maartens, A. P. & Brown, N. H. The many faces of cell adhesion during Drosophila muscle development. *Developmental biology* 401, 62-74, doi:10.1016/j.ydbio.2014.12.038 (2015).

19   Wahl, S. M., Feldman, G. M. & McCarthy, J. B. Regulation of leukocyte adhesion and signaling in inflammation and disease. *Journal of leukocyte biology* 59, 789-796 (1996).

20   Mitra, S. K. & Schlaepfer, D. D. Integrin-regulated FAK-Src signaling in normal and cancer cells. *Current opinion in cell biology* 18, 516-523, doi:10.1016/j.ceb.2006.08.011 (2006).

21   Bianchi-Smiraglia, A., Paesante, S. & Bakin, A. V. Integrin beta5 contributes to the tumorigenic potential of breast cancer cells through the Src-FAK and MEK-ERK signaling pathways. *Oncogene* 32, 3049-3058, doi:10.1038/onc.2012.320 (2013).

22   Lau, S. K. *et al.* EGFR-mediated carcinoma cell metastasis mediated by integrin alphavbeta5 depends on activation of c-Src and cleavage of MUC1. *PloS one* 7, e36753, doi:10.1371/journal.pone.0036753 (2012).

23   Bianconi, D., Unseld, M. & Prager, G. W. Integrins in the Spotlight of Cancer. *International journal of molecular sciences* 17, doi:10.3390/ijms17122037 (2016).

24   Ata, R. & Antonescu, C. N. Integrins and Cell Metabolism: An Intimate Relationship Impacting Cancer. *International journal of molecular sciences* 18, doi:10.3390/ijms18010189 (2017).

25   Desgrosellier, J. S. & Cheresh, D. A. Integrins in cancer: biological implications and therapeutic opportunities. *Nature reviews. Cancer* 10, 9-22, doi:10.1038/nrc2748 (2010).

26   Xu, F., Zhang, J., Hu, G., Liu, L. & Liang, W. Hypoxia and TGF-β1 induced PLOD2 expression improve the migration and invasion of cervical cancer cells by promoting epithelial-to-mesenchymal transition (EMT) and focal adhesion formation. *Cancer Cell Int* 17, 54-54, doi:10.1186/s12935-017-0420-z (2017).

27   Eckert, M. A. *et al.* ADAM12 induction by Twist1 promotes tumor invasion and metastasis via regulation of invadopodia and focal adhesions. *Journal of cell science* 130, 2036-2048, doi:10.1242/jcs.198200 (2017).

28   Wipff, P.-J. & Hinz, B. Integrins and the activation of latent transforming growth factor beta1 - an intimate relationship. *Eur J Cell Biol* 87, 601-615, doi:10.1016/j.ejcb.2008.01.012 (2008).

29   Bianchi-Smiraglia, A. *et al.* Integrin-beta5 and zyxin mediate formation of ventral stress

fibers in response to transforming growth factor beta. *Cell cycle (Georgetown, Tex.)* 12, 3377-3389, doi:10.4161/cc.26388 (2013).

30   Bianchi, A., Gervasi, M. E. & Bakin, A. Role of beta5-integrin in epithelial-mesenchymal transition in response to TGF-beta. *Cell cycle (Georgetown, Tex.)* 9, 1647-1659, doi:10.4161/cc.9.8.11517 (2010).

31   Lamouille, S., Xu, J. & Derynck, R. Molecular mechanisms of epithelial-mesenchymal transition. *Nature reviews. Molecular cell biology* 15, 178-196, doi:10.1038/nrm3758 (2014).

32   Berrier, A. L. & Yamada, K. M. Cell-matrix adhesion. *Journal of cellular physiology* 213, 565-573, doi:10.1002/jcp.21237 (2007).

33   Geiger, B. & Yamada, K. M. Molecular architecture and function of matrix adhesions. *Cold Spring Harb Perspect Biol* 3, a005033, doi:10.1101/cshperspect.a005033 (2011).

34   Lavelin, I. *et al.* Differential effect of actomyosin relaxation on the dynamic properties of focal adhesion proteins. *PloS one* 8, e73549, doi:10.1371/journal.pone.0073549 (2013).

35   Theocharis, A. D., Skandalis, S. S., Gialeli, C. & Karamanos, N. K. Extracellular matrix structure. *Adv Drug Deliv Rev* 97, 4-27, doi:10.1016/j.addr.2015.11.001 (2016).

36   Adutler-Lieber, S. *et al.* Engineering of synthetic cellular microenvironments: implications for immunity. *Journal of autoimmunity* 54, 100-111, doi:10.1016/j.jaut.2014.05.003 (2014).

37   Chautard, E., Fatoux-Ardore, M., Ballut, L., Thierry-Mieg, N. & Ricard-Blum, S. MatrixDB, the extracellular matrix interaction database. *Nucleic acids research* 39, D235-240, doi:10.1093/nar/gkq830 (2011).

38   Doyle, A. D., Carvajal, N., Jin, A., Matsumoto, K. & Yamada, K. M. Local 3D matrix microenvironment regulates cell migration through spatiotemporal dynamics of contractility-dependent adhesions. *Nature communications* 6, 8720, doi:10.1038/ncomms9720 (2015).

39   Singer, I. I., Kawka, D. W., Kazazis, D. M. & Clark, R. A. In vivo co-distribution of fibronectin and actin fibers in granulation tissue: immunofluorescence and electron microscope studies of the fibronexus at the myofibroblast surface. *The Journal of cell biology* 98, 2091-2106, doi:10.1083/jcb.98.6.2091 (1984).

40   Gunawan, F. *et al.* Focal adhesions are essential to drive zebrafish heart valve morphogenesis. *The Journal of cell biology* 218, 1039-1054, doi:10.1083/jcb.201807175 (2019).

41   Fischer, R. S., Lam, P.-Y., Huttenlocher, A. & Waterman, C. M. Filopodia and focal adhesions: An integrated system driving branching morphogenesis in neuronal pathfinding and angiogenesis. *Developmental biology* 451, 86-95, doi:10.1016/j.ydbio.2018.08.015 (2019).

42   Yue, J. *et al.* In vivo epidermal migration requires focal adhesion targeting of ACF7. *Nature communications* 7, 11692-11692, doi:10.1038/ncomms11692 (2016).

43   Haage, A. *et al.* Talin Autoinhibition Regulates Cell-ECM Adhesion Dynamics and Wound Healing In Vivo. *Cell Rep* 25, 2401-2416.e2405, doi:10.1016/j.celrep.2018.10.098 (2018).

44   Curtis, A. S. THE MECHANISM OF ADHESION OF CELLS TO GLASS. A STUDY BY INTERFERENCE REFLECTION MICROSCOPY. *The Journal of cell biology* 20, 199-215, doi:10.1083/jcb.20.2.199 (1964).

45   Abercrombie, M., Heaysman, J. E. & Pegrum, S. M. The locomotion of fibroblasts in culture. I. Movements of the leading edge. *Experimental cell research* 59, 393-398, doi:10.1016/0014-4827(70)90646-4 (1970).

46   Abercrombie, M., Heaysman, J. E. & Pegrum, S. M. The locomotion of fibroblasts in culture. II. "RRuffling". *Experimental cell research* 60, 437-444, doi:10.1016/0014-4827(70)90537-9 (1970).

47   Burridge, K. & Feramisco, J. R. Microinjection and localization of a 130K protein in living fibroblasts: a relationship to actin and fibronectin. *Cell* 19, 587-595, doi:10.1016/s0092-8674(80)80035-3 (1980).

48   Geiger, B. A 130K protein from chicken gizzard: its localization at the termini of microfilament bundles in cultured chicken cells. *Cell* 18, 193-205, doi:10.1016/0092-8674(79)90368-4 (1979).

49   Zaidel-Bar, R., Itzkovitz, S., Ma'ayan, A., Iyengar, R. & Geiger, B. Functional atlas of the integrin adhesome. *Nature cell biology* 9, 858-867, doi:10.1038/ncb0807-858 (2007).

50   Kuo, J.-C., Han, X., Hsiao, C.-T., Yates, J. R., 3rd & Waterman, C. M. Analysis of the myosin-II-responsive focal adhesion proteome reveals a role for β-Pix in negative regulation of focal adhesion maturation. *Nature cell biology* 13, 383-393, doi:10.1038/ncb2216 (2011).

51   Schiller, H. B., Friedel, C. C., Boulegue, C. & Fässler, R. Quantitative proteomics of the integrin adhesome show a myosin II-dependent recruitment of LIM domain proteins. *EMBO Rep* 12, 259-266, doi:10.1038/embor.2011.5 (2011).

52   Liu, J. *et al.* Talin determines the nanoscale architecture of focal adhesions. *Proceedings of the National Academy of Sciences of the United States of America* 112, E4864-4873, doi:10.1073/pnas.1512025112 (2015).

53   Paszek, M. J. *et al.* Scanning angle interference microscopy reveals cell dynamics at the nanoscale. *Nature methods* 9, 825-827, doi:10.1038/nmeth.2077 (2012).

54   Stubb, A. *et al.* Superresolution architecture of cornerstone focal adhesions in human pluripotent stem cells. *Nature communications* 10, 4756, doi:10.1038/s41467-019-12611-w (2019).

55   Orré, T., Rossier, O. & Giannone, G. The inner life of integrin adhesion sites: From single molecules to functional macromolecular complexes. *Experimental cell research* 379, 235-244, doi:10.1016/j.yexcr.2019.03.036 (2019).

56   Small, J. V., Rottner, K., Kaverina, I. & Anderson, K. I. Assembling an actin cytoskeleton for cell attachment and movement. *Biochimica et biophysica acta* 1404, 271-281 (1998).

57   Wu, C., Keivens, V. M., O'Toole, T. E., McDonald, J. A. & Ginsberg, M. H. Integrin activation and cytoskeletal interaction are essential for the assembly of a fibronectin matrix. *Cell* 83, 715-724, doi:10.1016/0092-8674(95)90184-1 (1995).

58   Kechagia, J. Z., Ivaska, J. & Roca-Cusachs, P. Integrins as biomechanical sensors of the microenvironment. *Nature reviews. Molecular cell biology* 20, 457-473, doi:10.1038/s41580-019-0134-2 (2019).

59   Shattil, S. J., Kim, C. & Ginsberg, M. H. The final steps of integrin activation: the end game. *Nature reviews. Molecular cell biology* 11, 288-300, doi:10.1038/nrm2871 (2010).

60   Laukaitis, C. M., Webb, D. J., Donais, K. & Horwitz, A. F. Differential dynamics of alpha 5 integrin, paxillin, and alpha-actinin during formation and disassembly of adhesions in migrating cells. *The Journal of cell biology* 153, 1427-1440 (2001).

61   Webb, D. J. *et al.* FAK-Src signalling through paxillin, ERK and MLCK regulates adhesion disassembly. *Nature cell biology* 6, 154-161, doi:10.1038/ncb1094 (2004).

62   Wiseman, P. W. *et al.* Spatial mapping of integrin interactions and dynamics during cell migration by image correlation microscopy. *Journal of cell science* 117, 5521-5534, doi:10.1242/jcs.01416 (2004).

63   Bellis, S. L., Miller, J. T. & Turner, C. E. Characterization of tyrosine phosphorylation of paxillin in vitro by focal adhesion kinase. *The Journal of biological chemistry* 270, 17437-17441 (1995).

64   Brown, M. C., Perrotta, J. A. & Turner, C. E. Identification of LIM3 as the principal determinant of paxillin focal adhesion localization and characterization of a novel motif on paxillin directing vinculin and focal adhesion kinase binding. *The Journal of cell biology* 135, 1109-1123 (1996).

65   Schaller, M. D. & Parsons, J. T. pp125FAK-dependent tyrosine phosphorylation of paxillin creates a high-affinity binding site for Crk. *Molecular and cellular biology* 15, 2635-2645 (1995).

66   Richardson, A., Malik, R. K., Hildebrand, J. D. & Parsons, J. T. Inhibition of cell spreading by expression of the C-terminal domain of focal adhesion kinase (FAK) is rescued by coexpression of Src or catalytically inactive FAK: a role for paxillin tyrosine phosphorylation. *Molecular and cellular biology* 17, 6906-6914 (1997).

67   Tsubouchi, A. *et al.* Localized suppression of RhoA activity by Tyr31/118-phosphorylated paxillin in cell adhesion and migration. *The Journal of cell biology* 159, 673-683, doi:10.1083/jcb.200202117 (2002).

1

1

68   Brown, M. C. & Turner, C. E. Paxillin: adapting to change. *Physiological reviews* 84, 1315-1339, doi:10.1152/physrev.00002.2004 (2004).

69   Wang, Y. & Gilmore, T. D. Zyxin and paxillin proteins: focal adhesion plaque LIM domain proteins go nuclear. *Biochimica et biophysica acta* 1593, 115-120 (2003).

70   Sen, A. *et al.* Paxillin mediates extranuclear and intranuclear signaling in prostate cancer proliferation. *The Journal of Clinical Investigation* 122, 2469-2481, doi:10.1172/JCI62044 (2012).

71   Woods, A. J. *et al.* Paxillin associates with poly(A)-binding protein 1 at the dense endoplasmic reticulum and the leading edge of migrating cells. *The Journal of biological chemistry* 277, 6428-6437, doi:10.1074/jbc.M109446200 (2002).

72   Woods, A. J., Kantidakis, T., Sabe, H., Critchley, D. R. & Norman, J. C. Interaction of paxillin with poly(A)-binding protein 1 and its role in focal adhesion turnover and cell migration. *Molecular and cellular biology* 25, 3763-3773, doi:10.1128/mcb.25.9.3763-3773.2005 (2005).

73   Hagel, M. *et al.* The adaptor protein paxillin is essential for normal development in the mouse and is a critical transducer of fibronectin signaling. *Molecular and cellular biology* 22, 901-915 (2002).

74   Choi, C. K. *et al.* Actin and alpha-actinin orchestrate the assembly and maturation of nascent adhesions in a myosin II motor-independent manner. *Nature cell biology* 10, 1039-1050, doi:10.1038/ncb1763 (2008).

75   Drees, B. *et al.* Characterization of the interaction between zyxin and members of the Ena/vasodilator-stimulated phosphoprotein family of proteins. *The Journal of biological chemistry* 275, 22503-22511, doi:10.1074/jbc.M001698200 (2000).

76   Reinhard, M., Jouvenal, K., Tripier, D. & Walter, U. Identification, purification, and characterization of a zyxin-related protein that binds the focal adhesion and microfilament protein VASP (vasodilator-stimulated phosphoprotein). *Proceedings of the National Academy of Sciences of the United States of America* 92, 7956-7960 (1995).

77   Rottner, K., Krause, M., Gimona, M., Small, J. V. & Wehland, J. Zyxin is not colocalized with vasodilator-stimulated phosphoprotein (VASP) at lamellipodial tips and exhibits different dynamics to vinculin, paxillin, and VASP in focal adhesions. *Molecular biology of the cell* 12, 3103-3113 (2001).

78   Furman, C. *et al.* Ena/VASP is required for endothelial barrier function in vivo. *The Journal of cell biology* 179, 761-775, doi:10.1083/jcb.200705002 (2007).

79   Hirata, H., Tatsumi, H. & Sokabe, M. Zyxin emerges as a key player in the mechanotransduction at cell adhesive structures. *Communicative & integrative biology* 1, 192-195 (2008).

80   Smith, M. A. *et al.* A zyxin-mediated mechanism for actin stress fiber maintenance and repair. *Developmental cell* 19, 365-376, doi:10.1016/j.devcel.2010.08.008 (2010).

81   Nix, D. A. & Beckerle, M. C. Nuclear-cytoplasmic shuttling of the focal contact protein, zyxin: a potential mechanism for communication between sites of cell adhesion and the nucleus. *The Journal of cell biology* 138, 1139-1147 (1997).

82   Cattaruzza, M., Lattrich, C. & Hecker, M. Focal adhesion protein zyxin is a mechanosensitive modulator of gene expression in vascular smooth muscle cells. *Hypertension (Dallas, Tex. : 1979)* 43, 726-730, doi:10.1161/01.hyp.0000119189.82659.52 (2004).

83   Lele, T. P. *et al.* Mechanical forces alter zyxin unbinding kinetics within focal adhesions of living cells. *Journal of cellular physiology* 207, 187-194, doi:10.1002/jcp.20550 (2006).

84   Castello, A. *et al.* Insights into RNA biology from an atlas of mammalian mRNA-binding proteins. *Cell* 149, 1393-1406, doi:10.1016/j.cell.2012.04.031 (2012).

85   Hirata, H., Tatsumi, H. & Sokabe, M. Mechanical forces facilitate actin polymerization at focal adhesions in a zyxin-dependent manner. *Journal of cell science* 121, 2795-2804, doi:10.1242/jcs.030320 (2008).

86   Uemura, A., Nguyen, T. N., Steele, A. N. & Yamada, S. The LIM domain of zyxin is sufficient for force-induced accumulation of zyxin during cell migration. *Biophysical journal* 101, 1069-1075, doi:10.1016/j.bpj.2011.08.001 (2011).

87   Drees, B. E., Andrews, K. M. & Beckerle, M. C. Molecular dissection of zyxin function reveals its involvement in cell motility. *The Journal of cell biology* 147, 1549-1560 (1999).

88   Crawford, A. W., Michelsen, J. W. & Beckerle, M. C. An interaction between zyxin and alpha-actinin. *The Journal of cell biology* 116, 1381-1393 (1992).

89   Yoshigi, M., Hoffman, L. M., Jensen, C. C., Yost, H. J. & Beckerle, M. C. Mechanical force mobilizes zyxin from focal adhesions to actin filaments and regulates cytoskeletal reinforcement. *The Journal of cell biology* 171, 209-215, doi:10.1083/jcb.200505018 (2005).

90   Hoffman, L. M. *et al.* Genetic ablation of zyxin causes Mena/VASP mislocalization, increased motility, and deficits in actin remodeling. *The Journal of cell biology* 172, 771-782, doi:10.1083/jcb.200512115 (2006).

91   Golsteyn, R. M., Beckerle, M. C., Koay, T. & Friederich, E. Structural and functional similarities between the human cytoskeletal protein zyxin and the ActA protein of Listeria monocytogenes. *Journal of cell science* 110 (Pt 16), 1893-1906 (1997).

92   Nix, D. A. *et al.* Targeting of zyxin to sites of actin membrane interaction and to the nucleus. *The Journal of biological chemistry* 276, 34759-34767, doi:10.1074/jbc.M102820200 (2001).

93   Fradelizi, J. *et al.* ActA and human zyxin harbour Arp2/3-independent actin-polymerization activity. *Nature cell biology* 3, 699-707, doi:10.1038/35087009 (2001).

94   Bear, J. E. & Gertler, F. B. Ena/VASP: towards resolving a pointed controversy at the barbed end. *Journal of cell science* 122, 1947-1953, doi:10.1242/jcs.038125 (2009).

95   Brühmann, S. *et al.* Distinct VASP tetramers synergize in the processive elongation of individual actin filaments from clustered arrays. *Proceedings of the National Academy of Sciences of the United States of America* 114, E5815-e5824, doi:10.1073/pnas.1703145114 (2017).

96   Damiano-Guercio, J. *et al.* Loss of Ena/VASP interferes with lamellipodium architecture, motility and integrin-dependent adhesion. *eLife* 9, doi:10.7554/eLife.55351 (2020).

97   Hoffman, L. M. *et al.* Targeted disruption of the murine zyxin gene. *Molecular and cellular biology* 23, 70-79 (2003).

98   Bubb, M. R., Spector, I., Beyer, B. B. & Fosen, K. M. Effects of jasplakinolide on the kinetics of actin polymerization. An explanation for certain in vivo observations. *The Journal of biological chemistry* 275, 5163-5170 (2000).

99   Amsellem, V. *et al.* The actin cytoskeleton-associated protein zyxin acts as a tumor suppressor in Ewing tumor cells. *Experimental cell research* 304, 443-456, doi:10.1016/j.yexcr.2004.10.035 (2005).

100   Sanchez-Carbayo, M. *et al.* Molecular profiling of bladder cancer using cDNA microarrays: defining histogenesis and biological phenotypes. *Cancer research* 62, 6973-6980 (2002).

101   Wang, W. *et al.* Analysis of methylation-sensitive transcriptome identifies GADD45a as a frequently methylated gene in breast cancer. *Oncogene* 24, 2705-2714, doi:10.1038/sj.onc.1208464 (2005).

102   Humphries, J. D. *et al.* Vinculin controls focal adhesion formation by direct interactions with talin and actin. *The Journal of cell biology* 179, 1043-1057, doi:10.1083/jcb.200703036 (2007).

103   Bakolitsa, C. *et al.* Structural basis for vinculin activation at sites of cell adhesion. *Nature* 430, 583-586, doi:10.1038/nature02610 (2004).

104   Jones, P. *et al.* Identification of a talin binding site in the cytoskeletal protein vinculin. *The Journal of cell biology* 109, 2917-2927 (1989).

105   Opazo Saez, A. *et al.* Tension development during contractile stimulation of smooth muscle requires recruitment of paxillin and vinculin to the membrane. *American journal of physiology. Cell physiology* 286, C433-447, doi:10.1152/ajpcell.00030.2003 (2004).

106   Thomas, S. M., Hagel, M. & Turner, C. E. Characterization of a focal adhesion protein, Hic-5, that shares extensive homology with paxillin. *Journal of cell science* 112 (Pt 2), 181-190 (1999).

107   Sathe, A. R., Shivashankar, G. V. & Sheetz, M. P. Nuclear transport of paxillin depends on focal adhesion dynamics and FAT domains. *Journal of cell science* 129, 1981-1988, doi:10.1242/jcs.172643

1

1

(2016).

108   Gertler, F. B., Niebuhr, K., Reinhard, M., Wehland, J. & Soriano, P. Mena, a relative of VASP and Drosophila Enabled, is implicated in the control of microfilament dynamics. *Cell* 87, 227-239 (1996).

109   Brindle, N. P., Holt, M. R., Davies, J. E., Price, C. J. & Critchley, D. R. The focal-adhesion vasodilator-stimulated phosphoprotein (VASP) binds to the proline-rich domain in vinculin. *The Biochemical journal* 318 (Pt 3), 753-757 (1996).

110   Reinhard, M., Rudiger, M., Jockusch, B. M. & Walter, U. VASP interaction with vinculin: a recurring theme of interactions with proline-rich motifs. *FEBS letters* 399, 103-107 (1996).

111   McGregor, A., Blanchard, A. D., Rowe, A. J. & Critchley, D. R. Identification of the vinculin-binding site in the cytoskeletal protein alpha-actinin. *The Biochemical journal* 301 (Pt 1), 225-233 (1994).

112   Xu, W., Baribault, H. & Adamson, E. D. Vinculin knockout results in heart and brain defects during embryonic development. *Development (Cambridge, England)* 125, 327-337 (1998).

113   Volberg, T. *et al.* Focal adhesion formation by F9 embryonal carcinoma cells after vinculin gene disruption. *Journal of cell science* 108 (Pt 6), 2253-2260 (1995).

114   Xu, W., Coll, J. L. & Adamson, E. D. Rescue of the mutant phenotype by reexpression of full-length vinculin in null F9 cells; effects on cell locomotion by domain deleted vinculin. *Journal of cell science* 111 (Pt 11), 1535-1544 (1998).

115   Mierke, C. T. *et al.* Vinculin facilitates cell invasion into three-dimensional collagen matrices. *The Journal of biological chemistry* 285, 13121-13130, doi:10.1074/jbc.M109.087171 (2010).

116   Thievessen, I. *et al.* Vinculin-actin interaction couples actin retrograde flow to focal adhesions, but is dispensable for focal adhesion growth. *The Journal of cell biology* 202, 163-177, doi:10.1083/jcb.201303129 (2013).

117   Coltella, N. *et al.* Role of the MET/HGF receptor in proliferation and invasive behavior of osteosarcoma. *FASEB journal : official publication of the Federation of American Societies for Experimental Biology* 17, 1162-1164, doi:10.1096/fj.02-0576fje (2003).

118   Patane, S. *et al.* MET overexpression turns human primary osteoblasts into osteosarcomas. *Cancer research* 66, 4750-4757, doi:10.1158/0008-5472.Can-05-4422 (2006).

119   Patane, S. *et al.* A new Met inhibitory-scaffold identified by a focused forward chemical biological screen. *Biochemical and biophysical research communications* 375, 184-189, doi:10.1016/j.bbrc.2008.07.159 (2008).

120   Pennacchietti, S. *et al.* Hypoxia promotes invasive growth by transcriptional activation of the met protooncogene. *Cancer cell* 3, 347-361 (2003).

121   Bottaro, D. P. *et al.* Identification of the hepatocyte growth factor receptor as the c-met proto-oncogene product. *Science (New York, N.Y.)* 251, 802-804, doi:10.1126/science.1846706 (1991).

122   Stoker, M., Gherardi, E., Perryman, M. & Gray, J. Scatter factor is a fibroblast-derived modulator of epithelial cell mobility. *Nature* 327, 239-242, doi:10.1038/327239a0 (1987).

123   Weidner, K. M., Behrens, J., Vandekerckhove, J. & Birchmeier, W. Scatter factor: molecular characteristics and effect on the invasiveness of epithelial cells. *The Journal of cell biology* 111, 2097-2108, doi:10.1083/jcb.111.5.2097 (1990).

124   Park, M. *et al.* Sequence of MET protooncogene cDNA has features characteristic of the tyrosine kinase family of growth-factor receptors. *Proceedings of the National Academy of Sciences* 84, 6379-6383, doi:10.1073/pnas.84.18.6379 (1987).

125   Birchmeier, C., Birchmeier, W., Gherardi, E. & Vande Woude, G. F. Met, metastasis, motility and more. *Nature Reviews Molecular Cell Biology* 4, 915-925, doi:10.1038/nrm1261 (2003).

126   Imamura, R. & Matsumoto, K. Hepatocyte growth factor in physiology and infectious diseases. *Cytokine* 98, 97-106, doi:10.1016/j.cyto.2016.12.025 (2017).

127   Cecchi, F., Rabe, D. C. & Bottaro, D. P. Targeting the HGF/Met signalling pathway in can-

cer. *Eur J Cancer* 46, 1260-1270, doi:10.1016/j.ejca.2010.02.028 (2010).

128   Scagliotti, G. V., Novello, S. & von Pawel, J. The emerging role of MET/HGF inhibitors in oncology. *Cancer Treat Rev* 39, 793-801, doi:10.1016/j.ctrv.2013.02.001 (2013).

129   Trusolino, L. & Comoglio, P. M. Scatter-factor and semaphorin receptors: cell signalling for invasive growth. *Nature reviews. Cancer* 2, 289-300, doi:10.1038/nrc779 (2002).

130   Whang, Y. M., Jung, S. P., Kim, M. K., Chang, I. H. & Park, S. I. Targeting the Hepatocyte Growth Factor and c-Met Signaling Axis in Bone Metastases. *International journal of molecular sciences* 20, doi:10.3390/ijms20020384 (2019).

131   Cheng, F. & Guo, D. MET in glioma: signaling pathways and targeted therapies. *J Exp Clin Cancer Res* 38, 270, doi:10.1186/s13046-019-1269-x (2019).

132   Zhang, H., Feng, Q., Chen, W. D. & Wang, Y. D. HGF/c-MET: A Promising Therapeutic Target in the Digestive System Cancers. *International journal of molecular sciences* 19, doi:10.3390/ijms19113295 (2018).

133   Boros, P. & Miller, C. M. Hepatocyte growth factor: a multifunctional cytokine. *Lancet* 345, 293-295, doi:10.1016/s0140-6736(95)90279-1 (1995).

134   Zarnegar, R. & Michalopoulos, G. K. The many faces of hepatocyte growth factor: from hepatopoiesis to hematopoiesis. *The Journal of cell biology* 129, 1177-1180, doi:10.1083/jcb.129.5.1177 (1995).

135   Cox, I. J. & Sheppard, C. J. Scanning optical microscope incorporating a digital framestore and microcomputer. *Appl Opt* 22, 1474-1474, doi:10.1364/ao.22.001474 (1983).

136   Brakenhoff, G. J., van der Voort, H. T., van Spronsen, E. A., Linnemans, W. A. & Nanninga, N. Three-dimensional chromatin distribution in neuroblastoma nuclei shown by confocal scanning laser microscopy. *Nature* 317, 748-749, doi:10.1038/317748a0 (1985).

137   Shimomura, O., Johnson, F. H. & Saiga, Y. Extraction, purification and properties of aequorin, a bioluminescent protein from the luminous hydromedusan, Aequorea. *J Cell Comp Physiol* 59, 223-239, doi:10.1002/jcp.1030590302 (1962).

138   Tsien, R. Y. The green fluorescent protein. *Annu Rev Biochem* 67, 509-544, doi:10.1146/annurev.biochem.67.1.509 (1998).

139   Axelrod, D. Cell-substrate contacts illuminated by total internal reflection fluorescence. *The Journal of cell biology* 89, 141-145, doi:10.1083/jcb.89.1.141 (1981).

140   Stout, A. L. & Axelrod, D. Evanescent field excitation of fluorescence by epi-illumination microscopy. *Appl Opt* 28, 5237-5242, doi:10.1364/ao.28.005237 (1989).

141   Gustafsson, M. G. Surpassing the lateral resolution limit by a factor of two using structured illumination microscopy. *J Microsc* 198, 82-87 (2000).

142   Schermelleh, L., Heintzmann, R. & Leonhardt, H. A guide to super-resolution fluorescence microscopy. *The Journal of cell biology* 190, 165-175, doi:10.1083/jcb.201002018 (2010).

143   Walde, M., Monypenny, J., Heintzmann, R., Jones, G. E. & Cox, S. Vinculin binding angle in podosomes revealed by high resolution microscopy. *PloS one* 9, e88251, doi:10.1371/journal.pone.0088251 (2014).

144   de Boer, P., Hoogenboom, J. P. & Giepmans, B. N. Correlated light and electron microscopy: ultrastructure lights up! *Nature methods* 12, 503-513, doi:10.1038/nmeth.3400 (2015).

145   Zonnevylle, A. C. *et al.* Integration of a high-NA light microscope in a scanning electron microscope. *J Microsc* 252, 58-70, doi:10.1111/jmi.12071 (2013).

146   Wouters, C. H. & Koerten, H. K. Combined light microscope and scanning electron microscope, a new instrument for cell biology. *Cell Biol Int Rep* 6, 955-959, doi:10.1016/0309-1651(82)90007-8 (1982).

147   Axelrod, D., Koppel, D. E., Schlessinger, J., Elson, E. & Webb, W. W. Mobility measurement by analysis of fluorescence photobleaching recovery kinetics. *Biophysical journal* 16, 1055-1069, doi:10.1016/s0006-3495(76)85755-4 (1976).

1

1

148   Koppel, D. E., Axelrod, D., Schlessinger, J., Elson, E. L. & Webb, W. W. Dynamics of fluorescence marker concentration as a probe of mobility. *Biophysical journal* 16, 1315-1329, doi:10.1016/s0006-3495(76)85776-1 (1976).

149   Peters, R., Peters, J., Tews, K. H. & Bähr, W. A microfluorimetric study of translational diffusion in erythrocyte membranes. *Biochimica et biophysica acta* 367, 282-294, doi:10.1016/0005-2736(74)90085-6 (1974).

150   Houtsmuller, A. B. *et al.* Action of DNA repair endonuclease ERCC1/XPF in living cells. *Science (New York, N.Y.)* 284, 958-961, doi:10.1126/science.284.5416.958 (1999).

151   Phair, R. D. & Misteli, T. High mobility of proteins in the mammalian cell nucleus. *Nature* 404, 604-609, doi:10.1038/35007077 (2000).

152   McNally, J. G., Müller, W. G., Walker, D., Wolford, R. & Hager, G. L. The glucocorticoid receptor: rapid exchange with regulatory sites in living cells. *Science (New York, N.Y.)* 287, 1262-1265, doi:10.1126/science.287.5456.1262 (2000).

153   Stenoien, D. L. *et al.* FRAP reveals that mobility of oestrogen receptor-alpha is ligand- and proteasome-dependent. *Nature cell biology* 3, 15-23, doi:10.1038/35050515 (2001).

154   Mochizuki, N. *et al.* Spatio-temporal images of growth-factor-induced activation of Ras and Rap1. *Nature* 411, 1065-1068, doi:10.1038/35082594 (2001).

155   Geverts, B., van Royen, M. E. & Houtsmuller, A. B. Analysis of biomolecular dynamics by FRAP and computer simulation. *Methods in molecular biology (Clifton, N.J.)* 1251, 109-133, doi:10.1007/978-1-4939-2080-8_7 (2015).

156   Carrero, G., McDonald, D., Crawford, E., de Vries, G. & Hendzel, M. J. Using FRAP and mathematical modeling to determine the in vivo kinetics of nuclear proteins. *Methods* 29, 14-28, doi:10.1016/s1046-2023(02)00288-8 (2003).

157   Shcherbakova, D. M. & Verkhusha, V. V. Chromophore chemistry of fluorescent proteins controlled by light. *Curr Opin Chem Biol* 20, 60-68, doi:10.1016/j.cbpa.2014.04.010 (2014).

158   Lukyanov, K. A., Chudakov, D. M., Lukyanov, S. & Verkhusha, V. V. Innovation: Photoactivatable fluorescent proteins. *Nature reviews. Molecular cell biology* 6, 885-891, doi:10.1038/nrm1741 (2005).

159   Patterson, G. H. & Lippincott-Schwartz, J. A photoactivatable GFP for selective photolabeling of proteins and cells. *Science (New York, N.Y.)* 297, 1873-1877, doi:10.1126/science.1074952 (2002).

160   Nienhaus, K. & Nienhaus, G. U. Fluorescent proteins for live-cell imaging with super-resolution. *Chem Soc Rev* 43, 1088-1106, doi:10.1039/c3cs60171d (2014).

161   Wang, S., Moffitt, J. R., Dempsey, G. T., Xie, X. S. & Zhuang, X. Characterization and development of photoactivatable fluorescent proteins for single-molecule-based superresolution imaging. *Proceedings of the National Academy of Sciences of the United States of America* 111, 8452-8457, doi:10.1073/pnas.1406593111 (2014).

162   Betzig, E. *et al.* Imaging intracellular fluorescent proteins at nanometer resolution. *Science (New York, N.Y.)* 313, 1642-1645, doi:10.1126/science.1127344 (2006).

163   Rust, M. J., Bates, M. & Zhuang, X. Sub-diffraction-limit imaging by stochastic optical reconstruction microscopy (STORM). *Nature methods* 3, 793-795, doi:10.1038/nmeth929 (2006).

164   Hess, S. T., Girirajan, T. P. & Mason, M. D. Ultra-high resolution imaging by fluorescence photoactivation localization microscopy. *Biophysical journal* 91, 4258-4272, doi:10.1529/biophysj.106.091116 (2006).

165   Verdaasdonk, J. S., Stephens, A. D., Haase, J. & Bloom, K. Bending the rules: widefield microscopy and the Abbe limit of resolution. *Journal of cellular physiology* 229, 132-138, doi:10.1002/jcp.24439 (2014).

166   Schneider, C. A., Rasband, W. S. & Eliceiri, K. W. NIH Image to ImageJ: 25 years of image analysis. *Nature methods* 9, 671-675 (2012).

167   Schindelin, J. *et al.* Fiji: an open-source platform for biological-image analysis. *Nature meth-*

ods 9, 676-682, doi:10.1038/nmeth.2019 (2012).

168   Arena, E. T. *et al.* Quantitating the cell: turning images into numbers with ImageJ. *Wiley Interdiscip Rev Dev Biol* 6, doi:10.1002/wdev.260 (2017).

169   Berman, H. M. *et al.* The Protein Data Bank. *Nucleic acids research* 28, 235-242, doi:10.1093/nar/28.1.235 (2000).

170   Liang, M. *et al.* Structural basis of the target-binding mode of the G protein-coupled receptor kinase-interacting protein in the regulation of focal adhesion dynamics. *The Journal of biological chemistry* 294, 5827-5839, doi:10.1074/jbc.RA118.006915 (2019).

171   Zhu, L. *et al.* Structural Basis of Paxillin Recruitment by Kindlin-2 in Regulating Cell Adhesion. *Structure* 27, 1686-1697.e1685, doi:10.1016/j.str.2019.09.006 (2019).

172   Waterhouse, A. *et al.* SWISS-MODEL: homology modelling of protein structures and complexes. *Nucleic acids research* 46, W296-w303, doi:10.1093/nar/gky427 (2018).

173   Stokes, P. H. *et al.* Mutation in a flexible linker modulates binding affinity for modular complexes. *Proteins* 87, 425-429, doi:10.1002/prot.25675 (2019).

174   Ball, L. J. *et al.* Dual epitope recognition by the VASP EVH1 domain modulates polyproline ligand specificity and binding affinity. *The EMBO journal* 19, 4903-4914, doi:10.1093/emboj/19.18.4903 (2000).

175   Kühnel, K. *et al.* The VASP tetramerization domain is a right-handed coiled coil based on a 15-residue repeat. *Proceedings of the National Academy of Sciences of the United States of America* 101, 17027-17032, doi:10.1073/pnas.0403069101 (2004).

176   Izard, T. *et al.* Vinculin activation by talin through helical bundle conversion. *Nature* 427, 171-175, doi:10.1038/nature02281 (2004).

1

Chapter 2

Dynamics of paxillin, vinculin, zyxin and VASP depend on focal adhesion location and orientation

Karin Legerstee[1], Bart Geverts[1], and Adriaan B. Houtsmuller[1]

1 Erasmus Medical Centre Rotterdam, Department of Pathology, Optical Imaging Centre, Rotterdam, The Netherlands.

Abstract

Focal adhesions (FAs) are multiprotein structures that link the intracellular cytoskeleton to the extracellular matrix. They mediate cell adhesion and migration, crucial to many (patho-) physiological processes. We examined in two cell types from different species the binding dynamics of functionally related FA protein pairs: paxillin and vinculin versus zyxin and VASP. In both cell types, photobleaching experiments showed that ~40% of paxillin and vinculin remained stably associated with an FA for over half an hour, comparable to the average FA lifetime. Zyxin and VASP predominantly displayed more transient interactions. Furthermore, we show protein binding dynamics are influenced by FA location and orientation. In FAs located close to the edge of the adherent membrane paxillin, zyxin and VASP were more dynamic and had larger bound fractions. Zyxin and VASP were also more dynamic and had larger bound fractions at FAs perpendicular compared to parallel to this edge. The increased dynamic binding of the key structural factor paxillin may increase the dynamics of the FA complex as a whole, while the directly actin-binding zyxin and VASP potentially enhance the coupling of actin to these FAs.

2

Introduction

Focal adhesions (FAs) are the main cellular structures linking the intracellular cytoskeleton to the extracellular matrix (ECM). They are typically several square micrometres in size[1,2]. On the membrane-facing side integrins, transmembrane receptors directly binding to the extracellular matrix (ECM), are the main FA components. A specialised form of actin linked to contractile myosin-II forms the edge of the FA on the cytoplasm-facing side, which we will refer to as F-actin. In between integrins and actin a large and diverse intracellular macromolecular protein assembly is present, with over 200 different reported proteins[3,4]. These include (trans)membrane receptors, other than integrins, adaptor proteins and many different signalling proteins such as kinases, phosphatases and G-protein regulators, which through post-translational modifications add significantly to FA complexity. FAs experience force, the strength of which depends on the combination of myosin-II contractility and the stiffness of the ECM. Because of their importance to the transmission of force from the cell to the ECM and in cell adhesion, FAs are crucial to cell migration. Migration and adhesion are key cellular functions required for many physiological and pathophysiological processes, like embryological development, the functioning of the immune system and also cancer, in particular metastasis[4-6].

Here we investigated FA location and FA orientation dependent dynamics of four FA proteins, the large scaffold proteins paxillin and vinculin, and two FA proteins that are closely linked to the actin associated with FAs, zyxin and vasodilator-stimulated phosphoprotein (VASP). As adaptor proteins paxillin and vinculin are among the proteins with the most potential binding partners within FAs[3]. In keeping with their having a linking, structural, role they are amongst the first proteins to be recruited to assembling focal adhesion complexes, especially the directly integrin-binding paxillin[7-11]. Vinculin has a head and a tail domain with a flexible linker in between, allowing vinculin to adopt open and closed conformations[12]. Its head domain shares many important binding partners and functions with paxillin, indeed paxillin itself is one of its binding partners[13-16]. However, while Paxillin has no direct interaction with actin, vinculin's tail domain can directly bind actin filaments as well as the actin-binding proteins α-actinin and the ENA/VASP-proteins[16-20]. Zyxin and VASP are recruited to assembling FAs at much later stages than paxillin or vinculin and are more closely linked to actin[10]. Apart from at FAs zyxin and VASP also cluster at actin-polymerisation complexes, which are periodically distributed along F-actin fibres[21-23]. To stimulate actin polymerisation along FAs zyxin, VASP and vinculin depend on each other for proper functioning[24-29]. Zyxin and VASP, without vinculin, also work

together in several other cellular processes such as efficient cell spreading and VASP depends on zyxin for its force-dependent recruitment to FAs[25,30-32].

In photobleaching experiments ~40% of paxillin and vinculin remained stably associated with an FA for over half an hour. Zyxin and VASP predominantly displayed more transient interactions. We also reveal that the binding dynamics of VASP, zyxin, vinculin and paxillin differ with FA location and FA orientation relative to the closest edge of the ventral, or adherent, portion of the plasma membrane. Several factors form gradients based on their distance from the ventral membrane edge, such as actin fibre thickness and connectivity, the concentration of (signalling) molecules and enzyme activity[33-40], effectively creating different local environments for FAs varying with their distance from the ventral membrane edge. Lastly, by using Monte Carlo based simulations we were able to provide a detailed quantification of the binding dynamics of these four proteins, as well as of the differences seen in FAs with different orientations or cellular locations[41].

Results

Focal adhesion proteins have stably associated fractions at similar ratios across cell types

First, through FRAP-experiments we examined the binding dynamics of fluorescently-labelled paxillin, vinculin, VASP and zyxin at FAs in two different cell-types from two different species; U2OS cells, a human bone cancer cell line, and MDCK dog kidney cells (Fig. 1). Paxillin and vinculin both take about six minutes to reach final recovery levels at ~60% of prebleach fluorescence intensity, whereas both zyxin and VASP recover within two to three minutes to approximately 80 and 90% of prebleach fluorescence intensity. The same pattern of final recovery levels, highest for VASP, intermediate for zyxin and lowest and strikingly similar for vinculin and paxillin, was seen in both U2OS and MDCK cells. To facilitate comparison of recovery rates, irrespective of bleach depth or final recovery levels, recovery curves were expressed relative to intensity immediately after bleaching (0) and final recovery levels (1) (Fig. 1c,d). This highlights the much faster recovery rates of VASP and zyxin versus the highly similar slow recovery rates of paxillin and vinculin. Prolonged FRAP experiments verified paxillin recovery levels remained stable up to 15 minutes post-bleach (Supplementary Fig. S1). To rule out that the incomplete recoveries were due to bleaching of a significant portion of the cytoplasmic protein pool by the intense bleach pulse, we performed experiments where FAs were bleached a second time (Supplementary Fig. S2). If the bleach pulses bleached a significant portion of the protein pool, fluorescence recovery levels after the second bleach pulse would be decreased as a fraction of
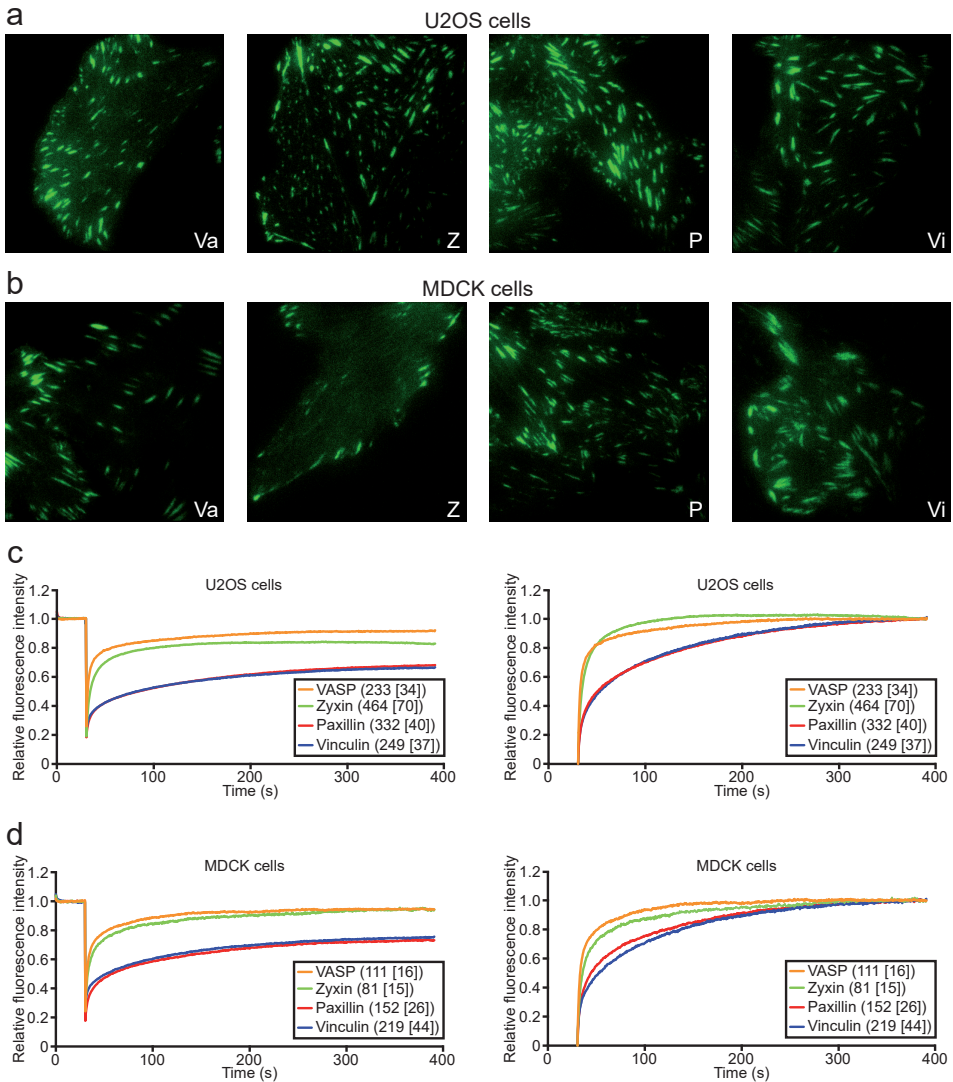
Figure 1. Focal adhesion proteins have stably bound fractions at similar ratios across cell types.
(a) TIRF images of the four studied proteins expressed in U2OS cells: VASP (Va), zyxin (Z), paxillin (P) and vinculin (Vi). **(b)** TIRF images of the four studied proteins expressed in MDCK cells. **(c)** FRAP-curves for U2OS cells stably expressing GFP-tagged FA proteins. In the left plot fluorescence intensity is expressed relative to prebleach levels, in the right plot relative to immediately postbleach (0) and final recovery levels (1) to facilitate comparison of the recovery rates irrespective of final recovery levels or bleach depths. The numbers between brackets indicate the number of bleached FAs from [number of cells]. **(d)** FRAP-curves for MDCK cells stably expressing GFP-tagged FA proteins.

the bleached proteins would exchange with other bleached proteins. However, after the second bleach pulse fluorescence recovery came to the exact same levels as after the first, demonstrating there is no significant bleaching of the fluorescent protein pool despite the fact that this control experiment contained a second
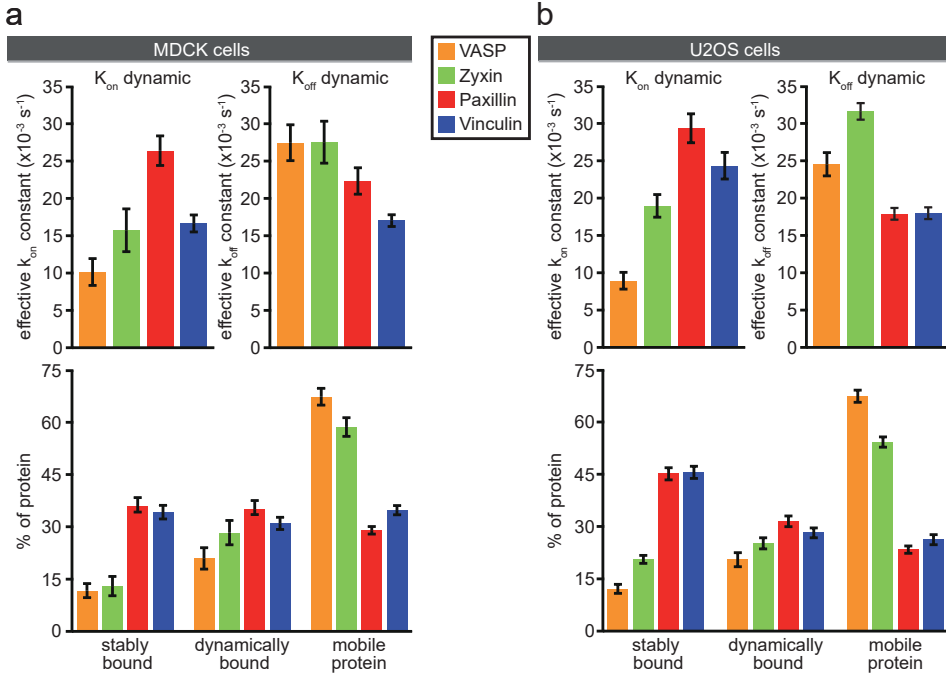
Figure 2. Quantification of the FRAP data.
(a) Parameters of FA protein dynamics in MDCK cells as determined by fitting the experimental curves shown in Fig. 1 to curves generated by Monte-Carlo based computer simulations. Bar charts of the effective on- and off-rate constants of the dynamically bound fractions (top panels) and the relative sizes of the stably bound, dynamically bound and mobile fractions (bottom panels). Error bars indicate 2xSEM. VASP n = 111 [16] , zyxin n = 81 [15], paxillin n = 152 [26], vinculin n = 219 [44] bleached FAs from [cells]. **(b)** Parameters of FA protein dynamics in U2OS cells. VASP n = 233 [34], zyxin n = 464 [70], paxillin n = 332 [40], vinculin n = 249 [37] bleached FAs from [cells].

bleach pulse. Instead, the incomplete recovery levels are due to a fraction of the protein pool being stably associated with FAs.

We quantified our data by fitting the experimentally-derived FRAP curves to curves generated by Monte Carlo based simulations[41] (Fig. 2). Briefly, the simulation goes through small time steps. In each step the simulated proteins, which are confined to a volume with the dimensions of a typical cell, have chances to step into a random direction, if they are freely diffusing. In addition, they have a chance to get immobilised (effective k_{on}) when close to predefined locations (FAs). Simulated proteins bound to an FA have chances to release (effective k_{off}). Similarly, proteins inside the laser beam during bleaching have a chance to get bleached. The simulation was systematically run with different k_{on}'s and k_{off}'s, leading to the medium and long bound fraction sizes, and their specific residence times. In this way a large database of computer generated FRAP-curves was created from which the one best fitting to the experimental data was selected. The k_{on}'s and

k_{off}'s used for the best fitting simulation were used to calculate residence times and fraction sizes[41] (for details see Materials and Methods). The stably bound fractions obtained in this way for U2OS and [MDCK] cells are (average ± 2x SEM = Standard Error of the Mean): 12.1 ± 1.30, [11.7 ± 2.02]% for VASP, 20.6 ± 1.14, [13.0 ± 2.80]% for zyxin, and as discussed above large and of strikingly similar size for paxillin and vinculin, at 45.1 ± 1.74, [36.0 ± 2.44]% for paxillin and 45.6 ± 1.74, [34.2 ± 1.97]% for vinculin. The simulations also provide accurate estimates of the more dynamically bound fractions: 20.5 ± 2.05, [20.9 ± 3.07]% for VASP, 25.2 ± 1.61%, [28.3 ± 3.51%] for zyxin 31.5 ± 1.54, [35.0 ± 2.51]% for paxillin and 28.2 ± 1.40, [31.0 ± 1.73]% for vinculin. The remainder of the protein pool was associated with FAs so briefly that its residence time was consistent with what would be expected for free diffusion. Hence, we will refer to this fraction as the mobile pool although its proteins may be very briefly immobilised at the FA complex. Additionally, fitting of the data allowed us to determine the average on- and off-rate constants for the dynamically and stably bound fractions, for the dynamic fractions these are plotted. For the stably bound fractions these did not differ significantly between the four proteins (data not shown). The average residence times of the stably bound fractions were over half an hour, which is comparable to previously reported FA lifetimes ranging from approximately 20 to 90 minutes[42-44]. We also examined the lifetime of 100 FAs from 5 cells in time lapse movies, which we found to be 55 ± 6 (2xSEM) minutes. This indicates that a substantial part of the investigated proteins in the stably bound fractions remain associated for the entire lifetime of an FA.

The effect of focal adhesion position and orientation on protein binding dynamics

Categorisation of focal adhesions based on their position and orientation

Several factors form gradients based on their distance from the edge of the ventral membrane, such as actin fibre thickness and connectivity, the concentration of (signalling) molecules and enzyme activity[33-40]. Such gradients effectively create different local environments for FAs varying with their distance from the ventral membrane edge. To investigate whether such variation in local environments influences FA protein dynamics, we further subdivided the FRAP data shown in Fig. 1.

First, all FAs were grouped on the basis of their distance from the closest ventral membrane edge. 'Outer' FAs are located close to this edge, 'inner' FAs are positioned further inwards with outer FAs located between them and the closest adherent membrane edge (Fig. 3a,b).
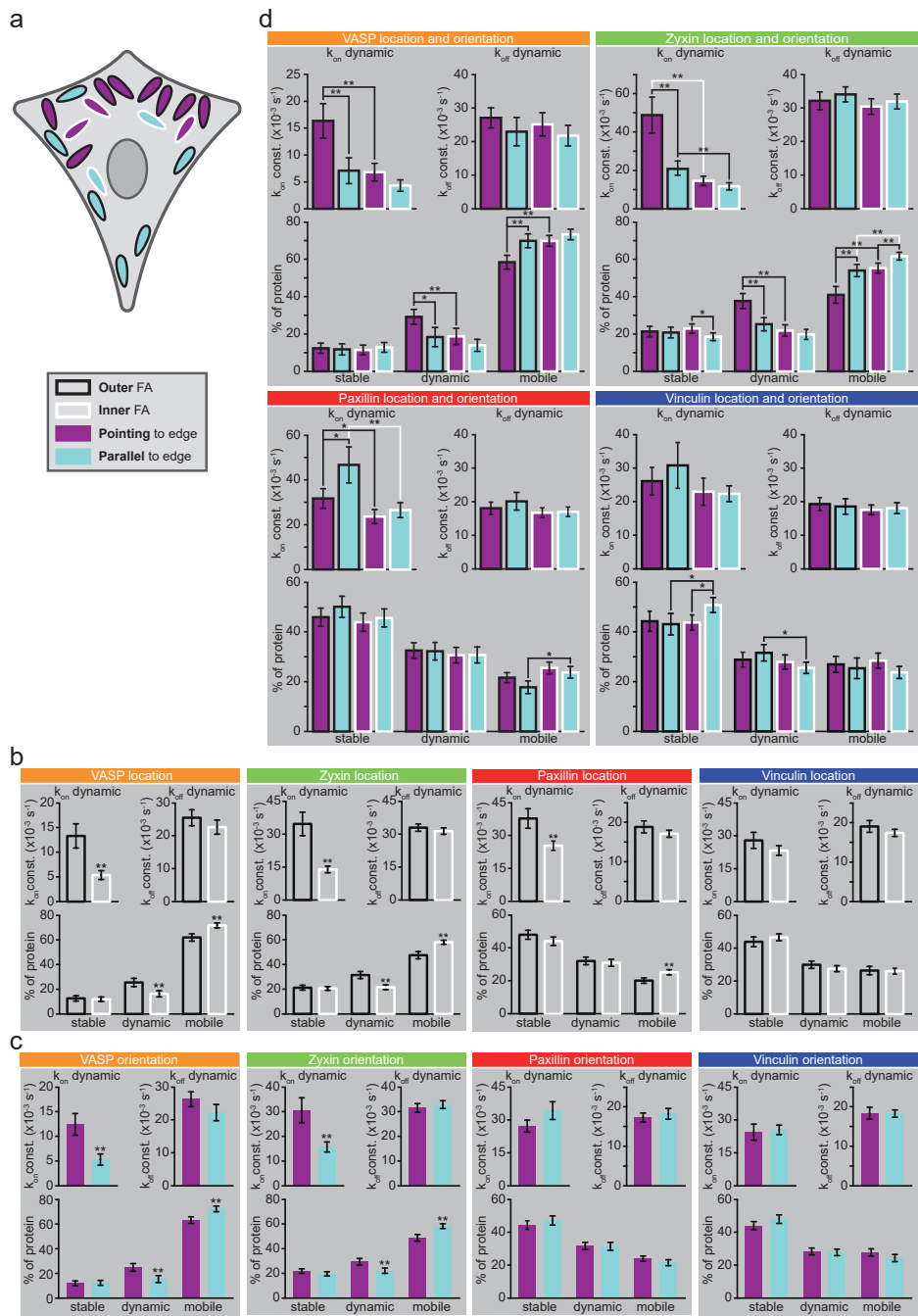
2

Figure 3. FA distance from and/or orientation relative to the closest edge of the ventral membrane influence its dynamics.
(a) Cartoon illustrating classification of FAs based on distance from or orientation relative to the closest edge of the ventral (adherent) portion of the plasma membrane. 'Outer' FAs (black outline) are

close to the edge of the ventral membrane, 'inner' FAs (white outline) are located away from the edge with outer FAs located in between. In 'pointing' FAs (purple) the longest axis is oriented more or less perpendicular to the closest membrane edge, and in 'parallel' FAs (blue) the longest axis is more or less parallel to the edge. **(b)** Quantification of U2OS cell FRAP data based on FA distance from the closest edge of the ventral membrane. VASP [34]: outer n = 100, inner n = 114, Zyxin [70]: outer n = 185, inner n = 260, Paxillin [40]: outer n = 120, inner n=200, Vinculin [37]: outer n = 91 inner n = 158 FAs from [cells]. Error bars indicate 2xSEM. Asterisks indicate significant p-values generated by two sided Mann Whitney test: * p < 0.01, ** p < 0.001 **(c)** Quantification of U2OS cell FRAP data based on FA orientation relative to the closest edge of the ventral membrane. VASP [34]: pointing n = 109, parallel n = 93, Zyxin [70]: pointing n = 199, parallel n = 209, Paxillin [40]: pointing n = 136, parallel n = 134, Vinculin [37]: pointing n = 119, parallel n = 95 FAs from [cells]. Error bars and asterisks as above. **(d)** Parameters obtained by fitting the FRAP data after categorising the FAs based on the combination of their distance from and their orientation relative to the closest edge of the ventral membrane. This is especially revealing for VASP and zyxin, as it shows that it are specifically the outer and pointing FAs that have strongly altered VASP and zyxin dynamics compared to all other FA types. N-numbers per protein for consecutively: outer and pointing, outer and parallel, inner and pointing and inner and parallel FAs: VASP: 64, 34, 45, 58, Zyxin: 90, 90, 104, 118, Paxillin: 65, 51, 67, 82, Vinculin: 56, 35, 63, 60. Error bars and asterisks as above.

In addition, we noticed that FAs are mostly orientated with their long axis either roughly perpendicular or roughly parallel to the closest adherent membrane edge. FAs were classified as 'pointing' when the angle between their long axis and the closest ventral membrane edge was 90° ± 30°. FAs were classified as 'parallel' when the angle between their long axis and the closest ventral membrane edge was 180° ± 30° (Fig. 3a,c). Of the 1278 bleached FAs (see Materials and methods for a specification per examined protein) 184 fell outside these criteria, which is 14%, whereas one third (60° / 180°) would be expected if FA orientation would be random.

Finally, the adhesions were grouped based on the combination of these two criteria which results in four groups: A outer and pointing, B outer and parallel, C inner and pointing and D inner and parallel FAs (Fig. 3a,d).

Differences in FA protein dynamics based on FA location

Zyxin and VASP exchange dynamics followed the same trend when comparing outer to inner FAs (Fig. 3b). At outer FAs the on-rate constant of the dynamically associated fraction was more than twice as large, leading to a significantly increased dynamically bound fraction and a significantly decreased mobile pool.

Similarly, for paxillin the on-rate constant of the dynamically associated fraction was significantly increased at the outer FAs while the mobile pool was significantly decreased. Unlike for zyxin/VASP this last was not caused by a significant increase of the dynamically associated fraction specifically, but rather by the sum of individually insignificant increases of the dynamically and the stably associated fractions.

Differences in FA protein dynamics based on FA orientation

Zyxin and VASP also showed similar trends in their dynamic behaviour when comparing parallel to pointing FAs (Fig. 3c). At pointing FAs the on-rate constant of the dynamically associated fraction is more than twice as large, resulting in a significantly increased dynamically bound fraction and a significantly decreased mobile pool.

For paxillin and vinculin none of the measured parameters were significantly altered in pointing FAs compared to parallel FAs.

Differences in FA protein dynamics based on both FA location and orientation

Having found that FA location and orientation separately correlate to the dynamics of FA associated proteins, we next examined the four possible combinations of FA location and orientation.

Again, the dynamics of zyxin and VASP followed a similar trend, with their dynamics at the outer and pointing FAs clearly standing out from their dynamics at any other FA type (Fig. 3d). Specifically, compared to either outer and parallel or to inner and pointing FAs the size and the on-rate constants of the dynamically associated fraction was significantly increased and the mobile pool was significantly decreased. For zyxin additional significant differences in dynamic behaviour were observed when comparing the remaining FA types, however these were all of a much smaller magnitude than those seen when comparing zyxin/VASP dynamics at outer and pointing FAs to zyxin/VASP dynamics at any other FA type.

For paxillin significant differences were also observed when comparing the four different FA types, but unlike for zyxin/VASP no single FA type clearly stands out from the rest. At the outer and pointing FAs the on-rate constant of the dynamically associated fraction is decreased compared to at the outer and parallel FAs, but increased compared to at the inner and pointing FAs. At the outer and parallel FAs the on-rate of the dynamically associated fraction is increased and the mobile pool decreased compared to at the inner and parallel FAs.

Similar to the lack of correlation between vinculin dynamic behaviour and FA location or orientation separately, the combination of FA location and orientation also had little effect, but there were some significant differences. At the inner and parallel FAs the stably bound fraction was increased compared to at either the outer and parallel or the inner and pointing FAs while the dynamically associated fraction was significantly decreased compared to at the outer and parallel FAs.

Discussion

Here we studied the dynamics of two pairs of functionally related focal adhesion proteins, paxillin/vinculin and zyxin/VASP, in two different, slow moving, non-fibroblast cell types on a collagen coating. The quantitative data were highly consistent between the cell types from different species, suggesting these findings are not cell-type specific and are relevant for FA function.

A large number of previous studies have examined the dynamics of paxillin, vinculin, zyxin or VASP in fibroblasts[11,45-59], but never together in the same study. Moreover, each study used different culturing and quantitative analysis methods, leading to considerable differences in reported quantitative parameters. For instance, for paxillin, half times to full recovery were between 1.5 and 41 seconds, the times until final recovery between 30 and 200 seconds, and mobile fractions between 60% and nearly 100%. The period fibroblasts were cultured on fibronectin prior to imaging ranged from 15 minutes to 48 hours which influences spreading level, a factor known to influence the maturation of FAs, which has been shown to inhibit vinculin dynamics[50]. Moreover, different culturing conditions may also affect FA composition, protein phosphorylation status and conformational states and these may influence protein dynamics[11,45,48-50,52,54,58]. The net result of this is a large variation in the reported quantitative parameters for these FA proteins, hampering comparison with the parameters presented here, as well as the parameters for the different proteins examined in different studies. However, it may still be noted that the speed of paxillin and vinculin recovery we observed was considerably slower than in previous studies, and we found larger stably associated fractions for these proteins. Both parameters were consistent between our two different cell types, which were from different species, suggesting they are not cell-type specific and are relevant for FA function. Yet neither of the two cell types used in this study show as much or as fast unstimulated migration as fibroblasts. Thus, the slow recovery and large immobile fractions we observed might be typical of cells displaying less or slower unstimulated migration.

We demonstrated that for each of the studied proteins three different dynamic pools are present in FAs: (1) a pool with stable associations (>30 minutes), (2) a dynamically exchanging pool with shorter interactions (~1 minute) and (3) a very dynamic pool with interactions so brief that they could not be distinguished from free diffusion (referred to as the mobile pool). In both cell types the stable fraction is small for VASP, somewhat larger for zyxin and largest and surprisingly similar for paxillin and vinculin (Fig. 4a). Consistently, previous studies measuring the recovery of both paxillin and vinculin also reported highly similar immobile fractions[51-54], but very different amongst studies. Since FAs show a sliding type of
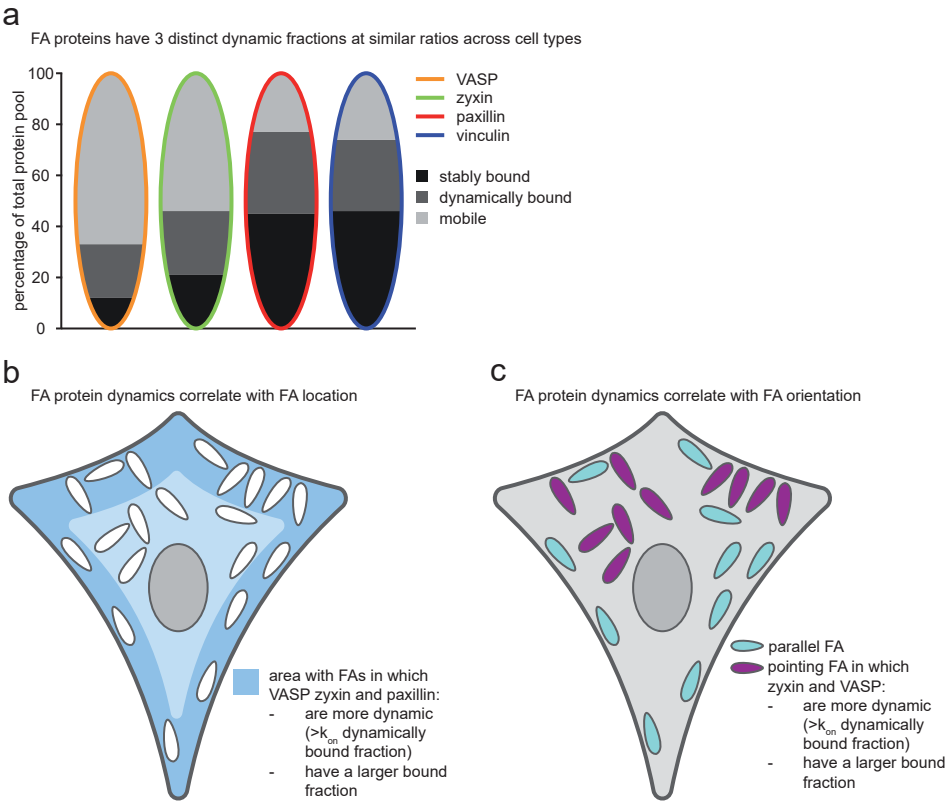
a

FA proteins have 3 distinct dynamic fractions at similar ratios across cell types

Legend:
- VASP
- zyxin
- paxillin
- vinculin

- stably bound
- dynamically bound
- mobile

y-axis: percentage of total protein pool

b

FA protein dynamics correlate with FA location

area with FAs in which VASP zyxin and paxillin:
- are more dynamic ($>k_{on}$ dynamically bound fraction)
- have a larger bound fraction

c

FA protein dynamics correlate with FA orientation

- parallel FA
- pointing FA in which zyxin and VASP:
  - are more dynamic ($>k_{on}$ dynamically bound fraction)
  - have a larger bound fraction

Figure 4. Schematic overview of the data.
(a) Model showing the ratio between the 3 dynamic fractions, stably bound, dynamically bound and mobile protein for each of the studied proteins as revealed by fitting of the experimental FRAP curves to curves generated by computer-based simulations **(b)** Schematic overview of how FA protein dynamics correlate with FA location, VASP, zyxin and paxillin are more dynamic (have a higher on-rate constant for the dynamically bound fraction) and a larger bound fraction at FAs located close to the ventral membrane edge. **(c)** Schematic overview of how FA protein dynamics correlate with FA orientation, VASP and zyxin are more dynamic (have a higher on-rate constant for the dynamically bound fraction) and a larger bound fraction at FAs orientated with their long axis more or less perpendicular to the ventral membrane edge.

movement, both in migrating and in stationary cells, they are typically regarded as highly dynamic complexes[60,61]. However, the average residence time of all stably associated fractions was relatively long compared to previously reported FA lifetimes and the average FA lifetime of 55 ± 6 minutes observed here[42-44], indicating the proteins in these fractions remain associated for a large part of the lifetime of an FA and revealing some properties of FAs are less dynamic than previously thought.

Furthermore, we show that protein binding dynamics differ with FA orientation and location relative to the closest edge of the ventral membrane (Fig. 4b,c). This

was especially true for zyxin and VASP, for which the on-rate constant of the dynamically associated fraction was more than twice as high at outer vs inner FAs and the same was true for pointing vs parallel FAs. Further investigation revealed dynamic on-rate constants were specifically increased at FAs that are outer as well as pointing. Increased on-rate constants can be the result of either increased numbers of available binding sites or of increased affinity for these sites. Because the off-rate constants of the dynamic fractions were not significantly altered, the increased on-rate constants lead to significantly increased sizes of the dynamically bound zyxin/VASP fractions at these FAs. A likely function of which is to facilitate the coupling of actin by increasing the number of available actin binding sites, as both proteins directly bind actin. Strong links between actin and FAs that lie close and perpendicular to the edge of the ventral membrane (i.e. are outer and pointing) are presumably needed to generate the force required to protrude or retract the ventral membrane. The effects of FA location and orientation on paxillin and vinculin dynamics are more subtle, for vinculin only the combination significantly correlated with its dynamics. For paxillin at outer FAs the on-rate constant of the dynamically associated fraction was significantly increased and the mobile pool significantly decreased, meaning an increased total (stable and dynamic) bound fraction. In spite of the increased on-rate constant, the dynamic fraction was not increased. This is due to the large decrease of the mobile pool, decreasing the number of paxillin molecules available for binding. With respect to biological function the increased total bound fraction of paxillin at outer FAs may be needed to deal with the increased force created by increased bound fractions of zyxin/VASP. Furthermore, an increase in the on-rate constant of the dynamically bound fraction of a structural component like paxillin, may stimulate the dynamics of the entire FA. This is supported by the increased on-rate constants of the dynamically bound VASP/zyxin fractions at outer FAs. It could be advantageous for FAs at the edge of the ventral membrane to be more dynamic when a cell is exploring its immediate environment by protruding its membrane at different areas, but is not yet committed to moving in a particular direction.

Overall it is remarkable how similar the dynamics of vinculin/paxillin are, and different from the also similar dynamics of zyxin/VASP, this last particularly with respect to the impact of FA orientation and location. The vinculin head domain and paxillin as well as zyxin/VASP share many functions and binding partners, including each other, potentially contributing to the similar binding dynamics. For the vinculin head domain and paxillin the most notable shared binding partner is talin, while zyxin/VASP both bind actin and work together in several cellular processes such as efficient cell spreading[13-16,25,30-32]. However,

vinculin's tail domain shares many functions and binding partners with zyxin/VASP, including zyxin/VASP themselves which depend on vinculin for many of the actin regulating processes they are involved in[16-20,24-29]. The remarkably similar vinculin/paxillin dynamics suggest that vinculin's head domain influences its dynamics more strongly than its tail domain. This is perhaps because vinculin, like paxillin, enters a newly forming FA complex when many of the proteins interacting with its head domain are already associated, while most of the interaction partners for its tail domain are not yet present. When at later stages the latter enter the FA complex, a large proportion of the vinculin molecules will already be extensively involved in interactions through their head domains. Later additional interactions through their tail domains will have little influence on their binding dynamics. Interestingly, in other studies looking at different aspects of protein behaviour at FAs, a split between paxillin/vinculin versus zyxin/VASP was also observed. For instance, zyxin/VASP dissociate from disassembling FAs earlier than paxillin/vinculin, including in response to actomyosin-II inhibition[21,54]. When stress fibres thicken, in response to mechanical stress or to the actin stabilizer jasplakinolide, VASP/zyxin rapidly translocate from FAs to the thickening stress fibres while vinculin/paxillin remain associated[28,62]. Zyxin is completely lost from FAs in response to actin polymerisation inhibition, while vinculin levels remain unchanged[48]. Overexpression of the zyxin LIM-domain causes the loss of endogenous zyxin and VASP from FAs while vinculin levels remain unchanged[27,63]. Thus, at FAs a distinction between paxillin/vinculin and VASP/zyxin behaviour seems to be a previously unrecognised recurring theme.

In summary, we examined the dynamics of two pairs of functionally related FA proteins, paxillin/vinculin and zyxin/VASP. For each protein we demonstrated the presence of a stably associating, a dynamically exchanging and a mobile pool within FAs. Moreover, we show there is a distinction between the dynamics of paxillin/vinculin and VASP/zyxin. A literature search revealed this distinction is a previously unrecognized but recurring theme in their behaviour at FAs. Furthermore, we show that protein binding dynamics differ with FA orientation and location. This is especially true for zyxin and VASP and most especially at FAs that are located close to the nearest ventral membrane edge and orientated with their long axis perpendicular to it. At these FAs there are significantly more zyxin and VASP proteins binding in a significantly more dynamic manner, potentially to facilitate the coupling of actin to these FAs since both proteins are directly actin-binding. The effects of FA location and orientation on paxillin and vinculin dynamics are more subtle, but it is noteworthy that at FAs close to the membrane edge paxillin binding is significantly more dynamic, presumably stimulating the dynamics of these FAs since paxillin is a key structural component. Overall, the

presented data add to unraveling and understanding the mechanisms by which FAs function in adhesion and cell migration.

Materials and Methods

Cell culture

MDCK cells were cultured in DMEM (Lonza) and U2OS cells in phenol-red free DMEM (Lonza) at 37 °C and 5% CO_2. Culture media were supplemented with 10% FCS (Gibco), 2mM L-glutamine (Lonza), 100 U/ml Penicillin and 100 μg/ml Streptomycine (Lonza) and to maintain stable cell lines with 100 μg/ml G418. Transfections were performed using Fugene (Promega), followed by selection with G418 when creating stable cell lines. For experiments 24 mm round glass coverslips were coated overnight at 4 °C with PureCol bovine collagen type I (Advanced Biomatrix) at a final concentration of 10 μg/ml. Cells were plated onto coated coverslips 24-48 h prior to imaging.

Constructs

The zyxin-GFP plasmid was created by replacing the mMaple3 in Zyxin-mMaple3 (Addgene101151) with eGFP from eGFP N1 (Clontech) as a BamHI NotI fragment.

The VASP-GFP, vinculin-GFP and paxillin-GFP plasmids were based on the VASP-mTurquoise (Addgene 55585), Vinculin-mTurquoise (Addgene 55587) and paxillin-mTurquoise (Addgene 55573) vectors, respectively. These use the multiple cloning site as a linker region between the protein and mTurquoise, hampering a simple colour swap. To still allow sticky-end ligation the protein, fluorescent label and empty vector backbone were all separately isolated as restriction fragments. These were ligated using sticky ends in 2 steps: (1) the protein to the fluorescent label (2) the created insert into the vector backbone. This strategy was applied to create the following constructs:

VASP-GFP: The vector backbone was isolated from paxillin-mTurquoise as an AgeI NotI fragment, VASP from VASP-mTurquoise as an AgeI BamHI fragment and GFP from eGFP N1 as a BamH1 Not1 fragment.

Vinculin-GFP: The vector backbone was isolated from paxillin-mTurquoise as a NheI NotI fragment, vinculin from vinculin-mTurquoise as a NheI EcoRI fragment and GFP from eGFP as an EcoRI NotI fragment.

Paxillin-GFP: The vector backbone was isolated from paxillin-mTurquoise as a BamHI NotI fragment, paxillin from paxillin-mTurquoise as a BamHI HindIII fragment and GFP from eGFP as a HindIII NotI fragment.

All constructs were checked through sequencing, one silent mutation was found (paxillin-GFP bp1461 C to G).

Time lapse TIRF imaging

Time lapse movies were made for 18 hours at 10 minute intervals on a Nikon Ti-Eclipse inverted microscope equipped with a TIRF unit and a 16 bit EM CCD camera (Photometrics) in TIRF mode using a 60x 1.45NA oil immersion objective (Apochromat TIRF). Cells were maintained at 37 °C and 5% CO_2 using a stage-top incubator (Tokai Hit). These were used to determine the lifetimes of a 100 FAs from 5 different cells.

FRAP experiments

Live-cell imaging

All FRAP data was acquired on a Nikon Ti-Eclipse inverted microscope equipped with a TIRF unit, a 3D FRAP scanning unit (Roper) and a 16 bit EM CCD camera (Photometrics) in TIRF mode and using a 60x 1.45NA oil immersion objective (Apochromat TIRF). Cells were maintained at 37 °C and 5% CO_2 using a stage-top incubator (Tokai Hit). Images were taken for 30 s prebleach and 6 minutes postbleach at 500 ms intervals. The FRAP unit allowed the efficient bleaching of 2 by 2 μm squares ~ 15-25 FAs spread over the field of view, which contained (portions of) several different cells, well within 300 ms. For U2OS cells the number of bleached FAs from [number of cells] were for VASP 233 [34], zyxin 464 [70], paxillin 332 [40], vinculin 249 [37] and for MDCK cells for VASP 111 [16], zyxin 81 [15], paxillin 152 [26] and vinculin 219 [44].

Data analyses

In ImageJ software[64] extended in the FIJI framework[65] ROIs were manually drawn around efficiently bleached (portions) of FAs, as well as a few unbleached FAs for control purposes and empty areas for background measurement. To control for monitor bleaching and/or bleaching of too high a proportion of the entire protein pool any experiments where the average intensity of the unbleached FAs fell below 90% of original levels were discarded. Separate experiments on MDCK cells expressing Paxillin-GFP, where the same FA was bleached a second time 4 minutes after the original bleach pulse and followed a further 4 minutes ruled out that a significant fraction of the fluorescent protein pool was bleached using our experimental setup (Supplemental Fig. S2). Data from any FAs not bleached to <20% of their average prebleach levels was excluded from analysis, as were any FAs that were not in a stable state. The resulting fluorescence intensity data was background-corrected and normalised to prebleach levels using the follow-

ing formula:

$$I_{norm} = \frac{I_t - I_{BGt}}{I_{pre} - I_{BGpre}}$$

Where I_{norm} is the normalised FA intensity, I_t is the raw intensity of the FA at time point t and I_{pre} is the average raw intensity of the FA during the entire prebleach period, I_{BGt} and I_{BGpre} are the corresponding intensities of the average background signal for the experiment.

To facilitate comparison of the recovery rates for the different proteins irrespective of their final recovery levels the data was also normalised in such a way as to set the first value after bleaching to zero and the final recovery level to 1 using the following formula:

$$I_{norm} = \frac{\left(I_t - I_{BGt}\right) - \left(I_0 - I_{BG0}\right)}{\left(I_{post} - I_{BGpost}\right) - \left(I_0 - I_{BG0}\right)}$$

Where I_{norm} is the normalised FA intensity, I_t is the raw intensity of the FA at time point t, I_0 at the first time point after bleaching and I_{post} the average raw intensity of the FA during the last 25 time points of the experiment, I_{BGt}, I_{BG0} and I_{BGpost} are the corresponding average background signals for the experiment.

Fitting of the experimentally derived FRAP curves using Monte-Carlo based simulations

For analysis of FRAP data, FRAP curves were normalized to prebleach values. A database of Monte Carlo based computer simulated FRAP curves was generated in which four parameters representing mobility properties were varied: long and medium immobile fractions (random values between 0% and 70%) and time spent in immobile state, ranging from medium residence times (random values between 20 and 100 s) to long residence times (random values between 600 and 3200 s). Database sizes of 5122/2027 simulated FRAP curves were used for the analysis of the FRAP data from the U2OS or MDCK cells respectively. The simulated curves are based on a model of diffusion in an ellipsoid volume representing the cell with ellipsoid volumes representing FAs and simple binding kinetics representing binding to the FA complex. Simulations were performed at unit time steps of 100 ms. Results of the simulation were evaluated every 500 ms corresponding to the experimental sample rate. The diffusion coefficient of 1 μm^2/s was based on separate experiments measuring free diffusion of paxillin-GFP in the cytoplasm. Diffusion was simulated by deriving novel positions ($x_{t+\Delta t}$, $y_{t+\Delta t}$, $z_{t+\Delta t}$) at each time step $t+\Delta t$ for all mobile molecules from their current positions (x_t, y_t, z_t) by $x_{t+\Delta t} = x_t + G(r_1)$, $y_{t+\Delta t} = y_t + G(r_2)$, and $z_{t+\Delta t} = z_t + G(r_3)$, where r_i

is a random number ($0 \leq r_i \leq 1$) chosen from a uniform distribution, and $G(r_i)$ is an inverse cumulative Gaussian distribution with $\mu = 0$ and $\sigma^2 = 2Dt$, where D is the diffusion coefficient and t is time measured in unit time steps.

Immobilisation in FAs was based on simple binding kinetics with two immobile fractions, a medium and a long fraction:

$$M_{imm,medium} \rightarrow M_{imm,long} \rightarrow M_{mob}$$

$$M_{mob} \rightleftarrows M_{imm,medium}$$

Where M_{mob} are the mobile molecules and $M_{imm,medium}$ and $M_{imm,long}$ are the molecules in the medium and the long immobile fractions respectively.

Each mobile molecule in the simulation can bind at the adhesion for a medium length of time with a given chance. Once a molecule becomes a part of the medium immobile fraction it has a chance to either become mobile again or to become a part of the long immobile fraction. Molecules in the long immobile fraction have a chance of becoming mobile again. These chances are defined in accordance with the following kinetics described by:

$$koff = \frac{1}{t_r}$$

Where k_{off} is the off rate constant in s^{-1} for the medium or the long immobile fraction and t_r is the average time in s spent immobile for molecules in this fraction.

$$k_{on,medium} = \frac{F_{imm,medium}}{1 - F_{imm,medium} - F_{imm,long}} \bullet (k_{off,medium} + k_{on,long})$$

Where $k_{on,medium}$ and $k_{on,long}$ are the effective on rate constants in s^{-1} for the medium/long immobile fractions and $F_{imm,medium}$/$F_{imm,long}$ are the relative number of medium/long immobile molecules respectively.

$$k_{on,long} = \frac{F_{imm,long}}{F_{imm,medium}} \bullet k_{off,long}$$

The ellipsoid volume of the cell was based on experimentally derived estimates of cell size, for U2OS cells this corresponds to a width of 24 μm, a length of 44 μm and a height of 2 μm, for MDCK to 15, 64 and 2 μm respectively. In each cell 2 ellipsoid volumes with widths of 1.5 μm, lengths of 2 μm and heights of 0.5 μm

were used to simulate FAs

The FRAP procedure was simulated on the basis of an experimentally derived 3D laser intensity profile providing a chance for each molecule to be bleached, based on its 3D position, during simulation of the bleach pulse. The number of fluorescent molecules in the ellipsoid volume of the bleached adhesion was used as the output of the simulation.

The experimentally derived FRAP curve for each individual FA was individually fitted to the simulated FRAP curves and the best fitting (least squares) curve was determined. For the parameters of interest, $k_{on,medium}$ and $k_{off,medium}$ we determined the interquartile range (IQR). Any FAs for which the best fitting curve resulted in a $k_{on,medium}$ or $k_{off,medium}$ outside of 1.5*IQR, the next best fitting curve was used iteratively until the parameter fell within 1.5*IQR range.

To give the resultant kinetic parameters for a set of FAs of interest the average was taken of the parameters corresponding to the best fitting curves for these FAs.

Classification of FAs

To examine the effects of FA location and/or orientation all FAs were classified. FAs were classified as 'outer' when they were located close to the ventral (adherent) membrane edge. FAs were classified as 'inner' when they were located further inwards, with another FA located between them and the closest membrane edge. FAs were classified as 'pointing' when they were orientated with their long axis 'perpendicular' (*i.e.* 90° ± 30°) to the closest ventral membrane edge. FAs were classified as 'parallel' when they were orientated with their long axis 'parallel' (*i.e.* 180° ± 30°) to the closest membrane edge. FAs outside these boundaries were discarded in these analyses, which for the FRAP data amounted to 31 of 233 FA for VASP (13%), 56 of 464 FAs for zyxin (12%), 62 of 332 FAs for paxillin (19%) and 35 of 249 FAs for vinculin (14%). Overall, from the FRAP data 184 of the 1278 bleached FAs (14%) fell outside the criteria for 'pointing' and 'parallel' and were discarded from analyses looking at FA orientation.

Statistical analysis

For analyses of the differences between two groups two-tailed Mann-Whitney U tests were used. For analyses of the differences between more than two groups two-tailed Kruskall-Wallis Rank Sum tests were used, if this generated a p-value <0.05 the specific groups with significant differences were determined using two-tailed Mann-Whitney U tests. To curtail the number of Mann Whitney U tests to be performed on the FRAP data separated based on FA location and orientation

into four groups only the differences between meaningful combinations were analysed limiting the number of tests to 4 per parameter: outer pointing versus inner pointing, outer parallel versus inner parallel, outer pointing versus outer parallel and inner pointing versus inner parallel. As a further precaution against an inflated type I error rate, for all FRAP data where the FAs were separated on the basis of FA location and/or orientation the p-value was adjusted to < 0.01 to denote significance

Acknowledgements

Author contributions

K.L. designed and performed microscopy experiments and wrote the manuscript; B.G. designed FRAP analysis software and performed the analyses; A.B.H. supervised the project, contributed to method and analysis development, supervised writing the manuscript and revised it.

References

1   Yamada, K. M. & Geiger, B. Molecular interactions in cell adhesion complexes. Current opinion in cell biology 9, 76-85 (1997).

2   Geiger, B., Bershadsky, A., Pankov, R. & Yamada, K. M. Transmembrane crosstalk between the extracellular matrix--cytoskeleton crosstalk. Nature reviews. Molecular cell biology 2, 793-805, doi:10.1038/35099066 (2001).

3   Zaidel-Bar, R., Itzkovitz, S., Ma'ayan, A., Iyengar, R. & Geiger, B. Functional atlas of the integrin adhesome. Nature cell biology 9, 858-867, doi:10.1038/ncb0807-858 (2007).

4   Winograd-Katz, S. E., Fassler, R., Geiger, B. & Legate, K. R. The integrin adhesome: from genes and proteins to human disease. Nature reviews. Molecular cell biology 15, 273-288, doi:10.1038/nrm3769 (2014).

5   Wahl, S. M., Feldman, G. M. & McCarthy, J. B. Regulation of leukocyte adhesion and signaling in inflammation and disease. Journal of leukocyte biology 59, 789-796 (1996).

6   Maartens, A. P. & Brown, N. H. The many faces of cell adhesion during Drosophila muscle development. Developmental biology 401, 62-74, doi:10.1016/j.ydbio.2014.12.038 (2015).

7   Laukaitis, C. M., Webb, D. J., Donais, K. & Horwitz, A. F. Differential dynamics of alpha 5 integrin, paxillin, and alpha-actinin during formation and disassembly of adhesions in migrating cells. The Journal of cell biology 153, 1427-1440 (2001).

8   Webb, D. J. et al. FAK-Src signalling through paxillin, ERK and MLCK regulates adhesion disassembly. Nature cell biology 6, 154-161, doi:10.1038/ncb1094 (2004).

9   Wiseman, P. W. et al. Spatial mapping of integrin interactions and dynamics during cell migration by image correlation microscopy. Journal of cell science 117, 5521-5534, doi:10.1242/jcs.01416 (2004).

10   Choi, C. K. et al. Actin and alpha-actinin orchestrate the assembly and maturation of nascent adhesions in a myosin II motor-independent manner. Nature cell biology 10, 1039-1050, doi:10.1038/ncb1763 (2008).

11   Pasapera, A. M., Schneider, I. C., Rericha, E., Schlaepfer, D. D. & Waterman, C. M. Myosin II activity regulates vinculin recruitment to focal adhesions through FAK-mediated paxillin phosphorylation. The Journal of cell biology 188, 877-890, doi:10.1083/jcb.200906012 (2010).

12   Bakolitsa, C. et al. Structural basis for vinculin activation at sites of cell adhesion. Nature 430, 583-586, doi:10.1038/nature02610 (2004).

13   Jones, P. et al. Identification of a talin binding site in the cytoskeletal protein vinculin. The Journal of cell biology 109, 2917-2927 (1989).

14   Turner, C. E. & Miller, J. T. Primary sequence of paxillin contains putative SH2 and SH3 domain binding motifs and multiple LIM domains: identification of a vinculin and pp125Fak-binding region. Journal of cell science 107 (Pt 6), 1583-1591 (1994).

15   Brown, M. C., Perrotta, J. A. & Turner, C. E. Identification of LIM3 as the principal determinant of paxillin focal adhesion localization and characterization of a novel motif on paxillin directing vinculin and focal adhesion kinase binding. The Journal of cell biology 135, 1109-1123 (1996).

16   Humphries, J. D. et al. Vinculin controls focal adhesion formation by direct interactions with talin and actin. The Journal of cell biology 179, 1043-1057, doi:10.1083/jcb.200703036 (2007).

17   McGregor, A., Blanchard, A. D., Rowe, A. J. & Critchley, D. R. Identification of the vinculin-binding site in the cytoskeletal protein alpha-actinin. The Biochemical journal 301 (Pt 1), 225-233 (1994).

18   Brindle, N. P., Holt, M. R., Davies, J. E., Price, C. J. & Critchley, D. R. The focal-adhesion vasodilator-stimulated phosphoprotein (VASP) binds to the proline-rich domain in vinculin. The Biochemical journal 318 (Pt 3), 753-757 (1996).

19   Gertler, F. B., Niebuhr, K., Reinhard, M., Wehland, J. & Soriano, P. Mena, a relative of VASP and Drosophila Enabled, is implicated in the control of microfilament dynamics. Cell 87, 227-239 (1996).

20   Reinhard, M., Rudiger, M., Jockusch, B. M. & Walter, U. VASP interaction with vinculin: a recurring theme of interactions with proline-rich motifs. FEBS letters 399, 103-107 (1996).

21   Rottner, K., Krause, M., Gimona, M., Small, J. V. & Wehland, J. Zyxin is not colocalized with vasodilator-stimulated phosphoprotein (VASP) at lamellipodial tips and exhibits different dynamics to vinculin, paxillin, and VASP in focal adhesions. Molecular biology of the cell 12, 3103-3113 (2001).

22   Furman, C. et al. Ena/VASP is required for endothelial barrier function in vivo. The Journal of cell biology 179, 761-775, doi:10.1083/jcb.200705002 (2007).

23   Hirata, H., Tatsumi, H. & Sokabe, M. Zyxin emerges as a key player in the mechanotransduction at cell adhesive structures. Communicative & integrative biology 1, 192-195 (2008).

24   Golsteyn, R. M., Beckerle, M. C., Koay, T. & Friederich, E. Structural and functional similarities between the human cytoskeletal protein zyxin and the ActA protein of Listeria monocytogenes. Journal of cell science 110 (Pt 16), 1893-1906 (1997).

25   Drees, B. et al. Characterization of the interaction between zyxin and members of the Ena/vasodilator-stimulated phosphoprotein family of proteins. The Journal of biological chemistry 275, 22503-22511, doi:10.1074/jbc.M001698200 (2000).

26   Fradelizi, J. et al. ActA and human zyxin harbour Arp2/3-independent actin-polymerization activity. Nature cell biology 3, 699-707, doi:10.1038/35087009 (2001).

27   Nix, D. A. et al. Targeting of zyxin to sites of actin membrane interaction and to the nucleus. The Journal of biological chemistry 276, 34759-34767, doi:10.1074/jbc.M102820200 (2001).

28   Yoshigi, M., Hoffman, L. M., Jensen, C. C., Yost, H. J. & Beckerle, M. C. Mechanical force mobilizes zyxin from focal adhesions to actin filaments and regulates cytoskeletal reinforcement. The Journal of cell biology 171, 209-215, doi:10.1083/jcb.200505018 (2005).

29   Hoffman, L. M. et al. Genetic ablation of zyxin causes Mena/VASP mislocalization, increased motility, and deficits in actin remodeling. The Journal of cell biology 172, 771-782, doi:10.1083/jcb.200512115 (2006).

2

30   Hoffman, L. M. et al. Targeted disruption of the murine zyxin gene. Molecular and cellular biology 23, 70-79 (2003).

31   Smith, M. A. et al. A zyxin-mediated mechanism for actin stress fiber maintenance and repair. Developmental cell 19, 365-376, doi:10.1016/j.devcel.2010.08.008 (2010).

32   Uemura, A., Nguyen, T. N., Steele, A. N. & Yamada, S. The LIM domain of zyxin is sufficient for force-induced accumulation of zyxin during cell migration. Biophysical journal 101, 1069-1075, doi:10.1016/j.bpj.2011.08.001 (2011).

33   Barsony, J. & Marx, S. J. Immunocytology on microwave-fixed cells reveals rapid and agonist-specific changes in subcellular accumulation patterns for cAMP or cGMP. Proceedings of the National Academy of Sciences of the United States of America 87, 1188-1192 (1990).

34   Neher, E. & Augustine, G. J. Calcium gradients and buffers in bovine chromaffin cells. The Journal of physiology 450, 273-301 (1992).

35   Ponti, A., Machacek, M., Gupton, S. L., Waterman-Storer, C. M. & Danuser, G. Two distinct actin networks drive the protrusion of migrating cells. Science (New York, N.Y.) 305, 1782-1786, doi:10.1126/science.1100533 (2004).

36   Nikolaev, V. O., Bunemann, M., Schmitteckert, E., Lohse, M. J. & Engelhardt, S. Cyclic AMP imaging in adult cardiac myocytes reveals far-reaching beta1-adrenergic but locally confined beta2-adrenergic receptor-mediated signaling. Circulation research 99, 1084-1091, doi:10.1161/01. RES.0000250046.69918.d5 (2006).

37   Lynch, M. J., Baillie, G. S. & Houslay, M. D. cAMP-specific phosphodiesterase-4D5 (PDE4D5) provides a paradigm for understanding the unique non-redundant roles that PDE4 isoforms play in shaping compartmentalized cAMP cell signalling. Biochemical Society transactions 35, 938-941, doi:10.1042/bst0350938 (2007).

38   Dixit, N. & Simon, S. I. Chemokines, selectins and intracellular calcium flux: temporal and spatial cues for leukocyte arrest. Frontiers in immunology 3, 188, doi:10.3389/fimmu.2012.00188 (2012).

39   Mehta, S. et al. Calmodulin-controlled spatial decoding of oscillatory Ca2+ signals by calcineurin. eLife 3, e03765, doi:10.7554/eLife.03765 (2014).

40   van Unen, J. et al. Plasma membrane restricted RhoGEF activity is sufficient for RhoA-mediated actin polymerization. Scientific reports 5, 14693, doi:10.1038/srep14693 (2015).

41   Geverts, B., van Royen, M. E. & Houtsmuller, A. B. Analysis of biomolecular dynamics by FRAP and computer simulation. Methods in molecular biology (Clifton, N.J.) 1251, 109-133, doi:10.1007/978-1-4939-2080-8_7 (2015).

42   Ren, X. D. et al. Focal adhesion kinase suppresses Rho activity to promote focal adhesion turnover. Journal of cell science 113 (Pt 20), 3673-3678 (2000).

43   Gupton, S. L. & Waterman-Storer, C. M. Spatiotemporal feedback between actomyosin and focal-adhesion systems optimizes rapid cell migration. Cell 125, 1361-1374, doi:10.1016/j. cell.2006.05.029 (2006).

44   Zaidel-Bar, R., Milo, R., Kam, Z. & Geiger, B. A paxillin tyrosine phosphorylation switch regulates the assembly and form of cell-matrix adhesions. Journal of cell science 120, 137-148, doi:10.1242/jcs.03314 (2007).

45   von Wichert, G., Haimovich, B., Feng, G. S. & Sheetz, M. P. Force-dependent integrin-cytoskeleton linkage formation requires downregulation of focal complex dynamics by Shp2. The EMBO journal 22, 5023-5035, doi:10.1093/emboj/cdg492 (2003).

46   Chandrasekar, I. et al. Vinculin acts as a sensor in lipid regulation of adhesion-site turnover. Journal of cell science 118, 1461-1472, doi:10.1242/jcs.01734 (2005).

47   Cohen, D. M., Kutscher, B., Chen, H., Murphy, D. B. & Craig, S. W. A conformational switch in vinculin drives formation and dynamics of a talin-vinculin complex at focal adhesions. The Journal of biological chemistry 281, 16006-16015, doi:10.1074/jbc.M600738200 (2006).

48   Lele, T. P. et al. Mechanical forces alter zyxin unbinding kinetics within focal adhesions of

living cells. Journal of cellular physiology 207, 187-194, doi:10.1002/jcp.20550 (2006).

49   Lele, T. P., Thodeti, C. K., Pendse, J. & Ingber, D. E. Investigating complexity of protein-protein interactions in focal adhesions. Biochemical and biophysical research communications 369, 929-934, doi:10.1016/j.bbrc.2008.02.137 (2008).

50   Mohl, C. et al. Becoming stable and strong: the interplay between vinculin exchange dynamics and adhesion strength during adhesion site maturation. Cell motility and the cytoskeleton 66, 350-364, doi:10.1002/cm.20375 (2009).

51   Wolfenson, H. et al. A role for the juxtamembrane cytoplasm in the molecular dynamics of focal adhesions. PloS one 4, e4304, doi:10.1371/journal.pone.0004304 (2009).

52   Horton, E. R. et al. Modulation of FAK and Src adhesion signaling occurs independently of adhesion complex composition. The Journal of cell biology 212, 349-364, doi:10.1083/jcb.201508080 (2016).

53   Wolfenson, H., Bershadsky, A., Henis, Y. I. & Geiger, B. Actomyosin-generated tension controls the molecular kinetics of focal adhesions. Journal of cell science 124, 1425-1432, doi:10.1242/jcs.077388 (2011).

54   Lavelin, I. et al. Differential effect of actomyosin relaxation on the dynamic properties of focal adhesion proteins. PloS one 8, e73549, doi:10.1371/journal.pone.0073549 (2013).

55   Schiefermeier, N. et al. The late endosomal p14-MP1 (LAMTOR2/3) complex regulates focal adhesion dynamics during cell migration. The Journal of cell biology 205, 525-540, doi:10.1083/jcb.201310043 (2014).

56   Feutlinske, F. et al. Stonin1 mediates endocytosis of the proteoglycan NG2 and regulates focal adhesion dynamics and cell motility. Nature communications 6, 8535, doi:10.1038/ncomms9535 (2015).

57   Doyle, A. D., Carvajal, N., Jin, A., Matsumoto, K. & Yamada, K. M. Local 3D matrix microenvironment regulates cell migration through spatiotemporal dynamics of contractility-dependent adhesions. Nature communications 6, 8720, doi:10.1038/ncomms9720 (2015).

58   Sathe, A. R., Shivashankar, G. V. & Sheetz, M. P. Nuclear transport of paxillin depends on focal adhesion dynamics and FAT domains. Journal of cell science 129, 1981-1988, doi:10.1242/jcs.172643 (2016).

59   Le Devedec, S. E. et al. The residence time of focal adhesion kinase (FAK) and paxillin at focal adhesions in renal epithelial cells is determined by adhesion size, strength and life cycle status. Journal of cell science 125, 4498-4506, doi:10.1242/jcs.104273 (2012).

60   Smilenov, L. B., Mikhailov, A., Pelham, R. J., Marcantonio, E. E. & Gundersen, G. G. Focal adhesion motility revealed in stationary fibroblasts. Science (New York, N.Y.) 286, 1172-1174 (1999).

61   Zamir, E. et al. Dynamics and segregation of cell-matrix adhesions in cultured fibroblasts. Nature cell biology 2, 191-196, doi:10.1038/35008607 (2000).

62   Bubb, M. R., Spector, I., Beyer, B. B. & Fosen, K. M. Effects of jasplakinolide on the kinetics of actin polymerization. An explanation for certain in vivo observations. The Journal of biological chemistry 275, 5163-5170 (2000).

63   Hirata, H., Tatsumi, H. & Sokabe, M. Mechanical forces facilitate actin polymerization at focal adhesions in a zyxin-dependent manner. Journal of cell science 121, 2795-2804, doi:10.1242/jcs.030320 (2008).

64   Schneider, C. A., Rasband, W. S. & Eliceiri, K. W. NIH Image to ImageJ: 25 years of image analysis. Nature methods 9, 671-675 (2012).

65   Schindelin, J. et al. Fiji: an open-source platform for biological-image analysis. Nature methods 9, 676-682, doi:10.1038/nmeth.2019 (2012).
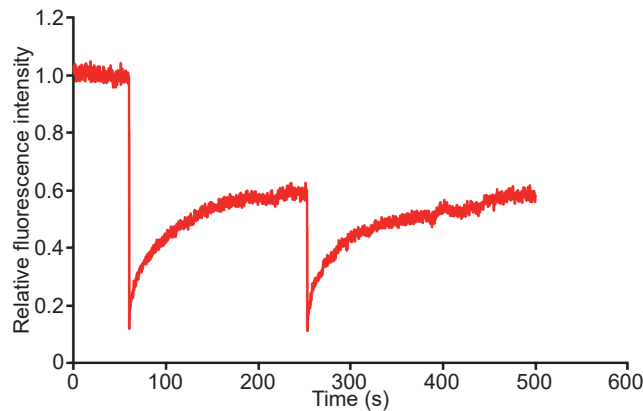
2

Supplementary Figures

S1
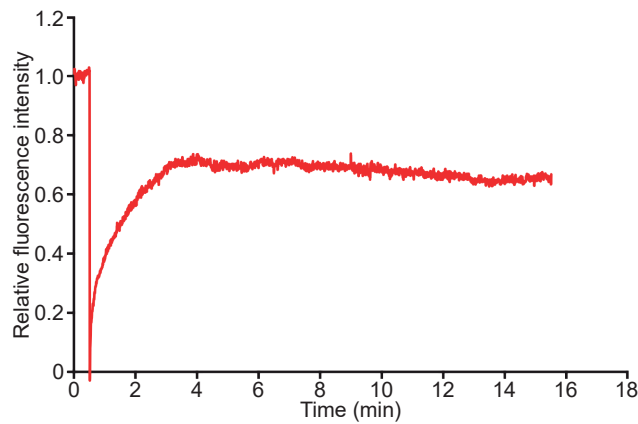
Supplementary Figure S1. Prolonged FRAP applied to paxillin in MDCK cells.
Fluorescence intensity of paxillin-GFP expressed relative to prebleach levels and intensity immediately after the bleach pulse.

S2

Supplementary Figure S2. Repeated FRAP applied to paxillin in MDCK cells.
Fluorescence intensity of paxillin-GFP expressed relative to prebleach levels. The bleach pulse was repeated after 3.5 minutes.

2

Chapter 3

A novel photoconversion assay reveals foci of stably bound proteins within focal adhesions

Karin Legerstee[1], Bart Geverts[1], Johan A. Slotman[1] and Adriaan B. Houtsmuller[1]

1 Erasmus Medical Centre Rotterdam, Department of Pathology, Optical Imaging Centre, Rotterdam, The Netherlands.

Abstract

Focal adhesions (FAs) are multiprotein structures that link the intracellular cytoskeleton to the extracellular matrix. They mediate cell adhesion and migration, crucial to many (patho-)physiological processes. We developed a photoconversion assay to specifically visualise the pool of stably bound proteins within subcellular structures and organelles and to distinguish this from its dynamically exchanging counterpart. We applied this assay to highlight the stably bound fractions of the key adaptor proteins paxillin and vinculin within focal adhesions (FAs). This revealed that while paxillin and vinculin are distributed evenly throughout FAs, their stably bound fractions form small clusters within the FA-complex. These clusters are mainly found at the proximal half of the FA, where actin fibres also enter. Furthermore, these clusters are more concentrated for paxillin than for vinculin, since the paxillin clusters were markedly smaller than the vinculin clusters, yet in previous photobleaching experiments we showed that at FAs the stably associated fraction of both proteins is ~40%. It is possible that the vinculin clusters are less concentrated due to their direct connection to actin which applies force, while the paxillin clusters might concentrate further due to their direct connection with the strongly clustering integrin receptors.

3

Introduction

Focal adhesions (FAs) are the main cellular structures linking the intracellular cytoskeleton to the extracellular matrix (ECM). They are typically several square micrometres in size[1,2]. On the membrane-facing side integrins, transmembrane receptors directly binding to the extracellular matrix, are the main FA components. A specialised form of actin linked to contractile myosin-II forms the edge of the FA on the cytoplasm-facing side, which we will refer to as F-actin. In between integrins and actin a large and diverse intracellular macromolecular protein assembly is present, with over 200 different reported proteins[3,4]. These include (trans)membrane receptors, other than integrins, adaptor proteins and many different signalling proteins such as kinases, phosphatases and G-protein regulators, which through post-translational modifications add significantly to FA complexity. FAs experience force, the strength of which depends on the combination of myosin-II contractility and the stiffness of the ECM. Because of their importance to the transmission of force from the cell to the ECM and in cell adhesion, FAs are crucial to cell migration. Migration and adhesion are key cellular functions required for many physiological and pathophysiological processes, like embryonic development, the functioning of the immune system and also cancer, in particular metastasis[4-6].

Here we examined the location of the stably bound fractions of the large scaffold proteins paxillin and vinculin. As adaptor proteins paxillin and vinculin are among the proteins with the most potential binding partners within FAs[3]. In keeping with their having a linking, structural, role they are amongst the first proteins to be recruited to assembling focal adhesion complexes, especially the directly integrin-binding paxillin[7-11]. Vinculin has a head and a tail domain with a flexible linker in between, allowing vinculin to adopt open and closed conformations[12]. Its head domain shares many important binding partners and functions with paxillin, indeed paxillin itself is one of its binding partners[13-16]. However, while Paxillin has no direct interaction with actin, vinculin's tail domain can directly bind actin filaments as well as the actin-binding proteins α-actinin and the ENA/VASP-proteins[16-20].

Taking advantage of a photoconvertible fluorescent protein in combination with a Fluorescence Recovery After Photobleaching (FRAP) set-up on a confocal microscope, we developed a dedicated assay to specifically reveal the location of the stably bound fraction of a protein within a structure, such as a focal adhesion. We applied this assay to paxillin and vinculin because in previous FRAP experiments we showed both proteins have strikingly large stably bound fractions of nearly 50% (Chapter 2). We visualised within FAs the spatial distribution of the stably
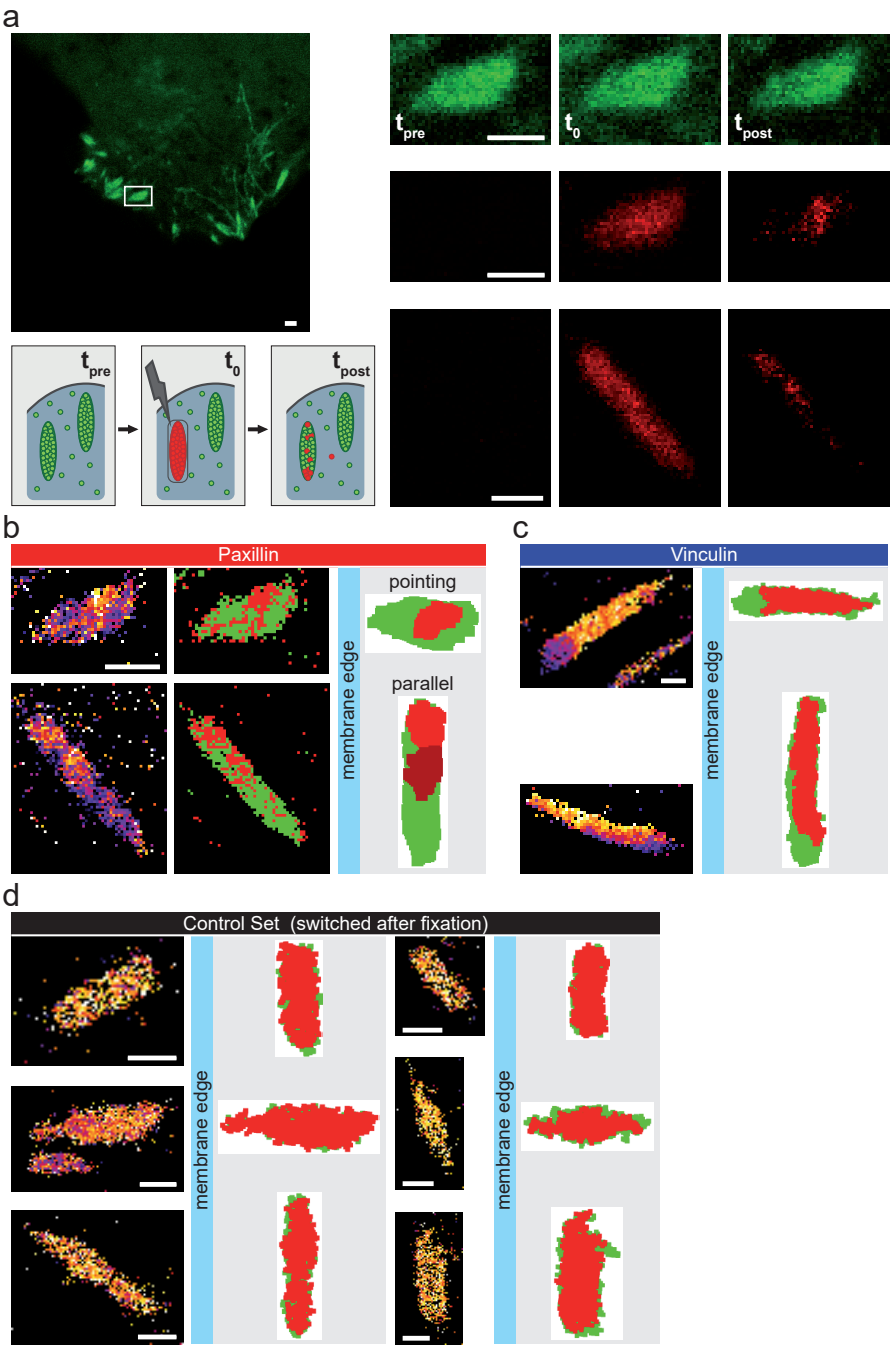
Figure 1. A dedicated assay to specifically visualise the spatial distribution of the stably bound fraction of a protein applied to paxillin and vinculin.
(a) Cartoon: Schematic overview of a photoconversion experiment. Cells express paxillin or vinculin tagged with the photoconvertible mMaple3. Before the photoconversion all FAs are green (t_{pre}). A

small region is exposed to a low intensity of 405 nm laser light, converting the mMaple in this area from green to red (t_0). After 3 minutes (three times the average residence times of the dynamically bound fractions), another image is taken (t_{post}). As the converted volume is small, most mMaple in the cytoplasm is not converted (green), so exchange in the converted FA will almost certainly lead to green proteins coming in. Therefore, at t_{post} the remaining red signal represents the stably associated fraction. Left image: green channel at t_{pre} for a representative pointing FA. Right images: magnification of the green and red channels at each time point for the boxed area, bottom row shows the red channel at each time point for a representative parallel FA. Scalebar: 1 μm **(b)** Analysis of the representative photoconverted paxillin FAs shown in a. 'Ratio view' (RV) images (left), show the ratio of the red signal at t_{post} over the red signal at t_0. Blue/purple indicates a low ratio, white/yellow a high ratio representing the stably bound fraction. To consistently select the high ratio pixels dynamic thresholds were applied to the RV images (middle image; above threshold pixels red, below threshold green). Stably bound areas were defined as above threshold areas of at least 0.05 μm². Plots were made with the stably bound area(s) in red and the rest of the FA in green (right). To facilitate comparison the distal FA side is always plotted to the left and pointing FAs were plotted with their long axis horizontal while parallel FAs were plotted with their long axis vertical. Scalebar: 1 μm. **(c)** Representative examples of analysed photoconversion data for vinculin. Left: RV images; right: rotated plots. Scalebar: 1 μm. **(d)** Representative examples of analysed control data of U2OS cells expressing paxillin-mMaple3 chemically fixed with paraformaldehyde prior to photoconversion. Scalebar: 1 μm.

bound fractions of paxillin and vinculin, which we found to be concentrated into specific areas along the FA rather than being distributed randomly throughout the FA. These areas are most often located in the proximal half of the FA where paxillin is concentrated in small regions and vinculin in larger less concentrated regions. To further investigate the cellular significance, we examined the effects of membrane dynamics as well as of FA location and orientation on the visualised stably bound areas. Several factors form gradients based on their distance from the ventral membrane edge, such as actin fibre thickness and connectivity, the concentration of (signalling) molecules and enzyme activity[21-28], effectively creating different local environments for FAs varying with their distance from the ventral membrane edge. We previously showed FA protein dynamics depend on both FA location and orientation (Chapter 2).

Results

Examining the spatial distribution of the stably bound fraction of a protein

A dedicated assay visualising the stably bound fraction of a protein within a macromolecular complex

We developed a novel photo conversion assay to specifically investigate the spatial distribution of the observed stably bound fractions of paxillin and vinculin. While traditional FRAP provides accurate estimates of the size of the stably bound fraction, the novel assay can be used to specifically visualise the proteins of this fraction within a macromolecular complex, distinguishing it from its dynamically exchanging counterpart. Here we used the photoconvertible fluorescent protein

mMaple3[29,30] in combination with a FRAP set-up on a confocal microscope (Fig. 1a). Successful implementation allowed us to specifically visualise the spatial location of the stably associated fractions of either vinculin or paxillin.

The photoconvertible fluorescent protein mMaple3 can be switched (converted) from emitting green fluorescence to emitting red fluorescence by exposure to 405 nm laser light at low intensity. In U2OS cells we expressed paxillin or vinculin tagged with mMaple3, which targeted to FAs highlighting them in green fluorescence (Fig. 1a, t_{pre}). Using a FRAP set-up on a confocal microscope we briefly exposed a small region of the cell, tightly enclosing one or two FAs, to 405 nm laser light. This switched the mMaple-tagged paxillin molecules, only within the exposed area, from emitting green fluorescence to emitting red fluorescence. Thus, the FA(s) within the exposed area emitted red fluorescence when excited at the appropriate wavelength (Fig. 1a, t_0). Next, we waited for three minutes, since this is ~3 times the average dynamic residence time for paxillin/vinculin, the vast majority of the dynamically binding proteins exchange. As only a small portion of the cell was briefly (in the hundreds of milliseconds range) exposed to the 405 nm laser light the unconverted green mMaple-tagged protein is present in vast excess compared to the converted red mMaple-tagged protein. Therefore, exchanging converted protein will almost certainly be replaced by unconverted protein, whereas stably associated converted proteins remain in the FA, revealing the spatial distribution of the stably and dynamically bound fractions of the studied proteins (Fig. 1a, t_{post}).

To improve visualisation of stably bound fractions within the context of entire FAs we made 'ratio view' (RV) images (Fig. 1b-d, left images). In these images a colour-coded scale is used to show on a pixel by pixel basis the ratio of the photoconverted signal still present at t_{post} over the converted signal present at t_0. Blue/purple pixels in the RV image indicate a low ratio of the converted signal after 3 minutes, visualising the dynamically bound fraction. White/yellow in the RV image means a high ratio of the converted signal at t_{post}, visualising the stably bound fraction.

To consistently differentiate between dynamically and stably bound areas, we applied a threshold to the RV images (Fig. 1b, middle images). To see if the stably bound fraction is spread evenly and randomly over the FA or is instead concentrated into specific areas, we examined above threshold areas of 0.05 μm^2 or larger. We created plots wherein these stably bound area(s) are plotted in (shades of) red and the rest of the FA in green (Fig. 1b-d, right images). To allow for easy comparison between FAs, for each FA we determined its distal side, the side which lies closest to the ventral membrane edge, then rotated the FA so that this
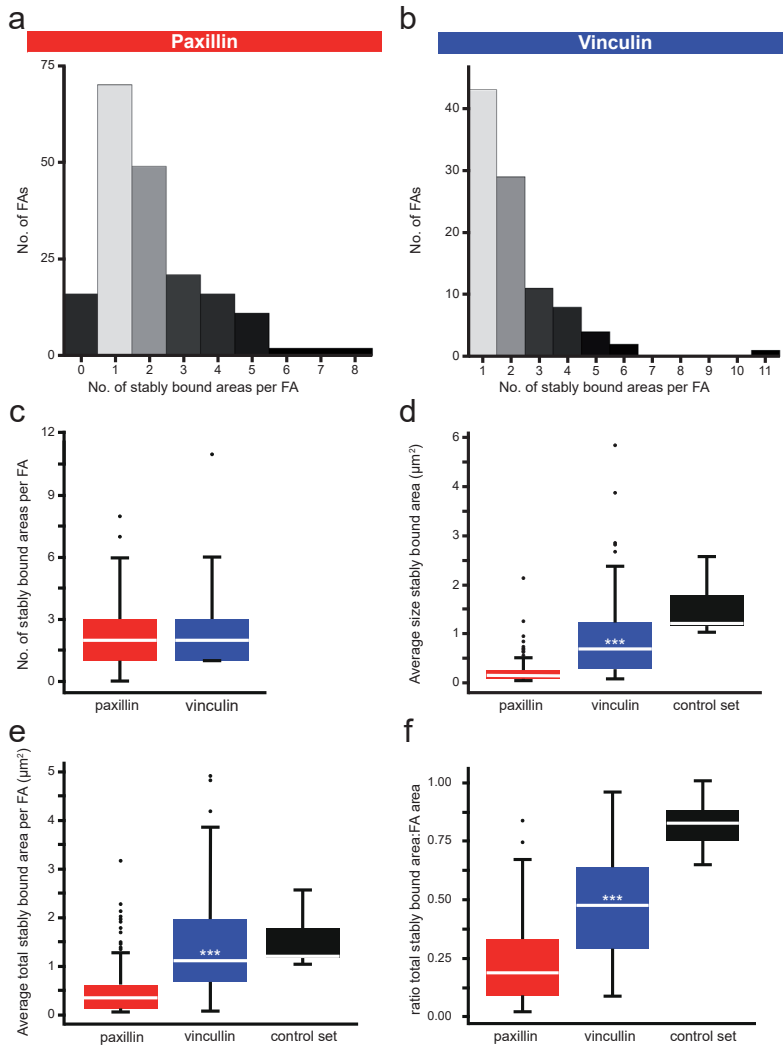
Figure 2. Quantification of the photoconversion experiments.
(a,b) Histograms of the number of stably bound areas (above threshold areas larger than 0.05 μm^2 after application of a dynamic threshold on the RV image) per FA for U2OS cells expressing paxillin-mMaple3 (a, n = 189 FAs in 153 cells) or vinculin-mMaple3 (b, n = 98 FAs in 84 cells). Note that for both proteins the largest number of FAs have one stably bound area. **(c)** Tukey style boxplots of the data shown in a and b. White lines denote medians and asterisks significant p-values in two sided Mann Whitney tests: *p<0.05, **p<0.01, ***p<0.001. **(d)** Tukey style boxplots of the surface area (μm^2) of the individual stably bound areas for FAs with at least 1 stably bound area (paxillin n = 173, vinculin n = 98, control n = 7). The control set contains cells expressing paxillin-mMaple3 which were chemically fixed prior to the photoconversion experiment. White lines and asterisks as in c. **(e)** Tukey style boxplots of the average total surface area (μm^2) covered by stably bound areas per FA for FAs with at least 1 stably bound area (for n see d). White lines and asterisks as in c. **(f)** Tukey style boxplots of the ratio of the total area of the FA covered by stably bound area(s) over the total FA surface area (for n see d). White lines and asterisks as in c.

side is always plotted to the left. FAs with their long axis more or less perpendicular to the ventral membrane edge, will be referred to as 'pointing FAs' and are plotted with their long axis horizontally, FAs with their long axis roughly parallel to this membrane edge are referred to as 'parallel FAs' and are plotted with this axis vertically (for a precise definition see Materials and Methods).

In addition, we performed control experiments where U2OS cells expressing paxillin-mMaple3 were chemically fixed prior to the photoconversion experiments (Fig. 1d). For these controls ratios were high throughout the FA in the RV images and the stably bound areas covered nearly the entire FA in the plots, as expected in fixed cells where proteins cannot exchange.

In principle it should not be necessary to create RV images to distinguish between the dynamically and the stably bound fractions, as the green fluorescence in the post exchange image should translate to the dynamically bound fraction. However, this last is only true if switching efficiencies are close to a hundred percent, otherwise the green signal is composed of a combination of proteins from the stably bound fraction that were not successfully switched and exchanged proteins from the dynamically bound fraction. In Figure 1a it can be seen that this is not the case since, apart from in the red channel, the FA was also still clearly visible in the green channel immediately after photoconversion (Fig. 1a, t_0), which was true for all converted FAs. This issue is resolved in the RV images by categorising both fractions on the basis of the ratio of the red signal still present after exchange of the dynamically bound fraction over the red signal present immediately after photoswitching. Meanwhile the green signal can be used to monitor the stability of the focal adhesion. Furthermore, the entire FA is clearly visible in the red channel at t_0, indicating a reasonable proportion of the tagged protein was converted throughout the FA, also true for all FAs. For this reason, even though we are clearly not photoconverting the whole population of tagged protein present in the FA, we are confident that the converted proportion of the tagged protein represents a fair and random sample taken from the entire population of tagged proteins associated with the FA, as is also shown by the control experiments on fixed samples.

Stably bound paxillin and vinculin are concentrated into specific areas within FAs

From the representative examples it seems that for the vinculin FAs the proportion of the FAs covered by the stably bound fraction was much larger than for the paxillin FAs. This was confirmed by a quantitative analysis of the stably bound areas for paxillin (n = 189 photoconverted FAs from 153 cells) and vinculin (n = 98 FAs from 84 cells). The number of stably bound areas per photoconverted FA did not differ significantly between paxillin and vinculin, for both proteins the medi-
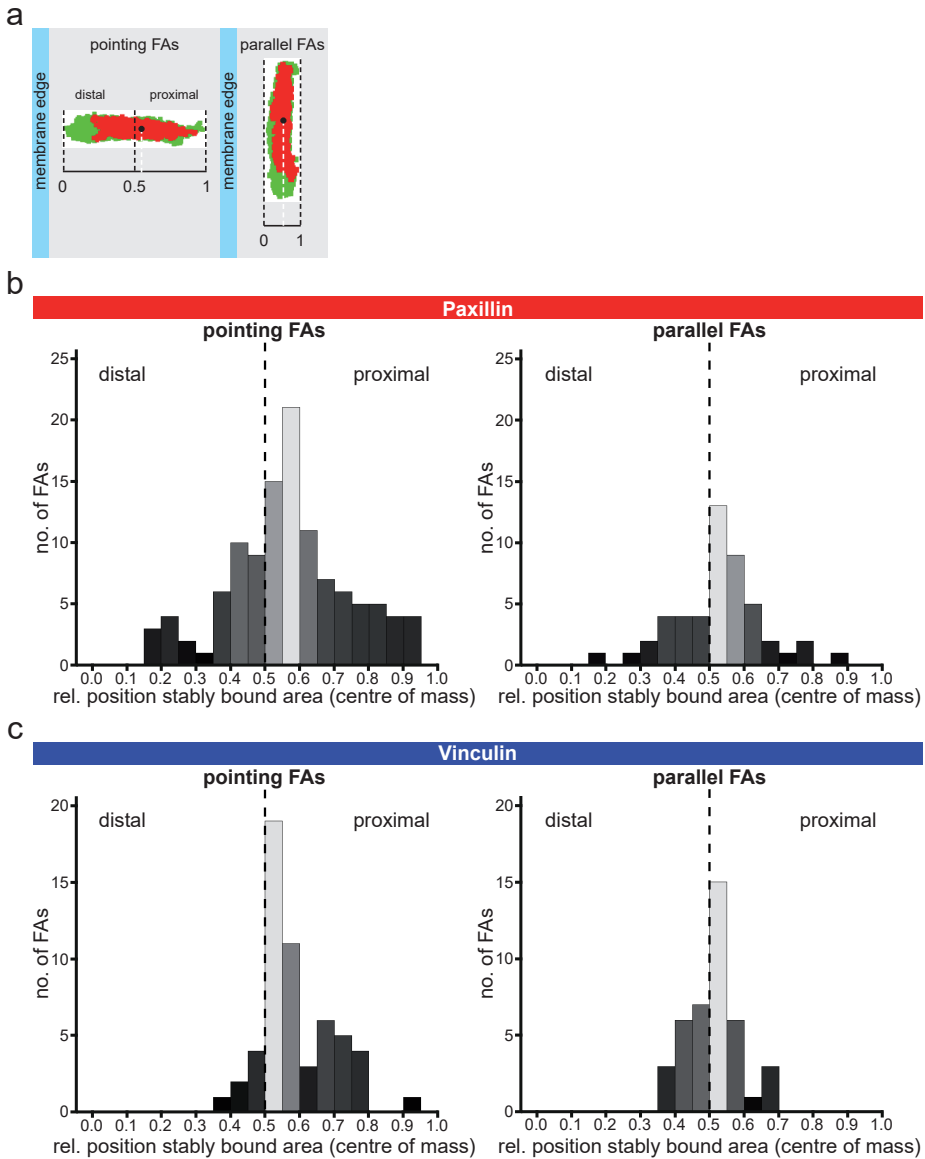
Figure 3. Stably bound paxillin and vinculin concentrate more often in the proximal half of FAs.
(a) Analysis of the location of the stably bound fraction of an FA relative to the closest ventral membrane edge. In the plots FAs are plotted with their distal side, which in the cells lies closest to the edge of the ventral membrane, on the left. The centre of mass of the stably bound area(s) is determined relative to the normalised length of the major axis of the FA for pointing FAs, or of the minor axis for parallel FAs. **(b)** Histogram of the centres of mass of the stably bound area(s) relative to the closest edge of the ventral membrane for all pointing (left, n = 113) or parallel FAs (right, n = 49) that have at least one stably bound area for cells expressing paxillin-mMaple3. **(c)** Histogram of the centres of mass of the stably bound area(s) relative to the closest edge of the ventral membrane for all pointing (left, n = 56) or parallel FAs (right, n = 41) that have at least one stably bound area for cells expressing vinculin-mMaple3.

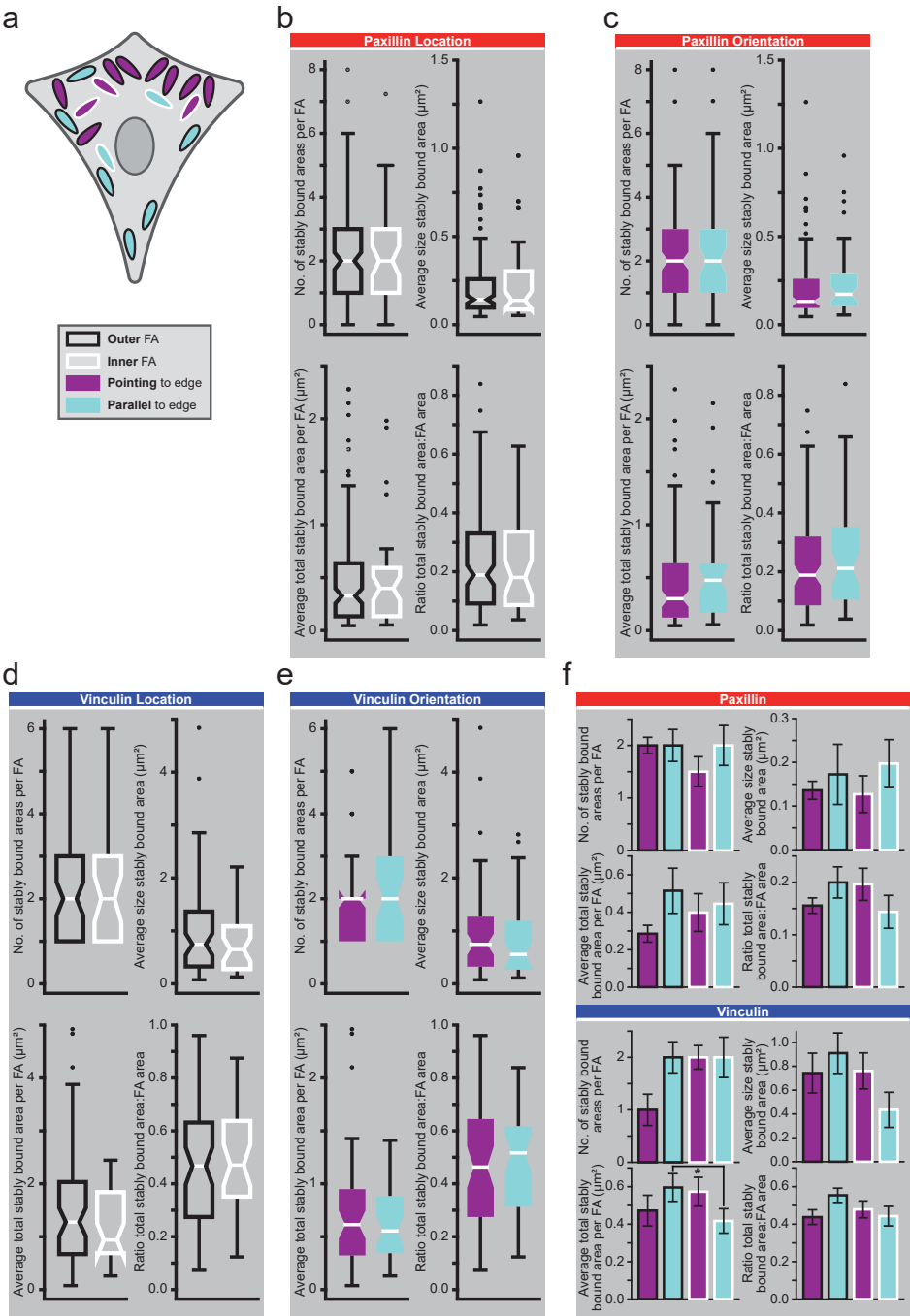**Figure 4. The effect of FA location and orientation on stably bound paxillin and vinculin clusters.**
(a) Cartoon illustrating classification of FAs based on distance from or orientation relative to the closest edge of the ventral (adherent) portion of the plasma membrane. 'Outer' FAs (black outline) are close to the edge of the ventral membrane, 'inner' FAs (white outline) are located away from the

edge. In 'pointing' FAs (purple) the major axis is orientated approximately perpendicular to the closest membrane edge, and in 'parallel' FAs (blue) the major axis is approximately parallel to the edge. **(b)** Quantification of photoconversion data for U2OS cells expressing paxillin-mMaple3 categorised based on FA location. From left to right and from top to bottom, Tukey style boxplots of: the number of stably bound areas per FA, the surface area (μm^2) of the individual stably bound clusters, the average total surface area covered by stably bound cluster(s) per FA and the ratio of the total area of the FA covered by stably bound cluster(s) over the total FA surface area for outer (n = 138) and inner (n = 48) FAs. For the last three sets of boxplots only data from FAs with at least 1 stably bound cluster was included (outer n = 138 and inner n = 43). White lines denote medians and notches their 95% confidence intervals. P-values in order: 0.56, 0.99, 0.96 and 0.87 (two-sided Mann Whitney tests. **(c)** Quantification of photoconversion data for U2OS cells expressing paxillin-mMaple3 categorised based on FA orientation. Tukey style boxplots in the same order as in b for pointing (n = 124) and parallel (n = 52) FAs. For the last three sets of boxplots only data from FAs with at least 1 stably bound cluster was included (pointing n = 113, parallel n = 49). Median and notches as in b. P-values in order: 0.22, 0.21, 0.11 and 0.36 (two-sided Mann Whitney tests). **(d)** Tukey style boxplots in the same order as in b for U20S cells expressing vinculin-mMaple3 for outer (n = 64) and inner (n = 33) FAs. Median and notches as in b. P-values in order: 0.70, 0.53, 0.49 and 0.71 (two-sided Mann Whitney tests). **(e)** Tukey style boxplots in the same order as in b for U2OS cells expressing vinculin-mMaple3 for pointing (n = 41) and parallel (n = 56) FAs. Median and notches as in b. P-values in order: 0.25, 0.53, 1 and 0.93 (two-sided Mann Whitney tests). **(f)** Bar plots of the median values for the same parameters and in the same order as the boxplots in b, for FAs categorised on the basis of the combination of location and orientation for U2OS cells expressing paxillin-mMaple3 (top) and vinculin-mMaple3 (bottom). N-numbers per protein for consecutively outer and pointing, outer and parallel, inner and pointing and inner and parallel FAs: paxillin: 100 [92], 32 [31], 24 [21], 20 [18] FAs and [FAs with at least 1 stably bound area] and vinculin: 39, 24 , 17 and 16 FAs. Error bars: standard error of the mean (SEM). Asterisk denotes significance (p = 0.044, two-sided Mann Whitney test). There are statistical trends towards larger individual stably bound vinculin clusters at outer and parallel compared to inner and parallel FAs (p = 0.12) and at inner and pointing compared to inner and parallel FAs (p = 0.16) and towards a smaller total surface area covered by paxillin clusters at outer and pointing compared to outer and parallel FAs (p = 0.14). All other p-values > 0.2 (two-sided Mann Whitney tests).

an value was two although the most common number of stably bound areas per FA was one (Fig. 2 a-c). However, the size of individual stably bound areas was more than 4 times smaller for paxillin than for vinculin, medians 0.14 and 0.69 μm^2 respectively (Fig. 2d). The summed stably bound area per FA, irrespective of the number of stably bound spots this area is spread over in the FA, was also more than three times smaller for paxillin than for vinculin (Fig. 2e). To determine the proportion of FAs covered by stably bound areas we divided the summed stably bound surface area per FA by the total surface area of that FA, making this value independent of FA size. For paxillin this value corresponded to less than one fifth of the FA (median 0.19), while for vinculin almost half (median 0.48) of the FA was covered by stably bound areas. Since we previously showed through FRAP experiments that the size of the stably bound fraction is nearly identical for paxillin and vinculin, this indicates that stably bound paxillin proteins are more concentrated at FAs than stably bound vinculin proteins (Chapter 2).

Stably bound paxillin and vinculin clusters are located at proximal FA ends

Additionally, for each photoconverted FA we calculated the average weighted (by area) gravitational centre for the stably bound area(s), which we expressed

relative to the major axis of the FA in the case of pointing FAs, or the minor axis of the FA for parallel FAs (Fig. 3a and below). This allows comparison of the location of the stably bound areas among all FAs irrespective of FA length. The stably bound fraction was located at the proximal FA half for 69% of all photoconverted paxillin FAs and for 75% of all converted vinculin FAs (Fig. 3b,c), which is the FA end where the F-actin fibre also enters the FA (Supplementary Fig. S1).

Examining the effects of focal adhesion position and orientation on clusters of stably bound FA proteins

Categorisation of focal adhesions based on their position and orientation

Several factors form gradients based on their distance from the edge of the ventral membrane, such as actin fibre thickness and connectivity, the concentration of (signalling) molecules and enzyme activity[21-28]. Such gradients effectively create different local environments for FAs varying with their distance from the ventral membrane edge. Through FRAP experiments we previously demonstrated FA protein dynamics depend on FA location and orientation relative to the ventral membrane edge (Chapter 2).

To investigate whether FA localisation and orientation also influence the stably bound paxillin and vinculin areas within FAs, we subdivided the data from all switched FAs. First, for FA location, all FAs were grouped on the basis of their distance from the closest ventral membrane edge. 'Outer' FAs are located close to this edge, 'inner' FAs are positioned further inwards with outer FAs located between them and the closest adherent membrane edge (Fig. 4a,b,d). In addition, for FA orientation, FAs were classified on the basis of our observation that most FAs are orientated with their long axis either roughly perpendicular or roughly parallel to the closest adherent membrane edge. FAs were classified as 'pointing' when the angle between their long axis and the closest ventral membrane edge was 90° ± 30°. FAs were classified as 'parallel' when the angle between their long axis and the closest ventral membrane edge was 180° ± 30° (Fig. 4a,c,e). Of the 287 switched FAs (see material and methods for a specification per examined protein) 14 fell outside these criteria, which is ~5%. Finally, the adhesions were grouped based on the combination of these two criteria which resulted in four groups: A outer and pointing, B outer and parallel, C inner and pointing and D inner and parallel FAs (Fig. 4a,f).

Effects of focal adhesion location and orientation on stably bound clusters of paxillin and vinculin

The robust effects of FA location and orientation on FA protein dynamics were not replicated in their effects on stably bound paxillin or vinculin clusters within
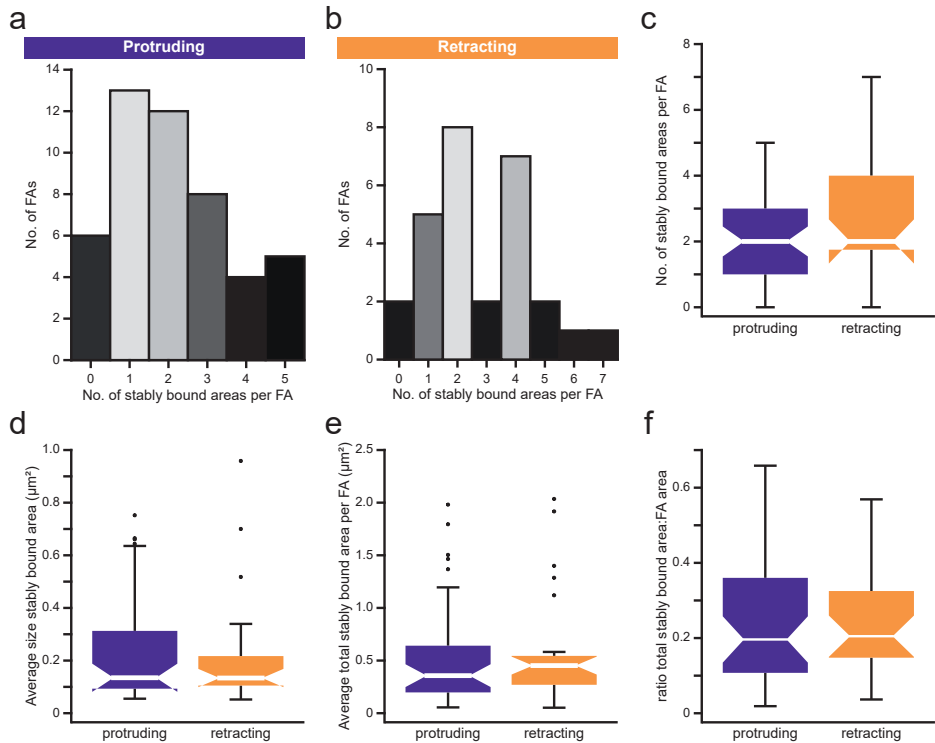
Figure 5. The influence of membrane dynamics on stably bound paxillin areas.
(a,b) Histograms of the number of stably bound areas per FA for U2OS cells expressing paxillin-mMaple3 for FAs near protruding membrane edges (a, n = 48) and for FAs near retracting membrane edges (b, n = 28) as determined from timelapse data (see material and methods). **(c)** Tukey style box-plots of the data shown in a and b. White lines denote medians. P-value is 0.12 in two-sided Mann Whitney test. **(d)** Tukey style boxplots of the surface area (μm^2) of the individual stably bound clusters for FAs with at least 1 stably bound cluster (protruding n = 42, retracting n = 26 FAs). White lines and statistical test as above, p = 0.91. **(e)** Tukey style boxplots of the average total surface area (μm^2) covered by stably bound areas per FA for FAs with at least one stably bound cluster (for n see d). White lines and statistical test as above, p = 0.59. **(f)** Tukey style boxplots of the ratio of the total area of the FA covered by stably bound area(s) over the total FA surface area (for n see d). White lines and statistical test as above, p = 0.89.

FAs. However, some interesting trends were observed. Although FA location did not seem to strongly impact stably bound paxillin clusters within FAs (Fig. 4b), the effect of FA orientation was more pronounced, with a trend towards a larger surface area of parallel FAs covered by stably bound paxillin cluster(s) than of pointing FAs (p = 0.11 in two-sided Mann Whitney test, Fig. 4c). For vinculin we were not able to show robust effects of either location or orientation separately on stably bound clusters within FAs (Fig. 4d,e), although there is some indication that the number of stably bound vinculin clusters might be larger at parallel compared to at pointing FAs. Categorising FAs on the basis of both location and orientation, seems to be more informative. Focusing exclusively on parallel

FAs, the total surface area covered by stably bound vinculin cluster(s) at FAs close to the adherent membrane edge was significantly larger than at FAs with a more inward position (Fig. 4f, outer and parallel vs inner and parallel p = 0.04 in two-sided Mann Whitney test). Looking at these same FAs there was also a trend towards larger sizes for individual stably bound vinculin clusters at outer and parallel FAs compared inner and parallel FAs (p = 0.12). Additionally, there was a trend towards larger individual vinculin clusters at inner and pointing compared to inner and parallel FAs (p = 0.16). For paxillin it appears that the above mentioned trend towards a smaller surface area covered by stably bound paxillin cluster(s) at pointing versus parallel FAs is mainly due to the effects seen at FAs close to the adherent membrane edge (outer and pointing vs outer and parallel FAs p = 0.14).

Effects of membrane dynamics on stably bound paxillin clusters

To further investigate the biological significance of the stably bound clusters we examined the correlation between membrane dynamics and stably bound paxillin clusters within FAs for a small data set for which we had timelapse data available (n= 48 FAs closest to a protruding membrane edge and 28 FAs nearest a retracting membrane edge). We observed a trend towards an increased number of stably bound areas for FA at retracting edges compared to at protruding edges (p = 0.12, two-sided Mann Whitney test) while all other cluster parameters seemed unaffected.

Discussion

Here we present a novel assay to specifically visualise the spatial distribution of stably associated proteins. A strong advantage of this new technique, over for example bleaching a single FA and following its recovery, is that the location of a stably bound fraction can be directly visualised. Moreover, the entire FA remains visible as converted (switched) proteins in the dynamic and mobile pools exchange with unconverted proteins. We successfully applied this assay to paxillin and vinculin in living cells. This revealed that stably bound paxillin and vinculin are accumulated in small clusters. Paxillin clusters are smaller than vinculin clusters (Fig. 2d and Fig. 6a). This indicates that paxillin clusters are more concentrated than vinculin clusters, since we previously showed through FRAP experiments that both have stably bound fractions of similar size (Chapter 2), This higher paxillin concentration may be caused by paxillin directly binding to integrins, which during the early phases of FA complex formation strongly cluster together. A recent study found this clustering to be even more pronounced than previously thought, with active and inactive integrins forming discrete
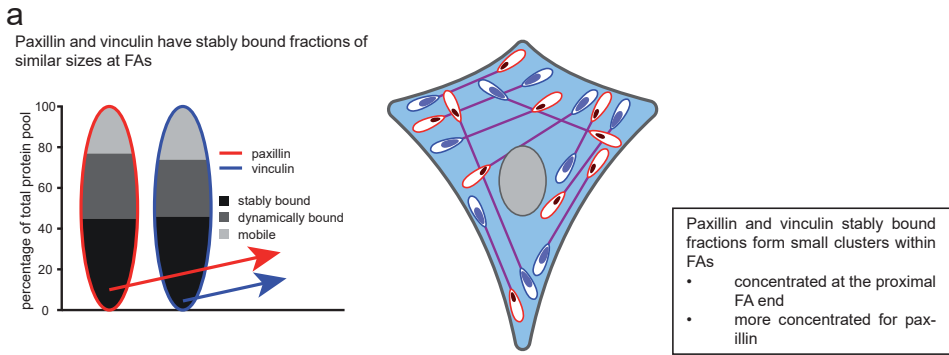
a

Paxillin and vinculin have stably bound fractions of
similar sizes at FAs

Paxillin and vinculin stably bound
fractions form small clusters within
FAs
- concentrated at the proximal
FA end
- more concentrated for pax-
illin

Figure 6. Schematic overview of the data.
(a) Left: Model showing the ratio between the 3 dynamic fractions, stably bound, dynamically bound and mobile protein for paxillin and vinculin as we previously showed by fitting experimental FRAP curves to curves generated by computer-based simulations (Chapter 2). Right: Schematic model of the location of stably bound paxillin and vinculin within FAs as revealed by the photoconversion assay. Stably bound paxillin and vinculin form small clusters that are most often located at the proximal FA end, for paxillin these cluster are more concentrated than for vinculin.

nanoclusters[31]. Conversely, vinculin directly binds to force-bearing F-actin potentially pulling the vinculin clusters further apart, which we observed using the novel assay. Within this context it is interesting that for pointing FAs the paxillin and vinculin small clusters are mostly located at the proximal half of the FA, the side of the FA where the F-actin stress fibre also enters. This ties in well with a previous study showing inactive vinculin is enriched at the FA tip closest to the edge of the ventral membrane, while active vinculin is enriched at the proximal tip, since activated vinculin is known to be more stably associated[32,33]. In any case we thus show that while paxillin and vinculin proteins are evenly distributed along the FA, their stably bound fractions form small clusters within the FA-complex, most frequently at its proximal end.

In the current study the robust effects of FA location and orientation on FA protein dynamics we showed previously (Chapter 2), were not replicated in their effects on stably bound paxillin or vinculin clusters within FAs. Nonetheless, we did find that the total surface area covered by stably bound vinculin cluster(s) within parallel FAs was significantly larger if they were located close to the membrane edge compared to if they had a more inward position (Fig. 4f, vinculin outer and parallel vs. inner and parallel, p = 0.04 two-sided Mann Whitney test). In the analyses of the data on individual stably bound vinculin clusters we also observed a trend towards smaller clusters at the inner parallel FAs, both in comparison to parallel FAs with a more outward position (outer and parallel vs. inner and parallel, p = 0.12), as well as in comparison to FAs with a similar inward position but with a pointing orientation (inner and parallel vs. inner and pointing, p = 0.16) For paxillin there was a trend towards a larger surface area

covered by paxillin stably bound clusters at parallel FAs compared to at pointing FAs (p = 0.11), which seemed to be mainly due to the effects of the outer FAs (outer and pointing vs outer and parallel p = 0.14). All these observations fit with the previously observed effects of FA location and orientation on paxillin and vinculin dynamics, in the sense that in the FRAP experiments for paxillin the largest differences were also observed between outer parallel and outer inner FAs (although these differences were in the k_{on} of the dynamic fraction rather than the stably bound fraction) and for vinculin there were differences in the stably bound fractions of both outer and parallel vs inner and parallel and between inner and pointing and inner and parallel FAs (Chapter 2). The observation of mainly trends in the different analyses (rather than statistically significant differences in the individual analyses) does not necessarily indicate that FA location and orientation do not affect the stably bound clusters. Instead, this may partially be due to the uneven distribution over the different groups of the FAs selected for photoswitching, for paxillin especially nearly three-quarter (74%) of the switched FAs are outer as this includes the original proof of concept data for which outer FAs were preferentially selected to minimize the potential of proteins outside the FA being switched. Despite this, some interesting trends are observed, next to the finding that the total surface area covered by stably bound vinculin cluster(s) within outer and parallel FAs is larger than at inner and parallel FAs, indicating this area warrants further investigation.

Our data on the correlation between membrane dynamics and stably bound paxillin clusters (Fig. 5), gave some interesting hints towards the significance of stably bound clusters within FAs to cellular behaviour or vice versa. The small size of the data sets for which we had timelapse data available (n = 48 at protruding and 28 FAs at retracting membrane edges) limited statistical analysis, however, there is an interesting statistical trend towards an increased number of stably bound clusters observed at FAs at retracting membrane edges compared to protruding edges. Both the relatively low p-value of 0.12 (two-sided Mann Whitney test) and the skewedness of the retracting dataset (Fig. 5b,c) warrants further investigation and suggests that in a larger dataset the number of stably bound paxillin clusters might be found to be significantly increased at FAs at retracting membranes, perhaps specifically at FAs with a certain location or orientation. In the current data set the other stably bound paxillin area parameters correlate much less strongly with membrane dynamics, suggesting the observed trend towards a larger number of paxillin clusters within FAs at retracting membrane edges reflects the separation of (one of the) existing stably bound paxillin clusters at these FAs, rather than the formation of a new cluster.

In summary, we presented and applied a novel assay to specifically visualise

the spatial distribution of stably associated proteins within macromolecular complexes in living cells. We showed that while paxillin and vinculin are distributed evenly throughout FAs, their stably bound fractions form small clusters within the FA-complex. These clusters were most frequently observed at the proximal FA end, the FA end where the F-actin stress fibre also enters and are significantly more concentrated for paxillin than for vinculin. The effects of FA orientation and location on stably bound paxillin and vinculin clusters were more subtle than their effects on FA protein dynamics in general, although the total surface area covered by stably bound vinculin cluster(s) within outer parallel FAs was larger than at parallel FAs with a more inward position.

Materials and Methods

Cell culture

U2OS cells were cultured in phenol-red free DMEM (Lonza) at 37°C and 5% CO_2. Culture medium was supplemented with 10% FCS (Gibco), 2mM L-glutamine (Lonza), 100 U/ml Penicillin and 100 μg/ml Streptomycine (Lonza) and to maintain stable cell lines with 100 μg/ml G418. Transfections were performed using Fugene (Promega), followed by selection with G418 when creating stable cell lines. For experiments 24 mm round glass coverslips were coated overnight at 4°C with PureCol bovine collagen type I (Advanced Biomatrix) at a final concentration of 10 μg/ml. Cells were plated onto coated coverslips 24-48h prior to imaging, for photoconversion experiments the medium was replaced ~1h prior to imaging with FluoroBrite DMEM (Thermo Fisher Scientific) to minimize autofluorescence.

Constructs

The paxillin-mMaple3 plasmid was based on the paxillin-mTurquoise (Addgene 55573). This vector uses the multiple cloning site as a linker region between the protein and mTurquoise, hampering a simple colour swap. To still allow sticky-end ligation the protein, fluorescent label and empty vector backbone were all separately isolated as restriction fragments. These were ligated using sticky ends in 2 steps: 1) the protein to the fluorescent label and 2) the created insert into the vector backbone. This strategy was applied to create paxillin-mMaple3:

The vector backbone was isolated from paxillin-mTurquoise as a BamHI NotI fragment and paxillin as a HindIII BamHI fragment. The mMaple3 was isolated from zyxin-mMaple3 (Addgene 101151) through PCR with primers GCAGAAC-CATCTCCCACAATGAC (FW) and CAAACTGAGGATGGAGGGCAAC (RV), the mMaple was isolated from the PCR product as an HindIII NotI product.

The paxillin was ligated to the mMaple3 which was then inserted into the vector backbone.

To create vinculin-mMaple3 the GFP in Vinculin-GFP (described in chapter 2) was replaced with mMaple3 from paxillin-mMaple3 as an EcoRI NotI fragment.

All constructs were checked through sequencing, no mutations were found.

Photoconversion experiments

Imaging

All photoconversion data was acquired on a Zeiss Elyra PS1 system equipped with a LSM 780 confocal unit set to confocal mode and using a 63x 1.4NA or a 100x 1.49NA oil immersion objective. For excitation a 561nm/488nm laser was used, the emission filters were set to 578-665nm/490-525nm for the green/cyan channel respectively, with a pinhole size of 59 μm and line averaging set to 4. For each experiment 2 images were taken of the green and red channel (t_{pre}), followed by the photoconversion of 1-2 FAs by exposing a small rectangle drawn tightly around the FA(s) to 25 iterations of low intensity 405nm laser light using the FRAP mode of the Zen software, immediately followed by the acquisition of another 2 images for both channels (t_0) and the starting of a stopwatch. When the stopwatch showed 3 minutes had passed another 2 images of both channels were acquired (t_{post}). For U2OS cells expressing paxillin-mMaple3 189 FAs were photoconverted from 153 cells, for U2OS cells expressing vinculin-mMaple3 98 FAs from 84 cells.

Data analysis

Data was analysed in the ImageJ software package in the Fiji framework, using a series of home-made macros. Firstly we made 'ratio view' (RV) images, where a fire-LUT was used to show on a pixel by pixel basis the ratio of the average intensity of the red signal for the two images taken at t_{post} over the average red signal for the two images taken at t_0 (RVimage=$I_{avgredpost}/I_{avgredt0}$). The fire-LUT was only applied to pixels that at t_{pre} in the green channel had an above-threshold value (variable threshold depending on the intensity of the background cytoplasmic signal), reliably selecting FAs and a limited number of relatively high intensity background cytoplasmic pixels. Next we saved the FAs as ROIs using the Fiji build-in dynamic 'moments' threshold on an average projection of the green channel at t_{pre} and differentiated between high (stably bound) and low (dynamically bound) ratio pixels by applying this same dynamic threshold to the RV image. This visualised the stably and dynamically bound fractions of the protein separately. To determine whether the stably bound fractions of paxillin

and/or vinculin concentrated into specific areas of the FA, we used Fiji's build-in 'analyse particles' on the thresholded RV images to group together any above threshold pixels together covering a surface area of at least 0.05 μm^2 and saved these as ROIs. For further analysis these ROIs were read into R using the Rstudio (R development Core Team, 2016), with custom-written R-scripts we plotted for each FA the ROI(s) corresponding to the stably bound area(s) in (shades of) red and the ROI corresponding to the rest of the FA in green, for easy comparison between FAs these plots are rotated relative to a virtual membrane to the left of these plots based on the orientation of the FA relative to the closest ventral membrane edge in the cell.

Classification of FAs

To examine the effects of FA location and/or orientation all FAs were classified. FAs were classified as 'outer' when they were located close to the ventral (adherent) membrane edge. FAs were classified as 'inner' when they were located further inwards, with another FA located between them and the closest membrane edge. FAs were classified as 'pointing' when they were orientated with their long axis 'perpendicular' (*i.e.* 90° ± 30°) to the closest ventral membrane edge. FAs were classified as 'parallel' when they were orientated with their long axis 'parallel' (*i.e.* 180° ± 30°) to the closest membrane edge. FAs outside these boundaries were discarded in these analyses. Of the FAs selected for the photoconversion experiments for paxillin 13 of 189 FAs (7%) and for vinculin 1 of 98 FAs (1%) were discarded from analyses involving FA orientation for these reasons.

Statistical analysis

For analyses of the differences between two groups two-tailed Mann-Whitney *U* tests were used. For analyses of the differences between more than two groups two-tailed Kruskall-Wallis Rank Sum tests were used, if this generated a p-value < 0.05 the specific groups with significant differences were determined using two-tailed Mann-Whitney *U* tests. To curtail the number of Mann Whitney *U* tests to be performed on the data separated based on FA location and orientation into four groups only the differences between meaningful combinations were analysed limiting the number of tests to 4 per parameter: outer pointing versus inner pointing, outer parallel versus inner parallel, outer pointing versus outer parallel and inner pointing versus inner parallel.

Author contributions

K.L. designed and performed microscopy experiments and wrote the manuscript; B.G. designed photoconversion analysis software and performed the analyses;

J.A.S. designed and wrote the photoconversion analysis software; A.B.H. supervised the project, contributed to method and analysis development, supervised writing the manuscript and revised it.

References

1   Yamada, K. M. & Geiger, B. Molecular interactions in cell adhesion complexes. *Current opinion in cell biology* **9**, 76-85 (1997).

2   Geiger, B., Bershadsky, A., Pankov, R. & Yamada, K. M. Transmembrane crosstalk between the extracellular matrix--cytoskeleton crosstalk. *Nature reviews. Molecular cell biology* **2**, 793-805, doi:10.1038/35099066 (2001).

3   Zaidel-Bar, R., Itzkovitz, S., Ma'ayan, A., Iyengar, R. & Geiger, B. Functional atlas of the integrin adhesome. *Nature cell biology* **9**, 858-867, doi:10.1038/ncb0807-858 (2007).

4   Winograd-Katz, S. E., Fassler, R., Geiger, B. & Legate, K. R. The integrin adhesome: from genes and proteins to human disease. *Nature reviews. Molecular cell biology* **15**, 273-288, doi:10.1038/nrm3769 (2014).

5   Wahl, S. M., Feldman, G. M. & McCarthy, J. B. Regulation of leukocyte adhesion and signaling in inflammation and disease. *Journal of leukocyte biology* **59**, 789-796 (1996).

6   Maartens, A. P. & Brown, N. H. The many faces of cell adhesion during Drosophila muscle development. *Developmental biology* **401**, 62-74, doi:10.1016/j.ydbio.2014.12.038 (2015).

7   Laukaitis, C. M., Webb, D. J., Donais, K. & Horwitz, A. F. Differential dynamics of alpha 5 integrin, paxillin, and alpha-actinin during formation and disassembly of adhesions in migrating cells. *The Journal of cell biology* **153**, 1427-1440 (2001).

8   Webb, D. J. *et al.* FAK-Src signalling through paxillin, ERK and MLCK regulates adhesion disassembly. *Nature cell biology* **6**, 154-161, doi:10.1038/ncb1094 (2004).

9   Wiseman, P. W. *et al.* Spatial mapping of integrin interactions and dynamics during cell migration by image correlation microscopy. *Journal of cell science* **117**, 5521-5534, doi:10.1242/jcs.01416 (2004).

10   Choi, C. K. *et al.* Actin and alpha-actinin orchestrate the assembly and maturation of nascent adhesions in a myosin II motor-independent manner. *Nature cell biology* **10**, 1039-1050, doi:10.1038/ncb1763 (2008).

11   Pasapera, A. M., Schneider, I. C., Rericha, E., Schlaepfer, D. D. & Waterman, C. M. Myosin II activity regulates vinculin recruitment to focal adhesions through FAK-mediated paxillin phosphorylation. *The Journal of cell biology* **188**, 877-890, doi:10.1083/jcb.200906012 (2010).

12   Bakolitsa, C. *et al.* Structural basis for vinculin activation at sites of cell adhesion. *Nature* **430**, 583-586, doi:10.1038/nature02610 (2004).

13   Jones, P. *et al.* Identification of a talin binding site in the cytoskeletal protein vinculin. *The Journal of cell biology* **109**, 2917-2927 (1989).

14   Turner, C. E. & Miller, J. T. Primary sequence of paxillin contains putative SH2 and SH3 domain binding motifs and multiple LIM domains: identification of a vinculin and pp125Fak-binding region. *Journal of cell science* **107 (Pt 6)**, 1583-1591 (1994).

15   Brown, M. C., Perrotta, J. A. & Turner, C. E. Identification of LIM3 as the principal determinant of paxillin focal adhesion localization and characterization of a novel motif on paxillin directing vinculin and focal adhesion kinase binding. *The Journal of cell biology* **135**, 1109-1123 (1996).

16   Humphries, J. D. *et al.* Vinculin controls focal adhesion formation by direct interactions with talin and actin. *The Journal of cell biology* **179**, 1043-1057, doi:10.1083/jcb.200703036 (2007).

17   McGregor, A., Blanchard, A. D., Rowe, A. J. & Critchley, D. R. Identification of the vinculin-binding site in the cytoskeletal protein alpha-actinin. *The Biochemical journal* **301 (Pt 1)**, 225-233 (1994).

18   Brindle, N. P., Holt, M. R., Davies, J. E., Price, C. J. & Critchley, D. R. The focal-adhesion vasodilator-stimulated phosphoprotein (VASP) binds to the proline-rich domain in vinculin. *The Biochemical journal* **318 (Pt 3)**, 753-757 (1996).

19   Gertler, F. B., Niebuhr, K., Reinhard, M., Wehland, J. & Soriano, P. Mena, a relative of VASP and Drosophila Enabled, is implicated in the control of microfilament dynamics. *Cell* **87**, 227-239 (1996).

20   Reinhard, M., Rudiger, M., Jockusch, B. M. & Walter, U. VASP interaction with vinculin: a recurring theme of interactions with proline-rich motifs. *FEBS letters* **399**, 103-107 (1996).

21   Barsony, J. & Marx, S. J. Immunocytology on microwave-fixed cells reveals rapid and agonist-specific changes in subcellular accumulation patterns for cAMP or cGMP. *Proceedings of the National Academy of Sciences of the United States of America* **87**, 1188-1192 (1990).

22   Neher, E. & Augustine, G. J. Calcium gradients and buffers in bovine chromaffin cells. *The Journal of physiology* **450**, 273-301 (1992).

23   Ponti, A., Machacek, M., Gupton, S. L., Waterman-Storer, C. M. & Danuser, G. Two distinct actin networks drive the protrusion of migrating cells. *Science (New York, N.Y.)* **305**, 1782-1786, doi:10.1126/science.1100533 (2004).

24   Nikolaev, V. O., Bunemann, M., Schmitteckert, E., Lohse, M. J. & Engelhardt, S. Cyclic AMP imaging in adult cardiac myocytes reveals far-reaching beta1-adrenergic but locally confined beta2-adrenergic receptor-mediated signaling. *Circulation research* **99**, 1084-1091, doi:10.1161/01.RES.0000250046.69918.d5 (2006).

25   Lynch, M. J., Baillie, G. S. & Houslay, M. D. cAMP-specific phosphodiesterase-4D5 (PDE4D5) provides a paradigm for understanding the unique non-redundant roles that PDE4 isoforms play in shaping compartmentalized cAMP cell signalling. *Biochemical Society transactions* **35**, 938-941, doi:10.1042/bst0350938 (2007).

26   Dixit, N. & Simon, S. I. Chemokines, selectins and intracellular calcium flux: temporal and spatial cues for leukocyte arrest. *Frontiers in immunology* **3**, 188, doi:10.3389/fimmu.2012.00188 (2012).

27   Mehta, S. *et al.* Calmodulin-controlled spatial decoding of oscillatory Ca2+ signals by calcineurin. *eLife* **3**, e03765, doi:10.7554/eLife.03765 (2014).

28   van Unen, J. *et al.* Plasma membrane restricted RhoGEF activity is sufficient for RhoA-mediated actin polymerization. *Scientific reports* **5**, 14693, doi:10.1038/srep14693 (2015).

29   McEvoy, A. L. *et al.* mMaple: a photoconvertible fluorescent protein for use in multiple imaging modalities. *PloS one* **7**, e51314, doi:10.1371/journal.pone.0051314 (2012).

30   Wang, S., Moffitt, J. R., Dempsey, G. T., Xie, X. S. & Zhuang, X. Characterization and development of photoactivatable fluorescent proteins for single-molecule-based superresolution imaging. *Proceedings of the National Academy of Sciences of the United States of America* **111**, 8452-8457, doi:10.1073/pnas.1406593111 (2014).

31   Spiess, M. *et al.* Active and inactive beta1 integrins segregate into distinct nanoclusters in focal adhesions. *The Journal of cell biology* **217**, 1929-1940, doi:10.1083/jcb.201707075 (2018).

32   Cohen, D. M., Kutscher, B., Chen, H., Murphy, D. B. & Craig, S. W. A conformational switch in vinculin drives formation and dynamics of a talin-vinculin complex at focal adhesions. *The Journal of biological chemistry* **281**, 16006-16015, doi:10.1074/jbc.M600738200 (2006).

33   Case, L. B. *et al.* Molecular mechanism of vinculin activation and nanoscale spatial organization in focal adhesions. *Nature cell biology* **17**, 880-892, doi:10.1038/ncb3180 (2015).

3

Supplementary Figures

S1
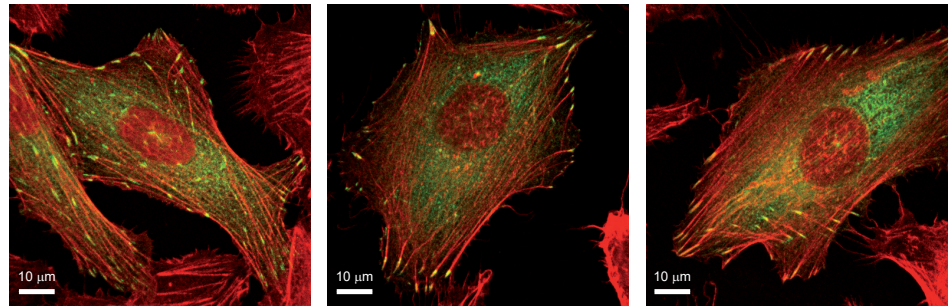
Supplementary Fig. S1 F-actin fibres enter pointing FAs at their proximal ends.
Overlay images of U2OS cells stably expressing paxillin-GFP (green) stained with phalloidin-CF405
to highlight the F-actin (red).

3

Chapter 4

Growth factor dependent changes in nanoscale architecture of focal adhesions

Karin Legerstee[1], Tsion E. Abraham[1],Wiggert A. van Cappellen[1], Alex Nigg[1], Johan A. Slotman[1] and Adriaan B. Houtsmuller[1]

1 Erasmus Medical Centre Rotterdam, Department of Pathology, Optical Imaging Centre, Rotterdam, The Netherlands.

Abstract

Focal adhesions (FAs) are flat elongated structures that mediate cell migration and link the cytoskeleton to the extracellular matrix. Along the vertical axis FAs were shown to be composed of three layers. We used structured illumination microscopy to examine the longitudinal distribution of four hallmark FA proteins, which we also used as markers for these layers. At the FA ends pointing towards the adherent membrane edge (heads), bottom layer protein paxillin protruded, while at the opposite ends (tails) intermediate layer protein vinculin and top layer proteins zyxin and VASP extended further. At the tail tips, only intermediate layer protein vinculin protruded. Importantly, head and tail compositions were altered during HGF-induced scattering with paxillin heads being shorter and zyxin tails longer. Additionally, FAs at protruding or retracting membrane edges had longer paxillin heads than FAs at static edges. These data suggest repositioning of layers along FAs is involved in cell movement.

4

Introduction

Focal adhesions (FAs) are the main cellular structures linking the intracellular cytoskeleton to the extracellular matrix (ECM). They are flat elongated structures 1-2 µm long, 300-500 nm wide and 200-300 nm thick[1,2]. On the membrane-facing side the main FA components are integrins, transmembrane receptors directly binding to the extracellular matrix (ECM). A specialised form of actin linked to contractile myosin-II forms the edge of the FA on the cytoplasm-facing side. FAs experience force, the strength of which depends on the combination of myosin-II contractility and the stiffness of the ECM. Because of their importance in cell adhesion and to the transmission of force from the cell to the extracellular matrix, FAs are crucial to most types of cell migration, including in vitro over a 2D surface, like the coverslips used in microscopic studies. Migration and adhesion in turn are key cellular functions required for many physiological and pathophysiological processes, like embryological development, the functioning of the immune system and also cancer, in particular metastasis[3-5]. A large and diverse intracellular macromolecular protein assembly is present between integrins and actin, with over 200 different reported proteins[4,6]. These include (trans)membrane receptors, adaptor proteins and many different signalling proteins such as kinases, phosphatases and G-protein regulators, which through post-translational modifications add significantly to FA complexity.

It is well established that these diverse proteins are not randomly distributed along the z-axis of the FA but form a layered nanostructure. A seminal study revealed the presence of three different layers: (1) the so-called integrin signalling layer (ISL) closest to the adherent membrane (within ~10-20 nm) which includes the cytoplasmic tails of the transmembrane integrin receptors, focal adhesion kinase and paxillin, (2) the actin-regulatory layer (ARL) at the top, where mainly directly actin-binding proteins such as zyxin, vasodilator-stimulated phosphoprotein (VASP) and α-actinin are found and (3) the force transduction layer (FTL) in between (from ~10-20 to ~50-60nm from the adherent membrane) of which talin is the most well-known protein and which is also where vinculin is found[7]. Later studies, using different techniques, confirmed the layered nanostructure of FAs along the z-axis[8-10].

Here we used the enhanced resolution provided by Structured Illumination Microscopy (SIM) to further examine the layered structure[11]. We selected four hallmark FA proteins to serve as markers for these layers: the large scaffold proteins paxillin (bottom ISL layer) and vinculin (middle FTL layer), and two FA proteins that are closely linked to the actin associated with FAs, zyxin and VASP (top ARL layer). As adaptor proteins, paxillin and vinculin are among the proteins with the
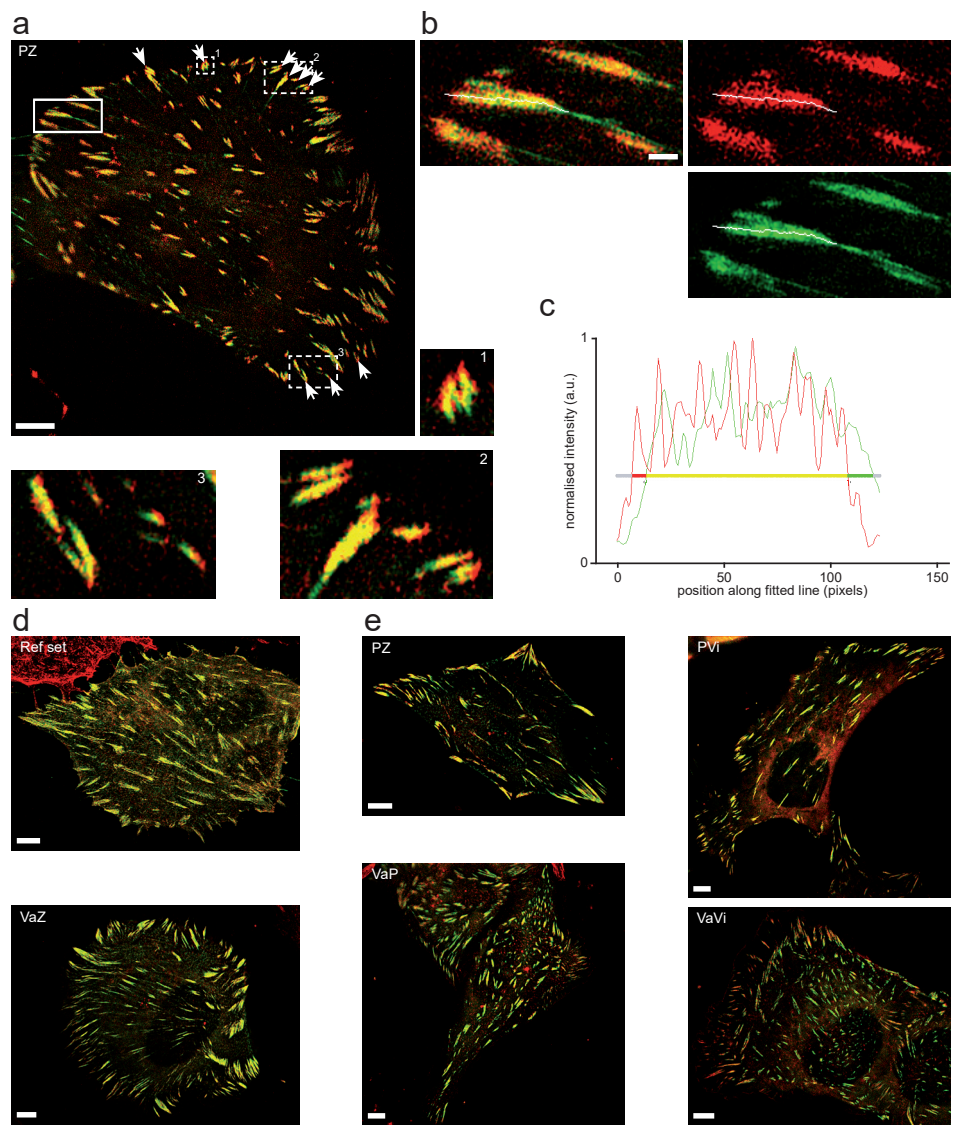
4

Figure 1. Measuring FA head and tail lengths using structured illumination microscopy.
(a) Representative merged SIM image of a U2OS cell co-expressing paxillin-mCherry and zyxin-GFP. Arrows indicate FAs with paxillin heads and zyxin tails. Numbered panels: magnifications of the corresponding dashed boxed areas. Scale bar 5 μm. **(b)** Magnification of the boxed area in a of the merged (left), red (right, top) and green (right, bottom) channels. The white line was automatically fit to the longitudinal axis of the FA (see Materials and Methods). Scale bar 1 μm. **(c)** Intensity profiles of the red and the green channels as measured along the line indicated in b, normalised to maximum values. The horizontal line indicates the threshold (40% of maximum intensity, see Materials and Methods). Yellow indicates that both signals are above threshold; red indicates that only the red channel is above threshold; green indicates only the green channel is above threshold; grey indicates both channels are below threshold. **(d)** Top panel: representative merged SIM image of U2OS cells co-expressing paxillin-mCherry and paxillin-GFP. Bottom panel: representative merged SIM image

of U2OS cells co-expressing two proteins from the same FA z-layer: VASP-mCherry and zyxin-GFP. Scale bar 5 µm. **(e)** Representative merged SIM image of U2OS cells co-expressing the indicated protein combinations (P: Paxillin, Vi: Vinculin, Va: VASP, Z: Zyxin), where the first is mCherry-tagged and the second is GFP-tagged. Scale bar 5 µm.

most potential binding partners within FAs[6]. In line with their linking, structural, role they are amongst the first proteins to be recruited to assembling FA complexes, especially the directly integrin-binding paxillin[12-16]. Unlike paxillin, vinculin can also directly bind actin filaments as well as the actin-binding proteins α-actinin and the ENA/VASP-proteins[17-24]. Zyxin and VASP are recruited to assembling FAs at much later stages than paxillin or vinculin and are more closely linked to actin[15]. In response to mechanical cues and during TGF-β induced EMT zyxin, VASP and vinculin stimulate actin polymerisation in a co-dependent manner[25-31].

We also studied the effect of increased cellular movement (scattering) on FA nanostructure by stimulating cells with Hepatocyte growth factor (HGF). HGF is known for its involvement in cancer, in particular for its promotion of metastasis through a variety of mechanisms, including strong increases in cell motility[32-37]. Thus, stimulation with HGF strongly increases the motility of cells in both 2D and 3D environments[35,38-40].

Results

The study presented here was motivated by observations we made in pilot experiments using dual colour superresolution (SIM) to visualise the distribution of paxillin-mCherry and zyxin-GFP within focal adhesions. We noted that in many FAs the central part, where paxillin and zyxin colocalised (yellow), was flanked by paxillin (red) at the FA end pointing towards the edge of the adherent membrane, further referred to as 'head', and by zyxin (green) at the opposite end, further referred to as 'tail' (Fig. 1a, arrows). We hypothesised that the observed shift along the long FA axis could be due to the fact that paxillin and zyxin are found in different FA z-layers (see Introduction), which may move with respect to each other during FA function. Therefore, we selected next to paxillin (bottom ISL layer) and zyxin (top ARL layer), two other hallmark FA proteins: VASP which is in the same layer as zyxin, and vinculin which resides in the middle FTL layer. We then used the enhanced resolution of structured illumination microscopy (SIM) to study their distribution within focal adhesions, in both live and chemically fixed cells. Fluorescently tagged constructs of these proteins were previously characterised and shown to be fully functional[7]. They were co-expressed in pairs in human bone cancer (U2OS) cells where they target to FAs, highlighting these in red (mCherry) and green (GFP) fluorescence (Fig. 1d,e, supplemental Fig. S1, S2).
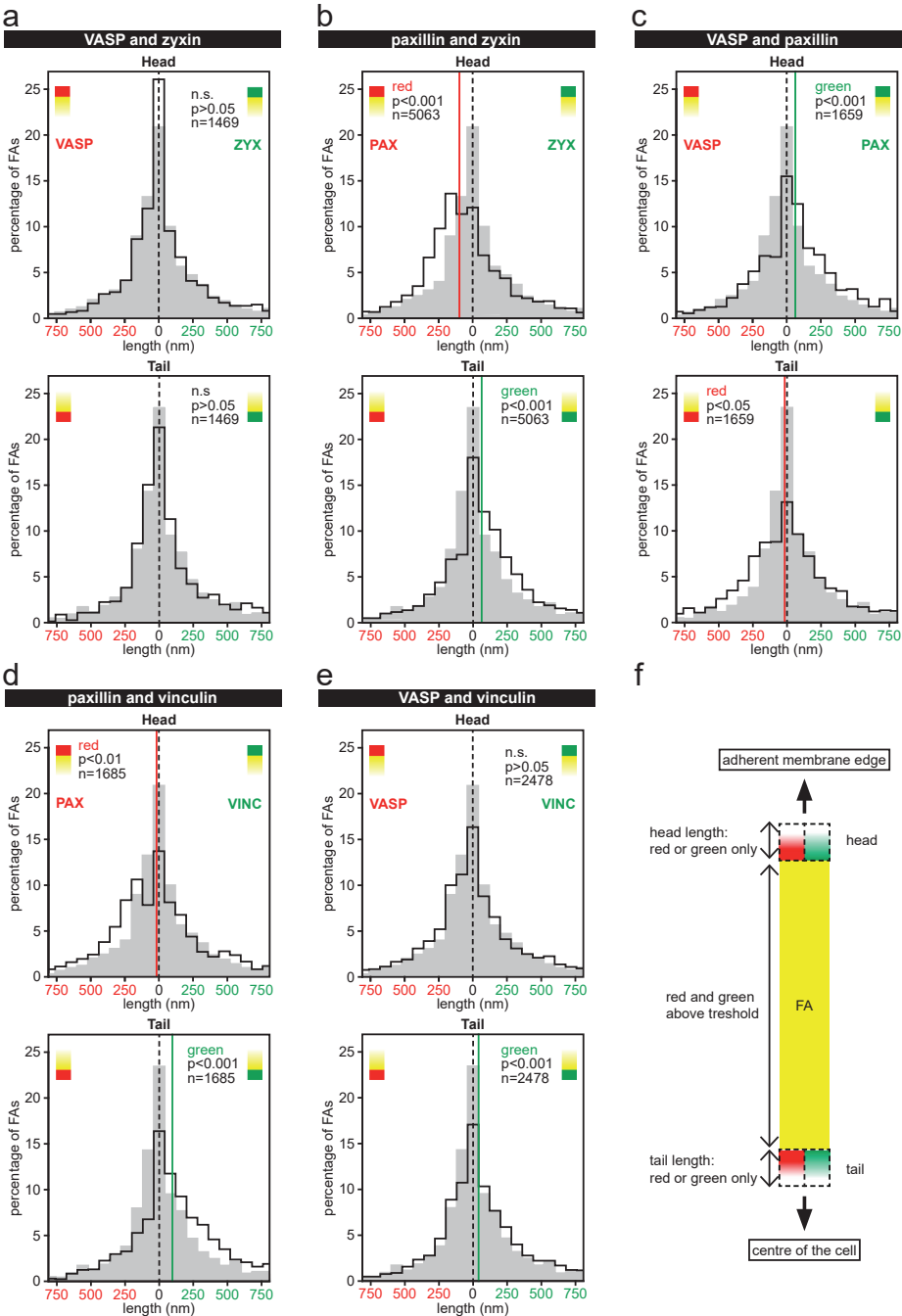
4

Figure 2. Histograms of the distribution of head and tail protrusion lengths.
(a-e) Histograms of FA head and tail protrusion lengths for the indicated protein pairs co-expressed in U2OS cells. Red protrusion lengths are plotted from right to left (analogous to negative values) and green from left to right. The histogram of the reference set, co-expressing mCherry and GFP-tagged

versions of paxillin in U2OS cells, is shown in grey. P-values generated by comparison of the experimental histogram and the reference histogram (grey) (two-sided Mann Whitney U tests), n represents the number of analysed FAs. Vertical lines: median protrusion lengths. Number of imaged cells from a to e: 15, 52, 17, 18 and 23. **(f)** Schematic representation of an FA in the two colour SIM images clarifying the method

To quantitatively study the distribution of pairs of the selected proteins along the long axes of focal adhesions, we developed a semi-automated method (see Materials and Methods). Briefly, in this method a line is fitted along the long axis of FAs and signal intensities for the proteins under investigation are determined along that line (Fig. 1b,c). Next, the head and tail protrusion lengths are determined. To calibrate the method we generated a reference set of 1630 FAs in 16 U2OS cells co-expressing paxillin-GFP and paxillin-mCherry (supplemental Fig. S1). Although mCherry- and GFP-tagged paxillin molecules are expected to be equally distributed within FAs, small apparent protrusion lengths were measured both at the heads and at the tails. These are due to noise and differences in signal-to-noise in the red and green channel (Fig. 1c). We subsequently generated two histograms, one of the distribution of apparent head and one of apparent tail protrusion lengths: green protrusion lengths were plotted from left to right and red protrusion lengths from right to left ('negative' green protrusion lengths). These two reference histograms were used to compare histograms generated in the same way from dual colour imaging the different FA-protein protein pairs. If, for example, the red stained protein protrudes at the tail, the histogram of tail protrusions will be shifted to the left. This shift then represents the median tail protrusion length (see Materials and Methods; Fig. 2a-e, grey distributions).

We first performed dual colour imaging SIM experiments on U2OS cells expressing the two FA proteins present in the same z-layer (top ARL-layer), zyxin-GFP and VASP-mCherry and generated histograms of the distribution of head and tail protrusions. No statistically significant difference was found between these histograms and the reference histograms (Fig. 2a), indicating that zyxin and VASP are similarly distributed along the FA. We then imaged each of these in combination with paxillin (bottom ISL-layer), expecting similar results in both combinations. Paxillin-mCherry and zyxin-GFP showed significantly shifted histograms indicating the presence of paxillin head protrusions and zyxin tail protrusions (Fig. 2b). As expected, similar results were obtained for paxillin-GFP and VASP-mCherry, *i.e.* paxillin head protrusions and VASP tail protrusions (Fig. 2c). Note that the use of paxillin-GFP in one, and paxillin-mCherry in the other experiment (colour swap), demonstrated that protrusion measurements are not influenced by difference in imaging red or green dyes, nor by differences in the photo-physical properties of these dyes. Paxillin-mCherry and Vinculin-GFP also showed significantly shifted histograms indicating paxillin head protrusions and

vinculin tail protrusions (Fig. 2d). When VASP-mCherry and vinculin-GFP were co-expressed, no significant head protrusions were observed (*i.e.* the histogram was not statistically different from the reference histogram), but at the tail, vinculin protruded significantly further than VASP (Fig. 2e). In summary, at FA heads paxillin protruded significantly further than vinculin, zyxin or VASP, while these latter three protruded significantly further at the tails with vinculin protruding the furthest.
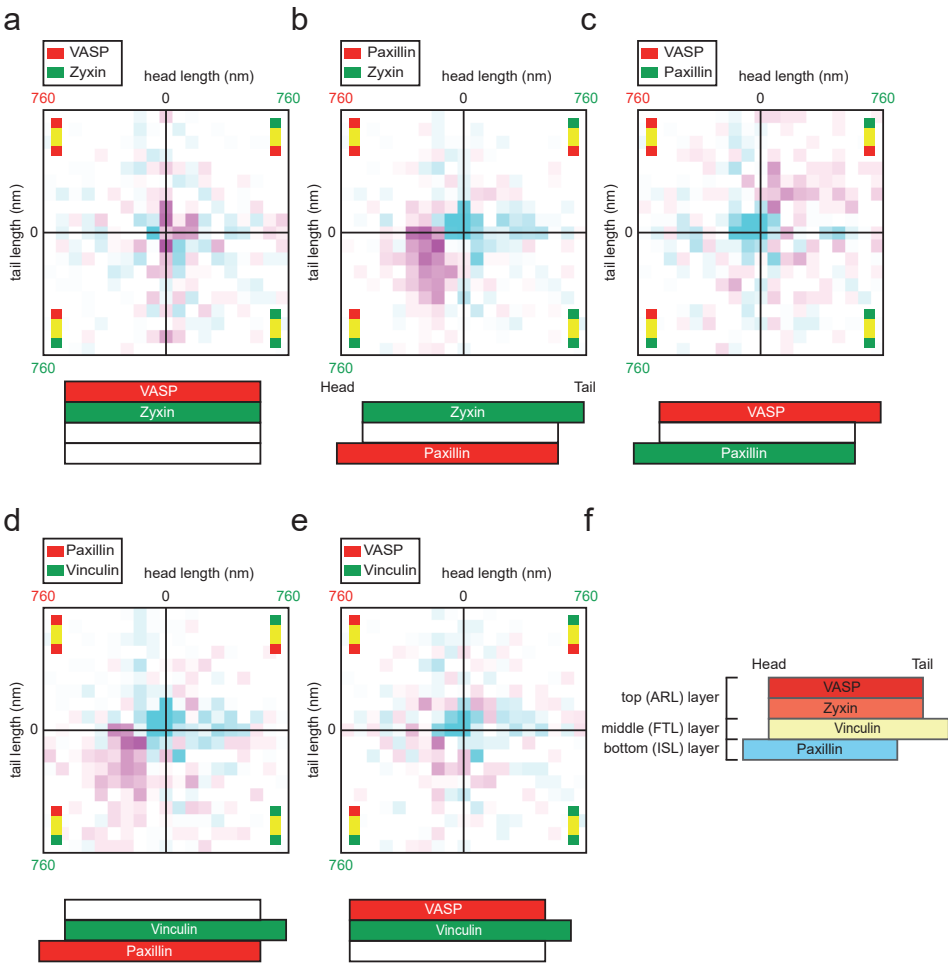

Figure 3. 2D histograms combining the head and tail protrusion lengths of individual FAs
(a-e) The data presented in Fig. 2 shown as 2D-histograms combining both the head (horizontal axis) and the tail (vertical axis) protrusion lengths for each individual FA. Colours represent the difference between the relative distributions of the reference set and the indicated protein pair. White: below threshold (see Materials and Methods), magenta: increase relative to reference set, cyan: decrease relative to reference set. Colour intensity represents magnitude of the change (for scale see Materials and Methods). Cartoons below provide a schematic summary of the data (not to scale). **(f)** A side view model for the longitudinal distribution of proteins along FAs based on the data from the different co-expressed FA protein pairs (not to scale).
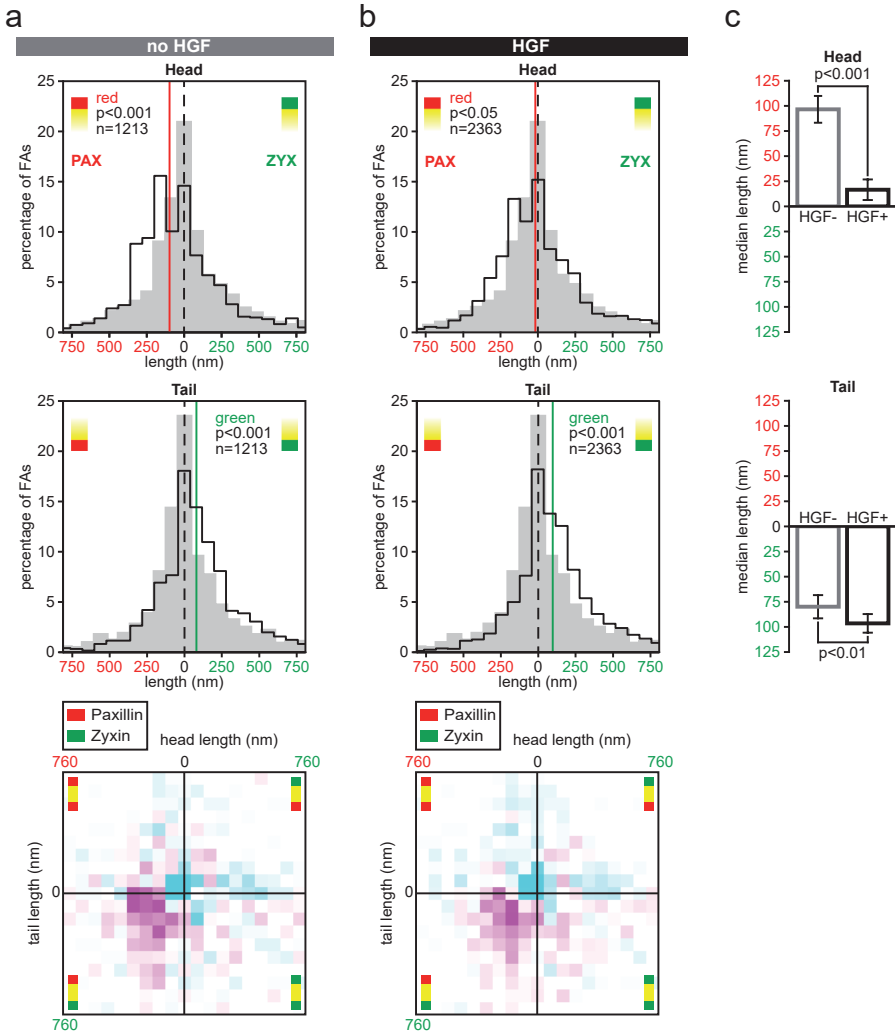
Figure 4. HGF treatment alters the longitudinal distributions of paxillin and zyxin along FAs.
(a) Histograms of head (top) and tail (middle) protrusion lengths for 12 U2OS cells co-expressing pax-illin-mCherry and zyxin-GFP and subjected to overnight serum-starvation. Histograms of protrusion lengths in the reference set shown in grey. P-values generated compared to the reference set (two-sided Mann Whitney *U* tests), n gives number of analysed FAs. Vertical lines: medians. Bottom: 2D-histogram combining head and tail protrusion length for each individual FA. Colours represent the difference compared to the relative distributions of the reference set. White: below threshold, magenta: increase relative to reference set, cyan: decrease relative to reference set. Colour intensity represents magnitude of the difference (for scale and threshold see Materials and Methods). **(b)** Histograms of head (top) and tail (middle) protrusion lengths for 21 U2OS cells co-expressing paxillin-mCherry and zyxin-GFP, subjected to overnight serum-starvation and treated with HGF at least three hours prior to imaging. Grey histograms, vertical lines, n-numbers and statistical tests as above. Bottom: 2D-histogram combining head and tail protrusion length for each individual FA. Colours as above. **(c)** Comparison of head (top) and tail (bottom) protrusion lengths for the serum starved HGF minus (grey) and the serum starved and HGF treated (black) cells, p-values are generated by two-sided Mann Whitney *U* tests.

We subsequently created 2-D histograms of the relative frequencies of com-bined head/tail lengths of individual FAs compared to the reference set (Fig. 3). These provide a visualisation of the relative frequency of the combination of a specific head and tail length compared to the relative frequency at which that combination occurred in the reference set. Values higher than in the reference set are shown in magenta and lower values in cyan. Colour intensity indicates the magnitude of the differences (see Materials and Methods for scale details). The VASP/zyxin protein set showed a distribution similar to the reference set, again indicating neither protein protruded significantly at either FA end (Fig. 3a). In the data sets including paxillin (Fig. 3b-d), the relative frequency of FAs with the combination of none to very short head and tail lengths was decreased compared to the reference set (cyan clusters at the centres of the histograms). The frequency of FAs with paxillin heads in combination with zyxin, vinculin or VASP tails was increased (magenta clusters in the respective quadrants of the histograms). The 2D-histogram of the VASP/vinculin set (Fig. 3e) clearly shows that the frequency of FAs with short head and tail protrusions is reduced (cyan cluster at the centre of the histogram), but the observed increases are small (no dark magenta) and they do not seem to cluster anywhere in the histogram. This is to be expected because neither protein extended significantly at the FA head, and only at the tail vinculin protruded significantly (Fig. 2e). Because there is no preference for either protein at the head, the increased frequency of FAs with vinculin tails is distributed over a large part of the lower half of the histogram, not clustered in a particular quadrant as is the case for the protein sets with paxillin, making the differences at individual bins less pronounced.

FA heads shorten and tails lengthen during scattering

Next, we examined the effect of HGF-induced scattering on the distribution of paxillin and zyxin along FAs. HGF, also known as the scattering factor, induces a scattering response in epithelial cells, including in U2OS cells[35,38-40]. During scattering cells display increased motility and undirected migration. In serum starved cells, not incubated in the presence of HGF (Fig. 4a) the same patterns were seen as before (Fig. 2b, 3b), with paxillin protruding significantly more often at the head and zyxin at the tail. Following HGF-stimulation however, the paxillin enriched head became significantly shorter (p < 0.001) to the point of nearly disappearing, with a length that is only just significantly different from the reference set (p = 0.045, Fig. 4b,c). At the same time, following HGF-treatment the length of the zyxin tail region was significantly increased (p < 0.01) (Fig. 4b,c). In the unstimulated cells the strongest increases in the 2-D histograms were seen further to the left than in the HGF-treated cells, indicating longer paxillin heads in combination with zyxin tails. Thus the differential longitudinal distribution
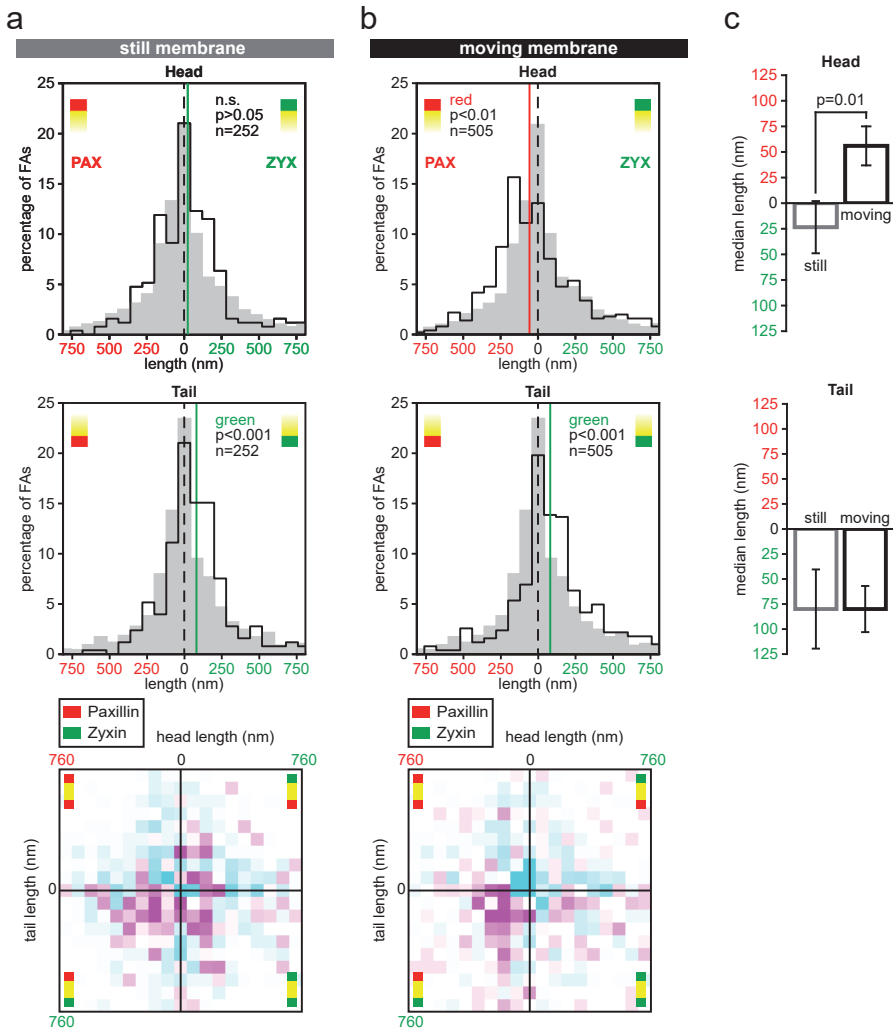
Figure 5. The longitudinal distributions of paxillin and zyxin differ for FAs near static compared to moving membrane edges.
(a) Histograms of head (top) and tail (middle) protrusion lengths for FAs near static membrane edges (not protruding or retracting) in U2OS cells co-expressing paxillin-mCherry and zyxin-GFP subjected to overnight serum-starvation and HGF-treatment. Histograms of the reference set plotted in grey. P-values generated compared to the reference set (two-sided Mann Whitney *U* tests), n gives number of analysed FAs. Vertical lines: median protrusion lengths. Bottom: 2D-histogram combining head and tail protrusion lengths for each individual FA. Colours represent the difference compared to the relative distributions of the reference set. White: below threshold, magenta: increase relative to reference set, cyan: decrease relative to reference set. Colour intensity represents magnitude of the difference (for scale and threshold see Materials and Methods) **(b)** Histograms of head (top) and tail (middle) protrusion lengths for FAs near moving membrane edges. Grey histograms, vertical lines, n-numbers and statistical tests as above. Bottom: 2D-histogram combining head and tail protrusion length for each individual FA. Colours as above. **(c)** Comparison of head/tail length for FAs near still (grey) and moving (black) ventral membrane edges, p-values are generated by two-sided Mann Whitney *U* test.

of FA proteins within FAs is altered in response to HGF, with paxillin heads shortening and zyxin tails lengthening.

FA head lengths correlate with membrane motility

Finally, we examined whether the lateral distribution of paxillin and zyxin along FAs correlated with the motility of the nearest ventral (adherent) membrane edge. Nine HGF-stimulated cells were reimaged approximately 30 minutes after the measurements shown in Fig. 4b, to analyse the movement of their ventral membrane edges (see Materials and Methods). 505 FAs were located close to a moving membrane edge and 252 FAs were located near a static membrane edge, while 266 FAs were disregarded from this analysis because of a more inward cellular position. At FAs near static membrane edges the paxillin enriched head was undetectable, which differed significantly from FAs near protruding or retracting edges that retained their paxillin enriched heads (Fig. 5). In contrast, FAs near both moving and still membrane edges have similar zyxin enriched tails. In the 2-D histograms this translates into the increases being spread all over the lower half of the histogram for static membrane edges. However, for FAs near moving membrane edges the strongest increases are clearly clustered in the lower left quadrant indicating FAs with paxillin heads combined with zyxin tails are seen more frequently.
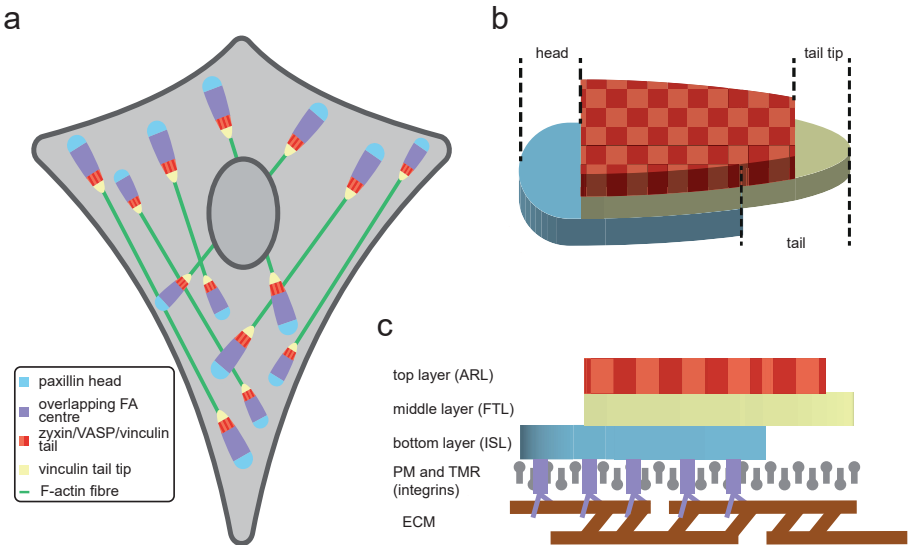

Figure 6. Schematic model of relative FA layer position.
(a) Schematic representation of the distribution of hallmark FA proteins paxillin, vinculin zyxin and VASP along the long axis of FAs within cells. For clarity the model is not drawn to scale. **(b,c)** Schematic representation of the position of the z-layers along the long axis of FAs based on the observed marker protein locations (not to scale). PM: plasma membrane, TMR: transmembrane receptor.

Discussion

Here we examined large numbers of FAs in cells co-expressing hallmark FA proteins in various combinations and showed that paxillin frequently protrudes at FA heads, zyxin and VASP at tails and vinculin at tail tips (Fig. 2, 3, 6a). Since these proteins each are present in a specific z-layer our data suggests these layers are shifted relative to each other, where in the most frequently observed configuration the layer closest to the ventral membrane (ISL) extends furthest at FA heads, the middle layer (FTL) at the tail tips and the top layer (ARL) at the tail (Fig. 3f, 6b).

We used multi-colour beads to perform separate channel alignments for all images. To rule out that other differences between the two dyes such as their different signal-to noise ratios impact their measured distributions, we performed a number of controls. As a first control, we created a reference set by imaging cells co-expressing red- and green-tagged versions of a single FA protein, paxillin (Fig. 2, grey histograms). This allowed to statistically test whether the head/tail lengths we observe for the image data sets of U2OS cells co-expressing different proteins are significantly different from those in the reference set. Secondly, when we examined the longitudinal distribution of two proteins from the same z-layer, zyxin and VASP, we found histograms that were not significantly different from the reference set, showing that VASP and zyxin are homogenously distributed along FAs (Fig. 2a). We used this finding for the final control where we swapped the tag of paxillin in the paxillin-mCherry zyxin-GFP versus the VASP-mCherry paxillin-GFP data sets (Fig. 2b vs 2c). Since VASP and zyxin have the same longitudinal distribution (Fig. 2A) this should produce similar head and tail protrusions but in opposite colours, which is indeed what we observed.

Our observation of vinculin protruding at tail tips corresponds remarkably well to previous studies showing that talin is stretched at these tips[7], since stretching of talin has been shown to unmask cryptic vinculin binding sites[41]. In other studies non-homogeneous protein distributions were also shown along FAs. For example, studies on large FAs at the trailing end of actively migrating cells showed that binding dynamics of paxillin vary along them[42-44]. For vinculin, it has been reported that its active form is enriched at the proximal FA tip (the tail) and its inactive form at the opposite FA end (the head)[45,46]. Also, active and inactive integrins were recently shown to form discrete nanoclusters[47]. Recently, we showed using FRAP and photoswitching in confocal mode (not for single molecule microscopy) that long term immobile paxillin and vinculin form small clusters within the FA complex that are enriched at the proximal half of the FA[48]. Lastly, in specialised FAs unique to pluripotent stem cells, termed cornerstone

4

FAs, β5-integrins and talin were shown to be specifically enriched around the edges of these FAs, while a third protein, the adaptor protein kank2, was shown to accumulate near these FAs specifically at the distal end[10].

We were also able to show that head and tail compositions were altered during HGF-induced scattering. HGF, or the scatter factor, is the natural ligand for the tyrosine receptor encoded for by the proto-oncogene c-Met[49-51]. The U2OS cells we used express the Met receptor[33] and stimulation with HGF has been shown to strongly increase the motility of U2OS cells in both 2D and 3D environments[35,38-40]. During HGF-induced scattering we observed that paxillin heads were shorter and zyxin tails longer than in unstimulated cells. Additionally, for the HGF-stimulated cells, FAs at protruding or retracting membrane edges had longer paxillin heads than FAs at static edges. Taken together these findings suggest that repositioning of layers along FAs plays a role in both overall cell movement and membrane movement.

With regard to the mechanism underlying the (re)arrangement of these layers along FAs, it is very tempting to speculate involvement of actin for two reasons. Firstly, of the proteins studied here, paxillin is the only one that does not directly bind actin and also the only protein absent from the tail region. Secondly, the tail protrudes at the FA tip where actin stress fibres enter FAs[44,52-54]. Mechanistically the actin might be playing a number of different roles. The absence of paxillin at the FA tail suggests that the FA tail is more loosely attached to the extracellular matrix, but instead forms an easily accessible handle for the actin to hold the FA. It may also be that over time the top two layers are pulled slightly apart from the bottom layer by the force exerted by the actin stress fibre since these layers are linked to the actin. The bottom layer, which is linked to the ECM-bound integrins, then stays in place, in that way also explaining the protrusion of the bottom layer at the head. Alternatively, the presence of the actin stress fibre at FA tails could be facilitating the binding of proteins directly binding actin (located in the top two layers), by providing a second binding platform for these proteins next to the FA complex itself.

In summary our data shows that FA layers are shifted with respect to each other along the long axis of FAs during movement, and that this is influenced by membrane motility as well as type of cellular movement, *i.e.* scattering or unstimulated.

Materials and Methods

Cell culture

U2OS cells were cultured in a humidified environment at 37°C and 5% CO_2 in phenol-red free DMEM (Lonza), supplemented with 10% FCS (Gibco), 2 mM L-glutamine (Lonza), 100 U/ml Penicillin, 100 µg/ml Streptomycine (Lonza) and, when maintaining stable cell lines, with 100 µg/ml G418. Transfections were performed using Fugene (Promega) followed by selection with G418 when creating stable cell lines. Stable cell lines were co-transfected with a second fluorescently labelled construct. For experiments 24 mm round glass coverslips were coated overnight at 4°C Celsius with PureCol bovine collagen type I (Advanced Bio-matrix) at a final concentration of 10 µg/ml. For channel alignment purposes TetraSpeck Microspheres 0.1 µm (ThermoFisher Scientific) were added to the coating. Cells were seeded onto the coated coverslips 16-24 h after transfection, then 24-48 h later imaged or chemically fixed (4% Paraformaldehyde), mounted using Vectashield Mounting Medium (Vector Laboratories) and stored at 4°C. For experiments examining the effects of HGF-induced scattering, prior to imaging cells were exposed to overnight serum starvation in 0.5% FCS containing DMEM, which 3-6 h prior to imaging was replaced with DMEM with 0.5% FCS (control) or DMEM with 0.5% FCS and 25 ng/ml HGF (HGF-treated).

Mammalian expression vectors

All fluorescent protein expression vectors were constructed using N1 (Clon-tech™-style) cloning vectors. They are based on mTurquoise or eGFP-tagged fusion constructs that have been previously characterised biochemically and/or cell biologically in the literature.

The Zyxin-GFP, Vinculin-GFP and Paxillin-GFP vectors were previously described[48]. The VASP-mCherry and Paxillin-mCherry constructs were based on the VASP-mTurquoise (Addgene 55585) and Paxillin-mTurquoise (Addgene 55573) vectors, respectively. These use the multiple cloning site as a linker region between the protein and mTurquoise, hampering a simple colour swap. To still allow sticky-end ligation the protein, fluorescent label and empty vector back-bone were all separately isolated as restriction fragments. These were ligated using sticky ends in 2 steps: 1) the protein to the fluorescent label and 2) the created insert into the vector backbone. This strategy was applied in the follow-ing manner:

For VASP-mCherry: The vector backbone was isolated from Paxillin-mTurquoise as an AgeI NotI fragment, VASP from VASP-mTurquoise as an AgeI BamHI frag-ment and mCherry from pmCherry N1 (Clontech) as a BamHI NotI fragment.

4

For Paxillin-mCherry: The vector backbone was isolated from Paxillin-mTurquoise as a BamHI NotI fragment, paxillin from Paxillin-mTurquoise as a BamHI HindIII fragment and mCherry from pmCherry as a HindIII NotI fragment.

All constructs were checked through sequencing, one silent mutation was found (Paxillin-GFP/Paxillin-mCherry bp1461 C to G). Furthermore, we confirmed all constructs localize properly (Fig. 1d,e, supplemental Fig. S1, S2).

Imaging

All data was acquired on a Zeiss Elyra PS1 system, an integrated microscope system with a structured Illumination unit and a LSM 780 confocal unit using a 63× 1.4NA oil objective. For live-cell imaging, cells were maintained at 37°C and 5% CO_2 using a stage-top incubator (Tokai Hit). For 3D-SIM imaging a grating was present in the light path. The grating was modulated in 5 phases and 5 rotations, and multiple z-slices were recorded with an interval of 110 nm on an Andor iXon DU 885, 1002 × 1004 EMCCD camera. GFP and mCherry were excited using 488 nm and 561 nm 100 mW diode lasers together with a BP 495-575 or 570-650 nm filter and a LP 750 nm filter. Raw images were reconstructed and channel alignment in x, y and z based on TetraSpeck beads was performed using the Zeiss Zen software. For the experiments looking at the effects of membrane motility, timelapse data was obtained for all positions using the LSM 780 confocal unit on the same microscope system at 10-30 minute intervals prior to the SIM imaging. Additionally either all positions were imaged at 15-30 minute intervals in confocal mode during the SIM imaging or the cells were reimaged in SIM mode 30 minutes after their initial SIM imaging.

Data analysis

Image analysis

Data was analysed in the ImageJ software package within the Fiji framework[55], using a series of macros we developed for this. From the reconstructed and channel aligned SIM data average projections were made of all z-slices (typically 3) with clearly visible FAs. A macro was used to roughly select the outlines of the FAs. Briefly, from a duplicate of the data to which a Gaussian blur with low σ was applied, another duplicate of the data to which a Gaussian blur with higher σ was applied, was subtracted. FAs were selected based on the Fiji build-in 'Otsu-dark' threshold, outlines were individually assessed and where needed corrected (mainly separation of touching FAs). Once all FAs were outlined a second macro was used to fit a line through the longitudinal axis of each FA. The 'fit ellipse' option was applied to find the centre of the FA, and the angle between the horizontal axis of the image and the longest axis of the FAs. These were used to fit a

line through the longitudinal axis of each FA by fitting a Gaussian to the intensity profile measured in a line perpendicular to the longest axis of the FA in the green channel. The fitted lines were terminated at both ends once the mean intensity of a 3 by 3 pixel sized box in both the green and the red channels fell below 30% of their maximum intensity along the line. For all FAs, intensity profiles along the fitted lines for both channels (red and green) were obtained. Distal and proximal ends were distinguished by determining which end was closest to a rectangle drawn around the cell (i.e. the distal FA end which we refer to as 'the head' in the manuscript).

Measuring FA head and tail protrusion lengths

The intensity profiles were loaded into R using the Rstudio (R development Core Team, 2016). Values were marked as positive for the channels based on a variable threshold (40% of the maximum value of the respective channel after application of a median filter with a window size of 5 pixels). The longest stretch of pixels along the line positive for both channels was determined, i.e. the main stretch of FA where both proteins overlap. This was hampered by the way noise manifests in reconstructed SIM images, as coloured noise due to the Fourier transformations applied in the SIM reconstruction, where even within bright high intensity patches small clusters of low intensity pixels are seen. To compensate for this, a gap of maximally 4 pixels (160 nm) negative for either/both channel(s) was allowed within the main stretch. The intensity data of the pixels surrounding the main stretch was examined to determine the FA head and tail lengths (Fig. 2f). If the pixel bordering the main stretch was positive for one of the channels, the identity of this channel and the number of consecutive pixels positive for this channel (again allowing for a gap of maximally 4 pixels) were taken as the head or tail lengths. Note that for conversion of these lengths to nanometres the position of the pixels was also taken into account, so the distance between 2 pixels in a straight line is 40 nm, but between two diagonal pixels is the square root of 3200, or ~57 nm. If the pixel bordering the main stretch was negative for both channels, the corresponding head or tail protrusion length was zero.

Reference set of paxillin-GFP and paxillin-mCherry

For analysis of the experimental data we first constructed a reference set by imaging and analysing 1630 FAs in 16 U2OS cells co-expressing paxillin-mCherry and paxillin-GFP which fully overlap. However, as expected, due to noise and other possible inaccuracies in the images, we still measured head and tail lengths. We found a small bias of 57 nm of measuring green head/tail lengths, for which we corrected all further measurements.

4

Representation and statistical analysis of the experimental data

The experimental data of all investigated protein pairs were plotted together with the data from the reference set as histograms with a bin size of 80 nm, with the measured head or tail red lengths to the left of zero and the measured head or tail green lengths to the right. This allowed us to test whether proteins protruded significantly at the head or tail in comparison to the reference set by using two-tailed Mann-Whitney *U* tests.

We also generated 2-D histograms to plot the head and tail lengths of the same FA as a single 2-D data point. 2-D histograms had 80 by 80 nm bins. The 2-D distribution of the reference set in the 2-D histogram was subtracted from the distribution of the protein set of interest and the distribution of the resulting increases and decreases (in percentage point) relative to the reference set were visualised as a 2-D histogram using a colour look up table (LUT), where values between 0 and 123 (corresponding to decreases of 3.45 to 0.13 percentage point) form a continuous range from cyan to white, values between 133 and 255 (corresponding to increases of 0.14 to 3.44 percentage point) a continues range from white to magenta and the intermediate values of 124 to 132 (corresponding to increases/decreases of less than 0.11 percentage point) are kept white for clarity.

Acknowledgements

Author contributions

Conceptualization, K.L, W.A.C and A.B.H; Methodology, K.L. and J.A.S; Software, K.L., A.N. and J.A.S.; Validation, A.B.H.; Formal Analysis, K.L. and J.A.S.; Investigation, K.L.; Resources, T.E.A.; Writing-Original Draft, K.L.; Writing- Review & Editing, K.L., J.A.S. and A.B.H.; Visualisation, K.L. and J.A.S; Supervision, W.A.C and A.B.H.

References

1   Yamada, K. M. & Geiger, B. Molecular interactions in cell adhesion complexes. *Current opinion in cell biology* **9**, 76-85 (1997).

2   Geiger, B., Bershadsky, A., Pankov, R. & Yamada, K. M. Transmembrane crosstalk between the extracellular matrix--cytoskeleton crosstalk. *Nature reviews. Molecular cell biology* **2**, 793-805, doi:10.1038/35099066 (2001).

3   Wahl, S. M., Feldman, G. M. & McCarthy, J. B. Regulation of leukocyte adhesion and signaling in inflammation and disease. *Journal of leukocyte biology* **59**, 789-796 (1996).

4   Winograd-Katz, S. E., Fassler, R., Geiger, B. & Legate, K. R. The integrin adhesome: from

genes and proteins to human disease. *Nature reviews. Molecular cell biology* **15**, 273-288, doi:10.1038/nrm3769 (2014).

5   Maartens, A. P. & Brown, N. H. The many faces of cell adhesion during Drosophila muscle development. *Developmental biology* **401**, 62-74, doi:10.1016/j.ydbio.2014.12.038 (2015).

6   Zaidel-Bar, R., Itzkovitz, S., Ma'ayan, A., Iyengar, R. & Geiger, B. Functional atlas of the integrin adhesome. *Nature cell biology* **9**, 858-867, doi:10.1038/ncb0807-858 (2007).

7   Kanchanawong, P. *et al.* Nanoscale architecture of integrin-based cell adhesions. *Nature* **468**, 580-584, doi:10.1038/nature09621 (2010).

8   Liu, J. *et al.* Talin determines the nanoscale architecture of focal adhesions. *Proceedings of the National Academy of Sciences of the United States of America* **112**, E4864-4873, doi:10.1073/pnas.1512025112 (2015).

9   Paszek, M. J. *et al.* Scanning angle interference microscopy reveals cell dynamics at the nanoscale. *Nature methods* **9**, 825-827, doi:10.1038/nmeth.2077 (2012).

10   Stubb, A. *et al.* Superresolution architecture of cornerstone focal adhesions in human pluripotent stem cells. *Nature communications* **10**, 4756, doi:10.1038/s41467-019-12611-w (2019).

11   Gustafsson, M. G. Surpassing the lateral resolution limit by a factor of two using structured illumination microscopy. *J Microsc* **198**, 82-87 (2000).

12   Laukaitis, C. M., Webb, D. J., Donais, K. & Horwitz, A. F. Differential dynamics of alpha 5 integrin, paxillin, and alpha-actinin during formation and disassembly of adhesions in migrating cells. *The Journal of cell biology* **153**, 1427-1440 (2001).

13   Webb, D. J. *et al.* FAK-Src signalling through paxillin, ERK and MLCK regulates adhesion disassembly. *Nature cell biology* **6**, 154-161, doi:10.1038/ncb1094 (2004).

14   Wiseman, P. W. *et al.* Spatial mapping of integrin interactions and dynamics during cell migration by image correlation microscopy. *Journal of cell science* **117**, 5521-5534, doi:10.1242/jcs.01416 (2004).

15   Choi, C. K. *et al.* Actin and alpha-actinin orchestrate the assembly and maturation of nascent adhesions in a myosin II motor-independent manner. *Nature cell biology* **10**, 1039-1050, doi:10.1038/ncb1763 (2008).

16   Pasapera, A. M., Schneider, I. C., Rericha, E., Schlaepfer, D. D. & Waterman, C. M. Myosin II activity regulates vinculin recruitment to focal adhesions through FAK-mediated paxillin phosphorylation. *The Journal of cell biology* **188**, 877-890, doi:10.1083/jcb.200906012 (2010).

17   McGregor, A., Blanchard, A. D., Rowe, A. J. & Critchley, D. R. Identification of the vinculin-binding site in the cytoskeletal protein alpha-actinin. *The Biochemical journal* **301 (Pt 1)**, 225-233 (1994).

18   Brindle, N. P., Holt, M. R., Davies, J. E., Price, C. J. & Critchley, D. R. The focal-adhesion vasodilator-stimulated phosphoprotein (VASP) binds to the proline-rich domain in vinculin. *The Biochemical journal* **318 (Pt 3)**, 753-757 (1996).

19   Gertler, F. B., Niebuhr, K., Reinhard, M., Wehland, J. & Soriano, P. Mena, a relative of VASP and Drosophila Enabled, is implicated in the control of microfilament dynamics. *Cell* **87**, 227-239 (1996).

20   Reinhard, M., Rudiger, M., Jockusch, B. M. & Walter, U. VASP interaction with vinculin: a recurring theme of interactions with proline-rich motifs. *FEBS letters* **399**, 103-107 (1996).

21   Humphries, J. D. *et al.* Vinculin controls focal adhesion formation by direct interactions with talin and actin. *The Journal of cell biology* **179**, 1043-1057, doi:10.1083/jcb.200703036 (2007).

22   Jones, P. *et al.* Identification of a talin binding site in the cytoskeletal protein vinculin. *The Journal of cell biology* **109**, 2917-2927 (1989).

23   Turner, C. E. & Miller, J. T. Primary sequence of paxillin contains putative SH2 and SH3 domain binding motifs and multiple LIM domains: identification of a vinculin and pp125Fak-binding region. *Journal of cell science* **107 (Pt 6)**, 1583-1591 (1994).

4

24   Brown, M. C., Perrotta, J. A. & Turner, C. E. Identification of LIM3 as the principal determinant of paxillin focal adhesion localization and characterization of a novel motif on paxillin directing vinculin and focal adhesion kinase binding. *The Journal of cell biology* **135**, 1109-1123 (1996).

25   Golsteyn, R. M., Beckerle, M. C., Koay, T. & Friederich, E. Structural and functional similarities between the human cytoskeletal protein zyxin and the ActA protein of Listeria monocytogenes. *Journal of cell science* **110 (Pt 16)**, 1893-1906 (1997).

26   Drees, B. *et al.* Characterization of the interaction between zyxin and members of the Ena/vasodilator-stimulated phosphoprotein family of proteins. *The Journal of biological chemistry* **275**, 22503-22511, doi:10.1074/jbc.M001698200 (2000).

27   Fradelizi, J. *et al.* ActA and human zyxin harbour Arp2/3-independent actin-polymerization activity. *Nature cell biology* **3**, 699-707, doi:10.1038/35087009 (2001).

28   Nix, D. A. *et al.* Targeting of zyxin to sites of actin membrane interaction and to the nucleus. *The Journal of biological chemistry* **276**, 34759-34767, doi:10.1074/jbc.M102820200 (2001).

29   Yoshigi, M., Hoffman, L. M., Jensen, C. C., Yost, H. J. & Beckerle, M. C. Mechanical force mobilizes zyxin from focal adhesions to actin filaments and regulates cytoskeletal reinforcement. *The Journal of cell biology* **171**, 209-215, doi:10.1083/jcb.200505018 (2005).

30   Hoffman, L. M. *et al.* Genetic ablation of zyxin causes Mena/VASP mislocalization, increased motility, and deficits in actin remodeling. *The Journal of cell biology* **172**, 771-782, doi:10.1083/jcb.200512115 (2006).

31   Bianchi-Smiraglia, A. *et al.* Integrin-beta5 and zyxin mediate formation of ventral stress fibers in response to transforming growth factor beta. *Cell cycle (Georgetown, Tex.)* **12**, 3377-3389, doi:10.4161/cc.26388 (2013).

32   Cecchi, F., Rabe, D. C. & Bottaro, D. P. Targeting the HGF/Met signalling pathway in cancer. *Eur J Cancer* **46**, 1260-1270, doi:10.1016/j.ejca.2010.02.028 (2010).

33   Scagliotti, G. V., Novello, S. & von Pawel, J. The emerging role of MET/HGF inhibitors in oncology. *Cancer Treat Rev* **39**, 793-801, doi:10.1016/j.ctrv.2013.02.001 (2013).

34   Trusolino, L. & Comoglio, P. M. Scatter-factor and semaphorin receptors: cell signalling for invasive growth. *Nature reviews. Cancer* **2**, 289-300, doi:10.1038/nrc779 (2002).

35   Patane, S. *et al.* MET overexpression turns human primary osteoblasts into osteosarcomas. *Cancer research* **66**, 4750-4757, doi:10.1158/0008-5472.Can-05-4422 (2006).

36   Boros, P. & Miller, C. M. Hepatocyte growth factor: a multifunctional cytokine. *Lancet* **345**, 293-295, doi:10.1016/s0140-6736(95)90279-1 (1995).

37   Zarnegar, R. & Michalopoulos, G. K. The many faces of hepatocyte growth factor: from hepatopoiesis to hematopoiesis. *The Journal of cell biology* **129**, 1177-1180, doi:10.1083/jcb.129.5.1177 (1995).

38   Coltella, N. *et al.* Role of the MET/HGF receptor in proliferation and invasive behavior of osteosarcoma. *FASEB journal : official publication of the Federation of American Societies for Experimental Biology* **17**, 1162-1164, doi:10.1096/fj.02-0576fje (2003).

39   Patane, S. *et al.* A new Met inhibitory-scaffold identified by a focused forward chemical biological screen. *Biochemical and biophysical research communications* **375**, 184-189, doi:10.1016/j.bbrc.2008.07.159 (2008).

40   Pennacchietti, S. *et al.* Hypoxia promotes invasive growth by transcriptional activation of the met protooncogene. *Cancer cell* **3**, 347-361 (2003).

41   del Rio, A. *et al.* Stretching single talin rod molecules activates vinculin binding. *Science (New York, N.Y.)* **323**, 638-641, doi:10.1126/science.1162912 (2009).

42   Webb, D. J., Brown, C. M. & Horwitz, A. F. Illuminating adhesion complexes in migrating cells: moving toward a bright future. *Current opinion in cell biology* **15**, 614-620 (2003).

43   Digman, M. A., Brown, C. M., Horwitz, A. R., Mantulin, W. W. & Gratton, E. Paxillin dynamics measured during adhesion assembly and disassembly by correlation spectroscopy. *Biophysi-*

4

cal journal **94**, 2819-2831, doi:10.1529/biophysj.107.104984 (2008).

44   Wolfenson, H. *et al.* A role for the juxtamembrane cytoplasm in the molecular dynamics of focal adhesions. *PloS one* **4**, e4304, doi:10.1371/journal.pone.0004304 (2009).

45   Chen, H., Cohen, D. M., Choudhury, D. M., Kioka, N. & Craig, S. W. Spatial distribution and functional significance of activated vinculin in living cells. *The Journal of cell biology* **169**, 459-470, doi:10.1083/jcb.200410100 (2005).

46   Case, L. B. *et al.* Molecular mechanism of vinculin activation and nanoscale spatial organization in focal adhesions. *Nature cell biology* **17**, 880-892, doi:10.1038/ncb3180 (2015).

47   Spiess, M. *et al.* Active and inactive beta1 integrins segregate into distinct nanoclusters in focal adhesions. *The Journal of cell biology* **217**, 1929-1940, doi:10.1083/jcb.201707075 (2018).

48   Legerstee, K., Geverts, B., Slotman, J. A. & Houtsmuller, A. B. Dynamics and distribution of paxillin, vinculin, zyxin and VASP depend on focal adhesion location and orientation. *Scientific reports* **9**, 10460, doi:10.1038/s41598-019-46905-2 (2019).

49   Bottaro, D. P. *et al.* Identification of the hepatocyte growth factor receptor as the c-met proto-oncogene product. *Science (New York, N.Y.)* **251**, 802-804, doi:10.1126/science.1846706 (1991).

50   Stoker, M., Gherardi, E., Perryman, M. & Gray, J. Scatter factor is a fibroblast-derived modulator of epithelial cell mobility. *Nature* **327**, 239-242, doi:10.1038/327239a0 (1987).

51   Weidner, K. M., Behrens, J., Vandekerckhove, J. & Birchmeier, W. Scatter factor: molecular characteristics and effect on the invasiveness of epithelial cells. *The Journal of cell biology* **111**, 2097-2108, doi:10.1083/jcb.111.5.2097 (1990).

52   Endlich, N., Otey, C. A., Kriz, W. & Endlich, K. Movement of stress fibers away from focal adhesions identifies focal adhesions as sites of stress fiber assembly in stationary cells. *Cell motility and the cytoskeleton* **64**, 966-976, doi:10.1002/cm.20237 (2007).

53   Hotulainen, P. & Lappalainen, P. Stress fibers are generated by two distinct actin assembly mechanisms in motile cells. *The Journal of cell biology* **173**, 383-394, doi:10.1083/jcb.200511093 (2006).

54   Wolfenson, H., Henis, Y. I., Geiger, B. & Bershadsky, A. D. The heel and toe of the cell's foot: a multifaceted approach for understanding the structure and dynamics of focal adhesions. *Cell motility and the cytoskeleton* **66**, 1017-1029, doi:10.1002/cm.20410 (2009).

55   Schindelin, J. *et al.* Fiji: an open-source platform for biological-image analysis. *Nature methods* **9**, 676-682, doi:10.1038/nmeth.2019 (2012).
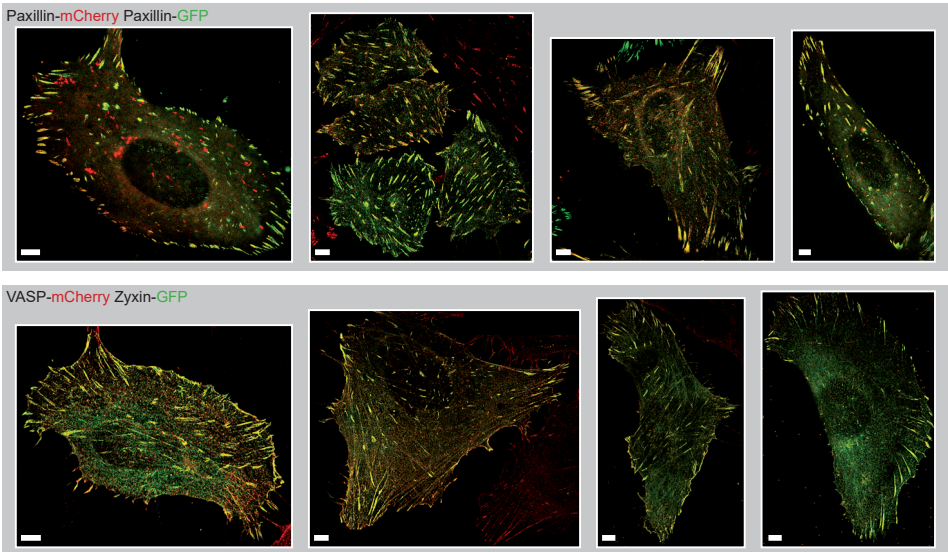
4

Supplementary Figures

S1

Figure S1. Representative merged dual colour SIM images.
Representative merged dual colour SIM images for U2OS cells co-expressing the indicated proteins.
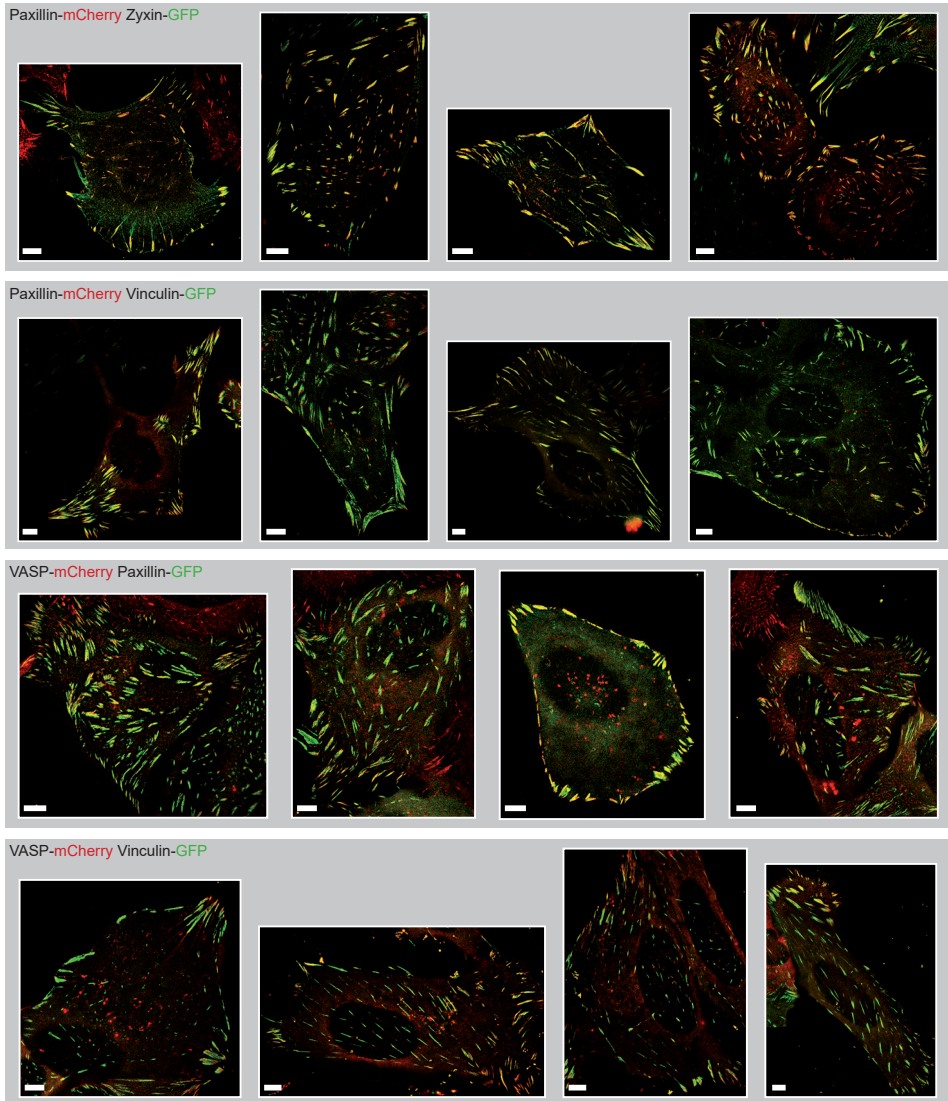Scale bar 5 μm.

S2

Figure S2. Representative merged dual colour SIM images.
Representative merged dual colour SIM images for U2OS cells co-expressing the indicated proteins.
Scale bar 5 μm.

Chapter 5

Correlative light and electron microscopy reveals fork-shaped structures at actin entry sites of focal adhesions

Karin Legerstee[1], Jason Sueters[2], Gert-Jan Kremers[1], Jacob P. Hoogenboom[2], Adriaan B. Houtsmuller[1]

1 Erasmus Medical Centre Rotterdam, Department of Pathology, Optical Imaging Centre, Rotterdam, The Netherlands.
2 Delft University of Technology, Department of Imaging Physics, Delft, The Netherlands

Abstract

Focal adhesions (FAs) are the main cellular structures to link the intracellular cytoskeleton to the extracellular matrix. FAs mediate cell adhesion, are important for cell migration and are involved in many (patho)-physiological processes. Here we examined FAs and their associated actin fibres using correlative fluorescence and scanning electron microscopy (SEM). We used fluorescence images of cells expressing paxillin-GFP to define the boundaries of FA complexes in SEM images, without using SEM contrast enhancing stains. We observed that SEM contrast was increased around the actin fibre entry site in 98% of FAs, indicating increases in protein density and possibly also phosphorylation levels in this area. In nearly three quarters of the FAs, these nanostructures had a fork shape, with the actin forming the stem and the high contrast FA areas the fork. In conclusion, the combination of fluorescent and electron microscopy allowed accurate localisation of a highly abundant, novel fork structure at the FA-actin interface.

5

Introduction

Focal adhesions (FAs) are the main cellular structures to link the intracellular cytoskeleton to the extracellular matrix (ECM). They are typically several square micrometres in size[1,2]. On the membrane-facing side the main FA components are integrins, transmembrane receptors which directly bind to the extracellular matrix (ECM). F-actin, or filamentous actin, forms the edge of the FA on the cytoplasm-facing side. In between integrins and actin a large and diverse intracellular macromolecular protein assembly is present, for which over 200 different proteins have been reported[3,4]. These include (trans)membrane receptors, other than integrins, adaptor proteins and many different signalling proteins such as kinases, phosphatases and G-protein regulators, which through post-translational modifications add significantly to FA complexity. FAs experience force, the strength of which depends on the combination of myosin-II contractility and the stiffness of the ECM. Because of their importance in cell adhesion and to the transmission of force from the cell to the extracellular matrix, FAs are crucial to most types of cell migration, including in vitro over a 2D-surface. Migration and adhesion are key cellular functions required for many physiological and patho-physiological processes, like embryological development, the functioning of the immune system and cancer, in particular metastasis[4-6].

The F-actin associated with FAs takes the shape of stress-fibres, a specialised form of actin associated with contractile myosin II and cytoskeletal proteins such as α-actinin[7]. There are two types of stress fibres associated with FAs: ventral stress fibres are associated with FAs at either end and typically transverse the whole cell, while dorsal stress fibres are linked to FAs on one end, typically near the cell front, then stretch upwards to the nucleus and the dorsal cell surface[8].

Here we examine FAs and their associated F-actin fibres using a correlative fluorescence microscopy and Scanning Electron Microscopy (SEM) approach. Because FAs are very dense protein complexes found at the very edge of the cell and directly attached to the ECM, they are well suited to studying with SEM. We used cells stably expressing a fluorescently tagged form of the major FA protein paxillin to mark the FAs and fluorescently tagged phalloidin to stain the F-actin network. Although FAs have frequently been visualised using SEM[9-15], overlaying the SEM images with the fluorescence images adds the possibility to clearly mark the FA boundaries in the SEM images. This revealed that FAs have a higher contrast in these images at the tip where actin fibres enter. Further examination revealed that these high contrasting FA areas and the associated F-actin fibre together have a forked shape, with the actin forming the stem and the high contrast areas within the FA forming the fork. Since no contrast-enhancing staining agent
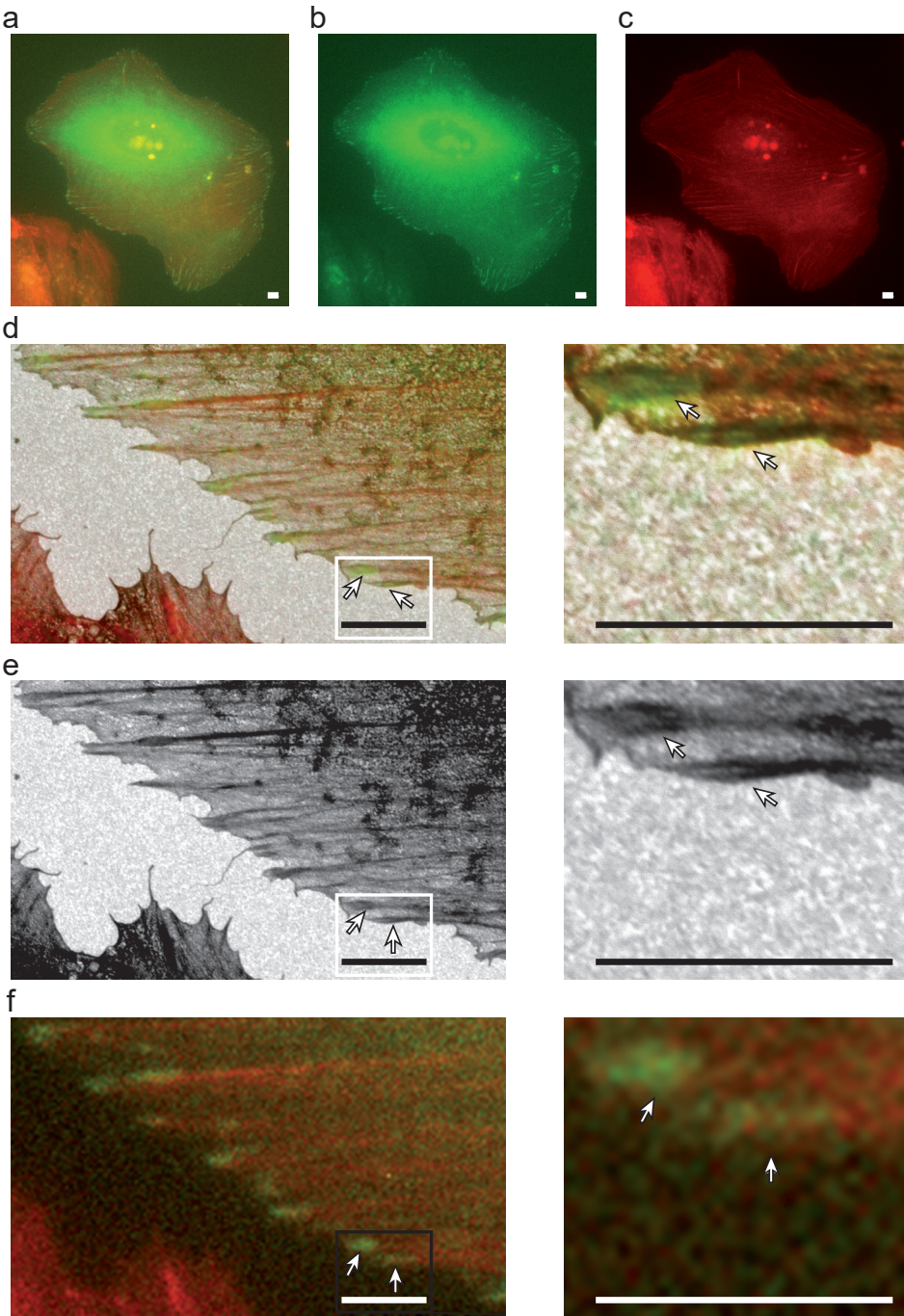
5

Figure 1. Overlay of fluorescent and SEM images reveals high contrast FA areas around the F-actin entry site.

Images of a U2OS cell stably expressing GFP-tagged paxillin and stained with phalloidin cultured on

a collagen-coated ITO coverslip. **(a)** Merged image, **(b)** green channel showing FAs where paxillin is localised, **(c)** red channel showing phalloidin stained F-actin. Scalebar: 5 μm. **(d)** Overlay image of a section of the fluorescent image in a with the corresponding SEM image (left), and zoom in of boxed area (right). Arrows indicate FAs with characteristic fork-shapes, where the fork is formed by higher contrast areas of the FA and the stem is formed by the F-actin fibre entering the FA. Scalebar: 5 μm. **(e)** SEM channel of the image in d. **(f)** Fluorescent channel of the image in d.

was applied this shows that protein density and possibly also phosphorylation levels are increased at the fork.

Results and discussion

Here we examine FAs and their associated F-actin fibres using correlative fluorescence and scanning electron microscopy. Indium-Tin-Oxide (ITO) coated glass coverslips were additionally coated with a thin layer of type-I collagen to mimic the ECM, providing a surface for the integrin receptors to bind to. The ITO-coated glass provides a conductive substrate, which allows SEM inspection of thin samples such as cultured cells without metal shadowing or other conductive coating and/or without additional staining[16-21]. Onto these coverslips human bone cancer (U2OS) cells were seeded, stably expressing GFP-tagged paxillin to visualise the FAs. The cells were given 36 hours to adhere and form clear FAs, followed by chemical fixation (4% paraformaldehyde), permeabilization and staining with phalloidin to fluorescently stain the F-actin fibres. Immediately before imaging, the samples were dehydrated (ethanol). During imaging we were able to switch between fluorescent and SEM imaging without moving the stage[17]. However, in vacuum, under these dehydrated, permeabilised conditions, the GFP signal was relatively weak[18,22]. Therefore we first made the fluorescent images then followed up with the SEM images. To create overlay images the two images were scaled to the same size followed by a manual overlay procedure, mainly on the basis of the F-actin network as due to the phalloidin staining this is clearly visible in both imaging modalities. Of the 122 FAs with associated actin fibres, 97 were clearly visible in both modalities and the remaining 25 were unclear in the SEM images. These latter FAs were located further from the edge of the adherent part of the plasma membrane, where the cell is thicker. In these areas the FAs were often lost in the signal from the rest of the cell including other fibre networks, as no specific markers or contrast agents were used and the SEM at the low energies used only penetrates the upper tens of nm of the sample.

FAs are visible in the SEM images but the overlay images are needed to clearly define the boundaries of the FAs (Fig. 1). Especially where the FA connects to its F-actin fibre it is almost impossible to determine from the SEM-images alone where the F-actin fibre ends and the FA begins. However, using the GFP-paxillin signal to mark the FA boundaries, it becomes clear that in the SEM images the
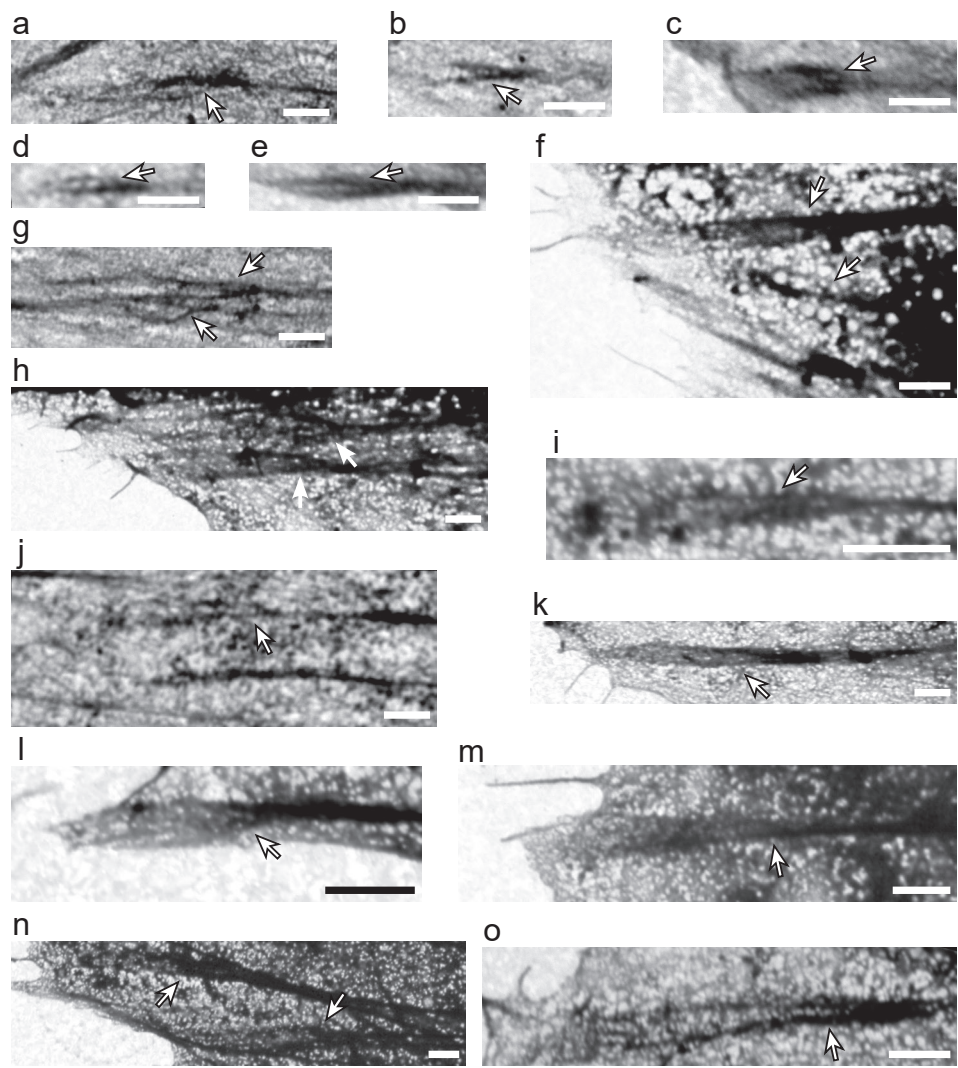
5

Figure 2. Representative examples of fork-shaped high contrast areas around the F-actin entry side.
(a-o) High-magnification SEM images of FAs in which the high contrast areas around the F-actin side forms the characteristic fork-like shape (arrows). Scalebar: 1 μm.

contrast of the FA complex is increased around the entrance point of the F-actin fibre. Note the SEM images show an apparent reverse contrast due to the comparatively high backscatter electron yield of the indium- and tin-containing sample substrate, so areas with less transmission and thus more electron-scattering biological material appear as darker areas, as first noted by Pluk et al[16]. Moreover, these overlays show that these high contrast areas are not part of the actin fibre but of the FA as identified on the basis of the paxillin fluorescent signal. Such high contrast areas were observed in 98% (95 FAs) of FAs (Table 1). Further ex-
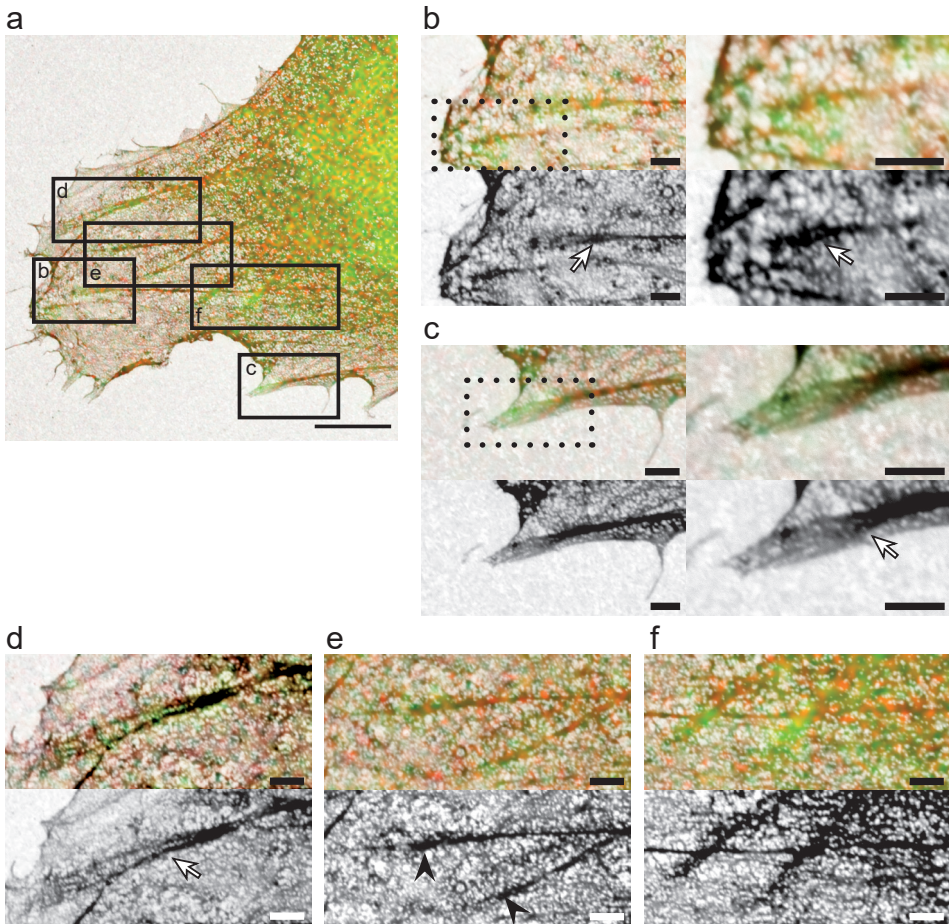
Figure 3. High contrast FA areas around F-actin entry site are a common feature.
(a) Overlay of SEM image and fluorescent image, with paxillin-stained FAs in green and phalloidin-stained actin in red. Boxes b-f indicate magnifications shown in panels b-f. Scalebar: 5 μm. **(b-e)** Magnifications of corresponding boxed areas in a. Top: overlay image; bottom SEM image. Scalebar: 1 μm. Arrows indicate FAs with characteristic fork-shaped high contrast areas around the F-actin entry site, arrow heads (in e) indicate FAs with high contrast areas not forming a fork-shape. For b and c right images are magnifications of the boxed areas in the left images. **(f)** Magnification of boxed area f in a. Top: overlay image; bottom: SEM image. For the shown FAs the shape of the high contrast areas could not be determined, probably due to the increased thickness of the cell at this more inward location. Scalebar: 1 μm.

amination showed that in almost three quarters of FAs, the high contrasting areas and the associated F-actin fibre are fork-shaped, with the actin as the stem and the high contrasting FA areas as the fork (Fig. 2 and 3). High contrasting areas within the focal adhesion (identified by the presence of paxillin fluorescence) were defined as forked when they were partially intersected by an area of lower contrast splitting the high contrast area into two sides (fork). The angle between the two sides of the fork varied between 7 and 48 degrees, with an average angle

	FAs with higher contrast at actin entry site	FAs with fork shape
Observer 1	97.9% (95 FAs)	73.2% (71 FAs)
Observer 2	97.9% (95 FAs)	74.2% (72 FAs)
% of overlap between observers	100%	94.8%
Average	97.9%	73.7%

Table 1. The majority of FAs have Fork shaped high contrast areas around the FA entry site.
Results of the categorisation of the 97 imaged FAs as independently categorised by two observers. The results for each observer, the percentage of FAs placed in the same category by both observers (% of overlap between observers) and the average results are given.

	FA length (long axis; μm)	Fork angle (°)	Fork length (% of FA axis)	Fork symmetry (% of FA axis)	Short side fork (% of FA axis)	Long side fork (% of FA axis)	Fork length (average; μm)	Fork length (short side μm)	Fork length (long side)
Average	3.30	20.2	59.7	17.0	51.1	68.2	1.98	1.69	2.26
Min	1.39	7.4	16.1	0.1	14.9	16.3	0.47	0.35	0.50
Max	7.42	47.6	90.3	65.4	88.8	99.2	5.76	5.76	5.77
SD	1.33	8.7	19.	15.1	20.6	20.5	1.06	1.03	1.17
SEM	0.02	1.0	2.2	1.8	2.4	2.4	0.01	0.01	0.02

Table 2. Quantitative analysis of the fork-shapes.
Results of a quantitative analysis of the observed fork shaped areas (n = 73). For each FA the longest and shortest side of the fork were measured and their lengths were calculated relative to the longest axis of the FA. In addition the angle between the two sides was measured. For fork symmetry the average difference in length between the long and the short side of the fork was calculated relative to the major axis of the FA.

of ~20 ± 2.0 degrees (± twice SEM). The average length of the fork was roughly two micrometers which corresponded to ~60 ± 4.5% of the long axis of the FA (Fig. 4 and Table 2). Looking at the two sides of the fork individually, the shortest side was on average ~51 ± 4.8% of the longitudinal FA axis (1.7 ± 0.03 μm) and the longest side ~68 ± 4.8% (2.3 ± 0.03 μm). With regard to symmetry, the average differences between the two sides of the fork was 17.0 ± 3.5% of the FA axis, with a minimum difference of only 0.1% and a maximum difference of 90.3%. Lastly, there was as a trend for longer FAs to have a smaller angle, suggesting the angle of the forks might decrease as FAs mature and grow (Fig. 4b).

To our knowledge this is the first report on forked structures with high contrast seen in FAs, possibly because by using correlative fluorescent images, the FA boundaries are clearly defined, whereas based on the SEM images alone the high contrast areas might easily be mistaken for parts of the actin fibre. However, with this new knowledge of exactly what to look for, we were now able to identify (hints of) the fork-shape in previously published EM images of FAs, that were ap-
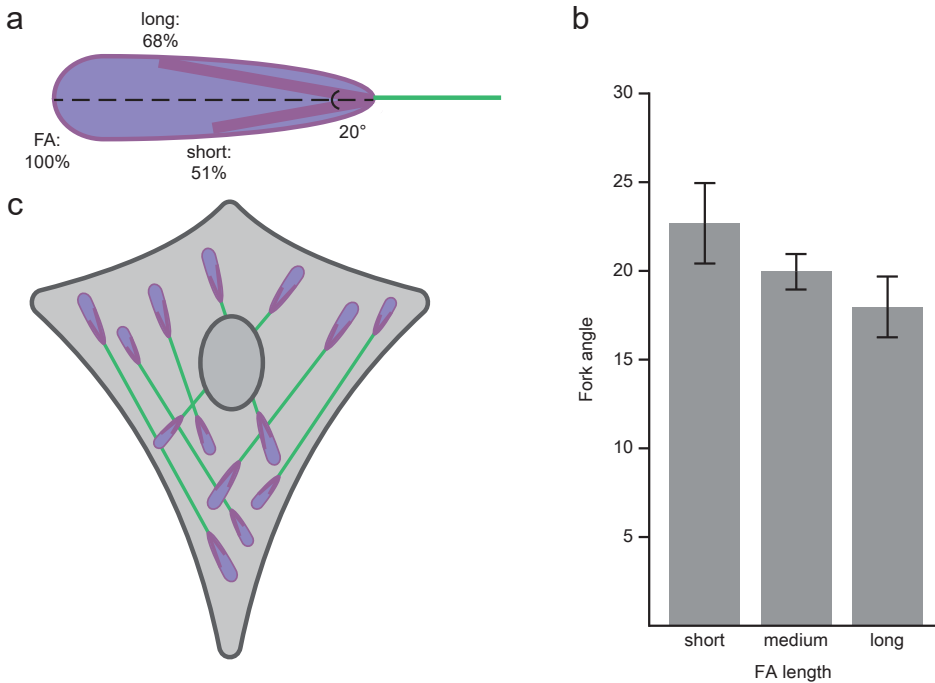
5

Figure 4. Quantitative measurements of the fork-shape.
(a) Schematic representation of the average fork-shape observed within FAs based on a quantitative analysis of all observed fork-shapes (see Materials and Methods) **(b)** There is a trend for the angle between the two sides of the fork to be decreased as the length of the FA increases. For this analysis the FAs were split into 3 groups, short: the 24 shortest FAs (ranging from 1.4 - 2.5 μm), medium: 24 FAs of medium length (ranging from 2.5 - 3.7 μm) and long: the 25 longest FAs (ranging from 3.7 - 7.4 μm). Error bars represent SEM.

parently not recognized at that time[10,23,24]. We also note that, while we followed a sample preparation procedure aimed specifically at preservation of fluorescence, these other works used EM-specific sample preparation protocols, indicating the fork-shapes observed here are not an artefact of our fixation procedure.

The nanoarchitecture along the z-axis of FAs has been well described previously[25]. Three different layers have been recognised: (1) the so-called integrin signalling layer (ISL) closest to the adherent membrane (within ~10 - 20 nm) which includes the cytoplasmic tails of the transmembrane integrin receptors, focal adhesion kinase and paxillin, (2) the actin-regulatory layer (ARL) at the top, where mainly directly actin-binding proteins such as zyxin, vasodilator-stimulated phosphoprotein (VASP) and α-actinin are found, and (3) the force transduction layer (FTL) in between (from ~10 - 20 to ~50 - 60 nm from the adherent membrane) of which talin is the most well-known.

The nanoscale structure along the lateral and longitudinal axis of FAs has been investigated to a lesser extent. Along the lateral axis FAs were shown to consist

5

of repeating linear subunits about 300 nm in width[26,27]. Along the longitudinal axis of FAs, different proteins (vinculin, zyxin, paxillin and integrins) were shown to form nanoclusters, suggesting the FA complex as a whole might also be composed of discrete nanoclusters[28-32]. Our data confirms heterogeneity along the longitudinal axis is a feature of the FA complex as a whole, since we are observing the FA complex in an unstained state instead of labelling a specific protein type. More importantly, we provide a location within the FA complex and a specific shape to this heterogeneity, namely a fork at the tip where the actin fibre enters the FA.

On a non-structural level, a few specific parameters have been shown to vary along the longitudinal axis of FAs, for example the binding dynamics of the hallmark FA protein paxillin as was shown in different studies using different approaches[33-36]. Traction forces and molecular tension of FA proteins are also non-uniformly distributed along the longitudinal axis[37,38]. Surprisingly, maximum forces are not found around entry sites of actin fibres, but instead at the opposite tips of the FA. It has been shown that the level of paxillin phosphorylation decreases when force is increased and indeed the level of paxillin phosphorylation has also been demonstrated to vary along FAs[39-41]. This could also be contributing to the formation of the observed high contrast areas, since here the force experienced by the proteins is the lowest, increasing the phosphorylation level of paxillin and perhaps other proteins as well. Strong local increases in the presence of slightly heavier elements than carbon, like phosphor, could further enhance the contrast in SEM images, in addition to a higher density of biological material.

A final example of heterogeneity along the longitudinal axis of FAs involves the activity of vinculin. Vinculin is a large adaptor FA protein like paxillin, but it has a head and a tail domain connected by a flexible linker, allowing vinculin to adopt open (active) and closed (inactive) conformations[42]. This allows assessment of vinculins activity levels through the use of a Foster resonance energy transfer (FRET) biosensor probe, which revealed that FAs at the retracting edge exhibit a gradient of vinculin activity along their lateral axis, with activity increasing towards the actin entry site[43]. A later study was able to generalise these results to FAs beyond the retracting edge[44]. It showed that inactive vinculin associates with the FA layer closest to the adherent membrane (ISL) by binding to phosphorylated paxillin, while talin causes vinculin activation and a shift to the higher FA layers where it binds actin. It was found that inactive vinculin in the ISL is significantly enriched at the FA tip where the actin fibre enters. As inactive vinculin binds to phosphorylated paxillin, this ties in well with studies showing that the forces at actin fibre entry sites are the lowest, leading to higher paxillin phosphorylation levels. The opposite FA tip is significantly enriched in activated vinculin located

in the higher FTL and ARL layers, again demonstrating a vinculin activation gradient along FAs. However, our data shows that heterogeneity along the x-axis is a general feature of FAs and extends beyond the activity levels of a single protein like vinculin. Differing levels in one protein alone would not explain the increased contrast in our SEM images around the actin fibre entry site.

Based on the literature, next to paxillin and vinculin, α-actinin is another protein likely to be involved in the formation of the observed forked shape. In a publication using a genetically coded tagged version of α-actinin specifically designed for use with EM, a forked shape analogous to ours can be clearly seen but was not specifically mentioned[24].

Summarizing, we show that the FA complex is altered around the actin fibre entry site leading to enhanced SEM contrast compared to the rest of the FA. In correlative fluorescence SEM images almost all FAs showed differential levels of contrast and in nearly three quarters of FAs this took the form of fork-shaped structures flanking the actin fibre entry point. Contrast is increased in SEM either when a structure is more dense or when more heavy elements are present, or both. Based on previous literature, it could be hypothesised that proteins likely to be involved in the formation of the fork-shaped structure are paxillin, which is more heavily phosphorylated around the actin entry site, vinculin, the inactive form of which binds to phosphorylated paxillin and is enriched around the entry site, and α-actinin which increases density around the entry site by accumulating here into a fork-shaped structure.

Materials and Methods

Cell culture

U2OS cells stably expressing GFP-tagged paxillin were cultured in phenol-red free DMEM (Lonza) at 37°C and 5% CO2. Culture media were supplemented with 10% FCS (Gibco), 2 mM L-glutamine, 100 U/ml Penicillin, 100 μg/ml Streptomycine and 100 μg/ml G418.

Sample preparation

For experiments Indium-Tin-Oxide (ITO) coated glass coverslips (22 x 22 x 0.17 mm, Optics Balzers) were coated overnight at 4°C with PureCol bovine collagen type I (Advanced Biomatrix) at a final concentration of 10 μg/ml. Cells were seeded onto coated coverslips and maintained for another 36 h at 37°C and 5% CO2. Cells are chemically fixed with 3.75% paraformaldehyde for 12 minutes and permeabilised with 0.2% Triton-X100 for 10 minutes, before and after each step the cells are washed thrice with PBS. We note that the formaldehyde fixa-

tives penetrate the cells rapidly but may be extracted by repeated washing. We used this procedure in order to preserve the fluorescence in the cells. The more commonly used osmium tetroxide fixate quenches the fluorescence, while glutaraldehyde, which would cross-link more permanently than paraformaldehyde, is auto-fluorescent. As documented in the manuscript, we found evidence for the appearance of the fork-like FA structure in EM images in literature under conditions where stronger fixation was used. Cells were stained with CF405M Phalloidin (Biotium) following the manufacturer's protocol. Just prior to imaging the samples were dehydrated using an ethanol sequence (2 minutes in 70%, 90%, 95%, and 100% ethanol successively).

Imaging

Integrated fluorescence microscopy and SEM was carried out using a SECOM integrated microscope (Delmic) retrofitted to a SEM (FEI Verios). The SECOM was equipped with an LED light source (Lumencor Spectra), which was used at 405 nm and 475 nm for Phalloidin and GFP respectively with 140 mW total excitation power. Emission was detected using a multi-band filter (Semrock LED-DA/FI/TR/Cy5-4X-A-000) and a CCD camera (Andor Zyla). Exposure time was typically set at 1 second. The ITO cover slide was mounted to the bottom of a SECOM sample holder ring using carbon tape. An extensive overview of imaging procedure in the integrated microscope was published previously[18]. Fluorescence images were recorded after closing the SEM chamber but before vacuum pump down. After recording the fluorescence images, the SEM was pumped to high vacuum mode and SEM images of selected regions of interest based on fluorescence expression were acquired. The sample was positioned at a working distance of 4.3 mm and back-scattered electrons were detected using a concentric backscatter detector (CBS). Images (4096 x 3775 pixels) were recorded at 2 keV electron energy, a current of 1.6 nA, and 10 μs pixel dwell time. Images in Figures 1, 2a, 2l and 2o were recorded at 3 keV energy and 0.4 nA.

Analysis

To make overlay images the EM image is opened in black and white as the background layer in Photosho-p. The fluorescence image is also opened in Photoshop, scaled to the same size as the SEM image (based on the known pixel dimensions) and placed as a separate layer in colour on top of the SEM background layer. The precise overlay is done by hand, mainly based on the F-actin network which due to phalloidin staining is clearly visible in both imaging dualities. To determine the prevalence of fork shaped high contrast areas (defined as any high contrast area that is partially intersected by an area of lower contrast, splitting the high contrast area into two sides) in the FAs of our data set all FAs were assigned

5

a number. In total 122 FAs were counted based on the fluorescent images and of these 97 were also clear enough in the SEM image to be able to determine the shape of the high contrast areas. The reasons to classify an FA as not clear enough in the SEM image to be able to determine the shape of the high contrast areas were in order of occurrence 1) the FA lies too far away from the edge of the cell where the cell is thin enough to image through with the SEM so the FA is lost in the signal coming from the cytoplasm/cytoskeleton of the cell 2) the FA is too small in the SEM image so while it is possible to make out the FA in the SEM image the resolution of the SEM image is not sufficient to allow the shape of the high contrast area to be determined or 3) the FA itself or the connecting F-actin fibre is not visible in the SEM image which doesn't allow anything to be said about the shape of a putative darker area at the place where the actin connects to the FA as this connection point is not visible. Of these 97 FAs two people independently counted the number of high contrast areas and the number of high contrast areas with a Y-shape, with very comparable results: 95 FAs have a high contrast area and for 71/72 FAs this area is fork shaped, we reported the average. To allow a more quantitative analysis of these fork shapes, all fork shapes and the longest axis of the FAs were also traced by hand using the Fiji inbuilt angle and line-drawing and measuring tools. Care was taken that for the angle measurements using the angle measurement tool only the beginning of the fork shape was used.

References

1   Yamada, K. M. & Geiger, B. Molecular interactions in cell adhesion complexes. *Current opinion in cell biology* **9**, 76-85 (1997).

2   Geiger, B., Bershadsky, A., Pankov, R. & Yamada, K. M. Transmembrane crosstalk between the extracellular matrix--cytoskeleton crosstalk. *Nature reviews. Molecular cell biology* **2**, 793-805, doi:10.1038/35099066 (2001).

3   Zaidel-Bar, R., Itzkovitz, S., Ma'ayan, A., Iyengar, R. & Geiger, B. Functional atlas of the integrin adhesome. *Nature cell biology* **9**, 858-867, doi:10.1038/ncb0807-858 (2007).

4   Winograd-Katz, S. E., Fassler, R., Geiger, B. & Legate, K. R. The integrin adhesome: from genes and proteins to human disease. *Nature reviews. Molecular cell biology* **15**, 273-288, doi:10.1038/nrm3769 (2014).

5   Wahl, S. M., Feldman, G. M. & McCarthy, J. B. Regulation of leukocyte adhesion and signaling in inflammation and disease. *Journal of leukocyte biology* **59**, 789-796 (1996).

6   Maartens, A. P. & Brown, N. H. The many faces of cell adhesion during Drosophila muscle development. *Developmental biology* **401**, 62-74, doi:10.1016/j.ydbio.2014.12.038 (2015).

7   Burridge, K. & Guilluy, C. Focal adhesions, stress fibers and mechanical tension. *Experimental cell research* **343**, 14-20, doi:10.1016/j.yexcr.2015.10.029 (2016).

8   Small, J. V., Rottner, K., Kaverina, I. & Anderson, K. I. Assembling an actin cytoskeleton for cell attachment and movement. *Biochimica et biophysica acta* **1404**, 271-281 (1998).

9   Biggs, M. J., Richards, R. G., Wilkinson, C. D. & Dalby, M. J. Focal adhesion interactions with topographical structures: a novel method for immuno-SEM labelling of focal adhesions in

5

S-phase cells. *J Microsc* **231**, 28-37, doi:10.1111/j.1365-2818.2008.02013.x (2008).

10   Biggs, M. J. *et al.* Adhesion formation of primary human osteoblasts and the functional response of mesenchymal stem cells to 330nm deep microgrooves. *Journal of the Royal Society, Interface* **5**, 1231-1242, doi:10.1098/rsif.2008.0035 (2008).

11   Biggs, M. J., Richards, R. G. & Dalby, M. J. Using immuno-scanning electron microscopy for the observation of focal adhesion-substratum interactions at the nano- and microscale in S-phase cells. *Methods in molecular biology (Clifton, N.J.)* **695**, 53-60, doi:10.1007/978-1-60761-984-0_4 (2011).

12   Friedmann, A., Hoess, A., Cismak, A. & Heilmann, A. Investigation of cell-substrate interactions by focused ion beam preparation and scanning electron microscopy. *Acta Biomater* **7**, 2499-2507, doi:10.1016/j.actbio.2011.02.024 (2011).

13   Martinez, E. *et al.* Focused ion beam/scanning electron microscopy characterization of cell behavior on polymer micro-/nanopatterned substrates: a study of cell-substrate interactions. *Micron* **39**, 111-116, doi:10.1016/j.micron.2006.12.003 (2008).

14   Richards, R. G. & Gwynn, I. A. Backscattered electron imaging of the undersurface of resin-embedded cells by field-emission scanning electron microscopy. *J Microsc* **177**, 43-52, doi:10.1111/j.1365-2818.1995.tb03532.x (1995).

15   Richards, R. G. *et al.* Immunogold labelling of fibroblast focal adhesion sites visualised in fixed material using scanning electron microscopy, and living, using internal reflection microscopy. *Cell Biol Int* **25**, 1237-1249, doi:10.1006/cbir.2001.0807 (2001).

16   Pluk, H., Stokes, D. J., Lich, B., Wieringa, B. & Fransen, J. Advantages of indium-tin oxide-coated glass slides in correlative scanning electron microscopy applications of uncoated cultured cells. *J Microsc* **233**, 353-363, doi:10.1111/j.1365-2818.2009.03140.x (2009).

17   Liv, N. *et al.* Simultaneous correlative scanning electron and high-NA fluorescence microscopy. *PloS one* **8**, e55707, doi:10.1371/journal.pone.0055707 (2013).

18   Peddie, C. J., Liv, N., Hoogenboom, J. P. & Collinson, L. M. Integrated light and scanning electron microscopy of GFP-expressing cells. *Methods in cell biology* **124**, 363-389, doi:10.1016/b978-0-12-801075-4.00017-3 (2014).

19   Voorneveld, P. W. *et al.* Loss of SMAD4 alters BMP signaling to promote colorectal cancer cell metastasis via activation of Rho and ROCK. *Gastroenterology* **147**, 196-208.e113, doi:10.1053/j.gastro.2014.03.052 (2014).

20   Joosten, B., Willemse, M., Fransen, J., Cambi, A. & van den Dries, K. Super-Resolution Correlative Light and Electron Microscopy (SR-CLEM) Reveals Novel Ultrastructural Insights Into Dendritic Cell Podosomes. *Frontiers in immunology* **9**, 1908, doi:10.3389/fimmu.2018.01908 (2018).

21   Pinotsi, D., Rodighiero, S., Campioni, S. & Csucs, G. An Easy Path for Correlative Electron and Super-Resolution Light Microscopy. *Scientific reports* **9**, 15526, doi:10.1038/s41598-019-52047-2 (2019).

22   Peddie, C. J. *et al.* Correlative super-resolution fluorescence and electron microscopy using conventional fluorescent proteins in vacuo. *Journal of structural biology* **199**, 120-131, doi:10.1016/j.jsb.2017.05.013 (2017).

23   Medalia, O. & Geiger, B. Frontiers of microscopy-based research into cell-matrix adhesions. *Current opinion in cell biology* **22**, 659-668, doi:10.1016/j.ceb.2010.08.006 (2010).

24   Shu, X. *et al.* A genetically encoded tag for correlated light and electron microscopy of intact cells, tissues, and organisms. *PLoS biology* **9**, e1001041, doi:10.1371/journal.pbio.1001041 (2011).

25   Kanchanawong, P. *et al.* Nanoscale architecture of integrin-based cell adhesions. *Nature* **468**, 580-584, doi:10.1038/nature09621 (2010).

26   Hu, S. *et al.* Structured illumination microscopy reveals focal adhesions are composed of linear subunits. *Cytoskeleton (Hoboken, N.J.)* **72**, 235-245, doi:10.1002/cm.21223 (2015).

27   Young, L. E. & Higgs, H. N. Focal Adhesions Undergo Longitudinal Splitting into Fixed-Width Units. *Curr Biol* **28**, 2033-2045.e2035, doi:10.1016/j.cub.2018.04.073 (2018).

28   Betzig, E. *et al.* Imaging intracellular fluorescent proteins at nanometer resolution. *Science (New York, N.Y.)* **313**, 1642-1645, doi:10.1126/science.1127344 (2006).

29   Shroff, H. *et al.* Dual-color superresolution imaging of genetically expressed probes within individual adhesion complexes. *Proceedings of the National Academy of Sciences of the United States of America* **104**, 20308-20313, doi:10.1073/pnas.0710517105 (2007).

30   Deschout, H. *et al.* Investigating Focal Adhesion Substructures by Localization Microscopy. *Biophysical journal* **113**, 2508-2518, doi:10.1016/j.bpj.2017.09.032 (2017).

31   Xu, L. *et al.* Nanoscale localization of proteins within focal adhesions indicates discrete functional assemblies with selective force-dependence. *Febs j* **285**, 1635-1652, doi:10.1111/febs.14433 (2018).

32   Spiess, M. *et al.* Active and inactive beta1 integrins segregate into distinct nanoclusters in focal adhesions. *The Journal of cell biology* **217**, 1929-1940, doi:10.1083/jcb.201707075 (2018).

33   Webb, D. J., Brown, C. M. & Horwitz, A. F. Illuminating adhesion complexes in migrating cells: moving toward a bright future. *Current opinion in cell biology* **15**, 614-620 (2003).

34   Digman, M. A., Brown, C. M., Horwitz, A. R., Mantulin, W. W. & Gratton, E. Paxillin dynamics measured during adhesion assembly and disassembly by correlation spectroscopy. *Biophysical journal* **94**, 2819-2831, doi:10.1529/biophysj.107.104984 (2008).

35   Wolfenson, H. *et al.* A role for the juxtamembrane cytoplasm in the molecular dynamics of focal adhesions. *PloS one* **4**, e4304, doi:10.1371/journal.pone.0004304 (2009).

36   Legerstee, K., Geverts, B., Slotman, J. A. & Houtsmuller, A. B. Dynamics and distribution of paxillin, vinculin, zyxin and VASP depend on focal adhesion location and orientation. *Scientific reports* **9**, 10460, doi:10.1038/s41598-019-46905-2 (2019).

37   Plotnikov, S. V., Pasapera, A. M., Sabass, B. & Waterman, C. M. Force fluctuations within focal adhesions mediate ECM-rigidity sensing to guide directed cell migration. *Cell* **151**, 1513-1527, doi:10.1016/j.cell.2012.11.034 (2012).

38   Sarangi, B. R. *et al.* Coordination between Intra- and Extracellular Forces Regulates Focal Adhesion Dynamics. *Nano letters* **17**, 399-406, doi:10.1021/acs.nanolett.6b04364 (2017).

39   Zaidel-Bar, R., Kam, Z. & Geiger, B. Polarized downregulation of the paxillin-p130CAS-Rac1 pathway induced by shear flow. *Journal of cell science* **118**, 3997-4007, doi:10.1242/jcs.02523 (2005).

40   Nayal, A. *et al.* Paxillin phosphorylation at Ser273 localizes a GIT1-PIX-PAK complex and regulates adhesion and protrusion dynamics. *The Journal of cell biology* **173**, 587-589, doi:10.1083/jcb.200509075 (2006).

41   Zaidel-Bar, R., Milo, R., Kam, Z. & Geiger, B. A paxillin tyrosine phosphorylation switch regulates the assembly and form of cell-matrix adhesions. *Journal of cell science* **120**, 137-148, doi:10.1242/jcs.03314 (2007).

42   Bakolitsa, C. *et al.* Structural basis for vinculin activation at sites of cell adhesion. *Nature* **430**, 583-586, doi:10.1038/nature02610 (2004).

43   Chen, H., Cohen, D. M., Choudhury, D. M., Kioka, N. & Craig, S. W. Spatial distribution and functional significance of activated vinculin in living cells. *The Journal of cell biology* **169**, 459-470, doi:10.1083/jcb.200410100 (2005).

44   Case, L. B. *et al.* Molecular mechanism of vinculin activation and nanoscale spatial organization in focal adhesions. *Nature cell biology* **17**, 880-892, doi:10.1038/ncb3180 (2015).

5

Appendix

Summary

Samenvatting

Scientific publications

Curriculum Vitae

PhD portfolio

Dankwoord

Summary

In multicellular organisms, different cells are organised together into tissues. A large three-dimensional network of proteins and sugars, the extracellular matrix (ECM), surrounds the cells in a tissue and provides additional structural support. To ensure tissue integrity it is important that most cells remain fixed in place. For this purpose, cells attach to each other as well as to the ECM. The attachment of cells to the ECM is mediated primarily by focal adhesions (FAs), complexes of up to hundreds of different bound proteins. In this thesis focal adhesions were studied using different advanced microscopy techniques, with all techniques providing different forms of information about these complex structures.

In **chapter 1** the role of focal adhesions in biology is discussed. They are especially important for processes in which cell migration plays a major role, such as embryonic development, the functioning of the immune system or metastasis of cancer cells. Furthermore, the main molecular components of focal adhesions are discussed, with special attention to the four FA proteins specifically examined in this thesis, paxillin, vinculin, zyxin and VASP. Finally, the advanced fluorescence microscopy techniques applied in the different chapters are introduced.

In **chapter 2** FA protein dynamics was studied using Fluorescence Recovery After Photobleaching (FRAP). Here, fluorescent (luminescent) proteins were coupled to the four selected FA proteins. Since FA proteins bind to and accumulate in focal adhesions, these also become fluorescent. The fluorescence of FAs was followed over time and plotted in FRAP curves. A number of focal adhesions were exposed to a bleach pulse. This laser pulse is powerful enough to destroy (bleach) fluorescent proteins, causing the FRAP curve to drop sharply. Fluorescence will increase again if the bleached proteins are able to exchange with other, unbleached, proteins. Analysis of FRAP curves showed that the dynamics of paxillin and vinculin in focal adhesions were surprisingly stable and similar, even in two different cell types from different species. Almost half of the paxillin and vinculin proteins bound in focal adhesions were stably bound with binding times comparable to the average FA lifetime. Zyxin and VASP were more dynamically associated with focal adhesions. In addition, we showed that the binding dynamics of FA proteins correlated with focal adhesion location and orientation. In focal adhesions close to the edge of the adherent cell membrane, paxillin, zyxin and VASP were more dynamically bound and had larger bound fractions than in FAs located further from this edge. Zyxin and VASP were also more dynamically bound and had larger bound fractions in FAs that were perpendicular to this membrane edge than in focal adhesions orientated parallel to it. The increased dynamics of an important structural protein such as paxillin, like in focal adhe-

A

sions close to the membrane edge, might increase the dynamics of the entire focal adhesion. A larger bound fraction of the actin-binding proteins zyxin and VASP potentially enhances actin coupling to the FAs in question.

In **chapter 3** a dedicated photoconversion assay to specifically visualise stably bound proteins within subcellular structures or organelles was developed. We successfully applied this technique to further investigate the large stably bound fractions of paxillin and vinculin in focal adhesions. This showed that, although paxillin and vinculin were uniformly distributed over FAs, the stable bound paxillin and vinculin proteins formed small clusters within focal adhesions. These clusters were much smaller for paxillin than for vinculin. This means that the stably bound paxillin proteins concentrated more strongly, since we showed in chapter 2 that the stably bound fractions of paxillin and vinculin are almost the same size. In addition, the stably bound protein clusters were significantly more likely to be at the focal adhesion half furthest from the adherent membrane edge. The actin fibre also enters the FA from this side. The effects of FA orientation and location appeared to be more subtle on the stably bound protein clusters than on FA protein binding dynamics, however the surface area of the stably bound vinculin clusters was significantly increased at parallel FAs close to the membrane edge compared to parallel FAs further away from this edge.

In **chapter 4** the distribution of the selected FA proteins along the long axis of focal adhesions was studied using the superresolution technique structured illumination microscopy. At the FA end closest to the edge of the adherent membrane ('head'), paxillin protruded further than the other three proteins. At the opposite FA end ('tail'), vinculin, zyxin and VASP protruded, with vinculin protruding the furthest. When cells were stimulated with HGF, the paxillin heads became shorter and the zyxin tails longer. In addition, focal adhesions at protruding or retracting membrane edges had longer paxillin heads than focal adhesions at static membrane edges. Taken together, this suggests movement influences the distribution of FA proteins along focal adhesions

Finally, in **chapter 5** the coupling between focal adhesions and actin was studied in detail, using a technique combining fluorescence microscopy and electron microscopy in a single microscope. This revealed that, for nearly all focal adhesions, the actin fibre entry site was darker in the electron microscopy images. This locally increased contrast indicates a higher protein density, possibly in combination with increased protein phosphorylation levels. In nearly three quarters of the focal adhesions, these areas of increased contrast had a forked nanostructure, with the actin fibre forming the stem of the fork and the focal adhesion areas with increased contrast forming the fork.

A

Samenvatting

In meercellige organismen zijn verschillende cellen samen gegroepeerd en georganiseerd als weefsels. Een groot driedimensionaal netwerk van eiwitten en suikers, de extracellulaire matrix (ECM), omgeeft de cellen van weefsels en voegt zo structurele ondersteuning toe. Om de weefselintegriteit te kunnen garanderen is het belangrijk dat de meeste cellen op hun plaats blijven. Daartoe hechten cellen zowel aan elkaar als aan de ECM. Het hechten van cellen aan de ECM gebeurt voornamelijk via focale adhesies (FA's), complexen van tot honderden verschillende aan elkaar gebonden eiwitten. In dit proefschrift zijn focale adhesies met verschillende geavanceerde microscopie technieken bestudeerd, waarbij alle technieken andere informatie over deze complexe structuren verschaffen.

In **hoofdstuk 1** wordt de rol van focale adhesies binnen de biologie besproken. Ze zijn vooral van belang voor processen waarbij celmigratie een grote rol speelt, zoals de embryonale ontwikkeling, het functioneren van het immuunsysteem of het uitzaaien van kankercellen. Verder wordt er ingegaan op de belangrijkste moleculaire componenten van focale adhesies, met speciale aandacht voor de vier FA-eiwitten die in dit proefschrift specifiek worden bekeken, paxillin, vinculin, zyxin en VASP. Tenslotte worden de geavanceerde fluorescentie microscopie technieken die in de verschillende hoofdstukken zijn toegepast geïntroduceerd.

In **hoofdstuk 2** werd de dynamiek van FA eiwitten bestudeerd door middel van Fluorescence Recovery After Photobleaching (FRAP). Hiervoor werden fluorescente (lichtgevende) eiwitten aan de vier geselecteerde FA-eiwitten gekoppeld. Doordat de FA-eiwitten binden en zich ophopen in focale adhesies werden deze hierdoor ook fluorescent. De fluorescentie van FA's werd gevolgd door de tijd en uitgezet in een grafiek, de FRAP-curve. Een aantal FA's werd belicht met een bleekpuls. Deze laserpuls is krachtig genoeg om fluorescente eiwitten kapot te maken (te bleken), zodat de FRAP-curve sterk daalt. De fluorescentie zal weer toenemen als de gebleekte eiwitten kunnen uitwisselen met andere, ongebleekte, eiwitten. Door analyse van FRAP-curves lieten we zien dat de dynamiek van paxillin en vinculin in focale adhesies verassend stabiel en vergelijkbaar was, in twee celtypes van verschillende diersoorten. Bijna de helft van de in focale adhesies gebonden paxillin en vinculin eiwitten was stabiel gebonden met bindingstijden die vergelijkbaar waren met de gemiddelde levensduur van FA's. Zyxin en VASP bonden veel dynamische aan focale adhesies. Daarnaast hebben we laten zien dat de bindingsdynamiek van FA-eiwitten verandert met de ligging en oriëntatie van een focale adhesie. In focale adhesies die dicht bij de rand van het gehechte celmembraan liggen waren paxillin, zyxin en VASP dynamischer gebonden en hadden zij grotere gebonden fracties dan in FA's

die verder dan deze rand liggen. Zyxin en VASP bonden ook dynamischer en hadden grotere gebonden fracties in focale adhesies die een loodrechte oriëntatie t.o.v. deze membraanrand hadden dan in focale adhesies die hier parallel aan lagen. De verhoogde dynamiek van een belangrijk structureel eiwit als paxillin, zoals voor focale adhesies dicht bij de membraanrand, zou de dynamiek van de complete focale adhesie kunnen vergroten, terwijl een grotere gebonden fractie van de direct aan actine bindende eiwitten zyxin en VASP potentieel de koppeling van actine aan de betreffende FA's versterkt.

In **hoofdstuk 3** werd een fotoconversie analysemethode gericht op het specifiek visualiseren van stabiel gebonden eiwitten binnen subcellulaire structuren en organellen ontwikkeld. Deze techniek werd toegepast om de grote stabiel gebonden fracties van paxillin en vinculin in focale adhesies verder te kunnen onderzoeken. Dit liet zien dat, ondanks dat paxillin en vinculin uniform verdeeld waren over focale adhesies, de stabiele gebonden paxillin en vinculin eiwitten kleine clusters vormden binnen focale adhesies. Deze clusters waren vele malen kleiner voor paxillin dan voor vinculin. Dit betekent dat de stabiel gebonden paxillin eiwitten sterker concentreerde, aangezien we in hoofdstuk 2 lieten zien dat de stabiel gebonden fracties van deze eiwitten vrijwel even groot zijn. De stabiel gebonden eiwitclusters bevonden zich bovendien significant vaker aan de helft van de focale adhesie die het verst van de rand van het gehechte membraan af ligt, de FA-kant waar ook de actinevezel binnenkomt. De effecten van FA oriëntatie en ligging t.o.v. de membraanrand op de stabiel gebonden eiwitclusters bleken subtieler dan op de bindingsdynamiek van FA-eiwitten, maar het oppervlak van de stabiel gebonden vinculin clusters was significant groter voor parallel georiënteerde FA's dicht bij de membraanrand dan voor parallelle FA's die hier verder vandaan lagen.

In **hoofdstuk 4** werd de distributie van de geselecteerde FA-eiwitten langs de lange as van focale adhesies bestudeerd door middel van de superresolutie techniek structured illumination microscopie. Aan het uiteinde van het FA complex dat het dichtst bij de rand van het gehechte celmembraan ligt ('head'), stak paxillin verder uit dan de drie andere eiwitten. Aan het tegenoverliggende FA-uiteinde ('tail') staken juist vinculin, zyxin en VASP uit, waarbij vinculin het verst uitstak. Wanneer cellen gestimuleerd werden met HGF werden de paxillin heads korter en de zyxin tails langer. Bovendien hadden focale adhesies bij een uitstulpend of terugtrekkend celmembraan langere paxillin heads dan focale adhesies bij een stilliggende membraanrand. Samen suggereert dit dat beweging de distributie van FA eiwitten langs de lange as van focale adhesies beïnvloedt.

Tenslotte werd in **hoofdstuk 5** de koppeling tussen focale adhesies en actine

A

in detail bestudeed met een techniek waarbij fluorescentie microscopie en elektronen microscopie in één apparaat worden gecombineerd. Dit liet zien dat vrijwel alle focale adhesies in de elektronenmicroscopie plaatjes donkerder kleuren rond de aanhechtingsplaats van de actine vezel. Dit lokaal verhoogde contrast duidt op een hogere eiwitdichtheid, wellicht in combinatie met een toename van de eiwit fosforylatie. In bijna driekwart van de focale adhesies vormden deze gebieden van verhoogd contrast een gevorkte nanostructuur, waarbij de actinevezel de stam van de vork vormt en de focale adhesie gebieden met verhoogd contrast de vork.

A

Scientific publications

✧ **Karin Legerstee**, Bart Geverts, Johan A. Slotman, Adriaan B. Houtsmuller, *Dynamics and distribution of paxillin, vinculin, zyxin and VASP depend on focal adhesion location and orientation.* Sci Rep 9, 10460, 2019

✧ **Karin Legerstee,** Tsion E. Abraham, Wiggert A. van Cappellen, Alex Nigg, Johan A. Slotman, Adriaan B. Houtsmuller, *Growth factor dependent changes in nanoscale architecture of focal adhesions* – submitted

✧ **Karin Legerstee,** Jason Sueters, Gert-Jan Kremers, Jacob P. Hoogenboom, Adriaan B. Houtsmuller, *Correlative light and electron microscopy reveals fork-shaped structures at actin entry sides of focal adhesions* - manuscript in preparation

A

Curriculum vitae

Personal details

Name: Karin Legerstee

Date and place of birth: 21ˢᵗ August 1986, Utrecht

Education

2012-2020

⬦ *PhD position Department of Patholgy, Erasmus MC, Rotterdam*
  – Promotor: Prof. dr. A.B. Houtsmuller
  – Copromotor: Dr. W.A. van Cappellen
  – Multimodal Microscopy of Focal Adhesions

2008-2011

⬦ *Master's degree Biomedical sciences, Neuroscience and Cognition, Experimental and Clinical Neuroscience, Utrecht University*
  – Major Research Project
    Rudolf Magnus Institute, University Medical Centre (UMC) Utrecht
    The intracellular signalling cascade activated by RGMa-signalling through neogenin
  – Minor Research Project
    Department of Pharmacology, University of Cambridge
    Examining Carbachol signalling through Adenylyl Cyclase 2 using live single cell imaging
  – Master Thesis
    Rudolf Magnus Institute, University Medical Centre (UMC) Utrecht
    Cytoplasmic FMRP-interacting protein (Cyfip1) – A key player in the pathophysiology of the fragile X syndrome?
  – X-track honours programme, graduate school of Life Sciences, Utrecht University
  – Editor in the editorial board of the student-run Journal of Neuroscience and Cognition

A

2005-2008

✧ *Bachelor's degree Biomedical sciences, cum laude, Utrecht University*
Specialising in the fields of neuroscience, cellular biology and immunology

1998-2005

✧ *Context and Language Integrated Learning Programme, cum laude, Anna van Rijn College, Nieuwegein*
  − vwo-diploma track Nature and Health
  − International Baccalaureate (IB) Diploma Programme Certificate for the subject English A2 Higher Level (the highest IB certificate to be obtained by non-native speakers)

A

PhD Portfolio

Personal details

Name:	Karin Legerstee
Erasmus MC department:	Pathology
Research school:	Molmed
PhD-period:	2012-2020
Promotor(s):	Prof. dr. A.B. Houtsmuller and dr. W.A. van Cappellen
Supervisor:	Prof dr. A.B. Houtsmuller

PhD training

- ✧ *Courses*

  - Workshop on photoshop and Illustrator CS5
    2012

  - Imaging life at the molecular level
    2012

  - Course on Molecular Medicine
    2012

  - Follow-up workshop on Indesign CS6
    2013

  - OIC AMIE symposium
    2013

  - Basic course on 'R'
    2014

- ✧ *Seminars and workshops*

  - Annual molecular medicine day (poster)
    2012-2015

  - Annual MGC day
    2013-2014

A

- – Invadosome (presentation)

  2013

- – MGC PhD-retreat (presentation)

  2014

- – The Netherlands Society for Microscopy Annual Meeting (poster)

  2012-2016

◇ *International conferences*

- – EMBO spatial (Israel)

  2013

- – Labelling and Nanoscopy (Germany)

  2014

◇ *Teaching*

- – Supervision HBO student final Master project

  2015

- – Practicals OIC microscopy courses for master students

  2012-2015

- – Practicals OIC microscopy courses for PhD students

  2013-2015

- – Teachers assistant Java programming course

  2018

A

Dankwoord

Veel mensen hebben bijgedragen aan mijn promotietraject, bedankt daarvoor.

Ten eerste natuurlijk Adriaan, mijn promotor. Bedankt dat je mij de kans hebt gegeven om binnen jouw groep te komen werken. Dat betekende de kans om focale adhesies met allerlei verschillende microscopen te bekijken en verschillende analyse-methodes op de verkregen beelden toe te passen, maar óók de kans om onderwijs te geven en een student te begeleiden. Kortom precies dat waar ik tijdens mijn sollicitatiegesprek al enthousiast over was. Dat sollicitatiegesprek duurde trouwens een halve dag, omdat je me meteen alle microscopen van het OIC liet zien en me aan iedereen ging voorstellen. Dat enthousiasme bleek typerend te zijn, bedankt daarvoor, het werkte aanstekelijk. En als tweede Gert, bedankt dat je mijn co-promotor wilde zijn. Ik kon ten alle tijden bij je binnen komen vallen met vragen en dan maakte je altijd tijd om met mij mee te denken.

Vervolgens wil ik Alessandra Cambi, Niels Galjart en Lodewyk Wessels bedanken voor hun bereidheid plaats te nemen in mijn leescomissie. Alessandra, bedankt voor de prettige samenwerking aan podosomen, ik heb er veel van opgestoken. Lodewijk, de regelmatige journalclubs hebben me geholpen met het inlezen in het focale adhesie vakgebied.

Dan iedereen van de Houtsmullergroep en het OIC, vanaf dag één voelde ik me welkom. Als eerste mijn paranimf Tsion. In het lab heb je me met van alles en nog wat geholpen, van hulp bij kweken of kloneren tot het bedienen van de confocal, je maakte er altijd tijd voor. Maar ik wil je vooral bedanken voor je vrolijke aanwezigheid, bij elke kantoorverhuizing was ik opgelucht dat we kantoorgenoten bleven! Hierbij noem ik ook Ilona en Fatma, volgens mij dreven we onze mannelijke kantoorgenoten soms tot wanhoop met ons 'vrouwelijke geklets' maar ik wil jullie bedanken voor die gezelligheid en de inzichten op werkgebied die er vaak uit voortvloeiden. De gezamenlijke lunches vond ik ook fijn, de groep wisselde, maar Bert-Jaap, Maarten, Martijn en later Johan en Bart, jullie probeerde er altijd tijd voor te maken. Soms werd het werk besproken, meestal juist niet, maar het gaf mij altijd nieuwe energie. En daglicht op dagen die ik verder in het donker bij een microscoop doorbracht! Bert-Jaap, jou wil ik ook bedanken voor je (luister)boekenserie tip. Met ruim 450 uur zorgde deze enkele serie ervoor dat ik me anderhalf jaar lang niet verveelde tijdens de busreis van en naar Rotterdam, én dat ik nooit meer aan een boekenserie begin zonder eerst te checken uit hoeveel bladzijdes deze bestaat. Maarten, bedankt voor je hulp met R, ik heb er veel aan gehad. Martijn, je hebt me wegwijs gemaakt op de TIRF. Johan, bedankt voor al je hulp met SIM, zowel bij het bedienen van de

A

microscoop als bij de daarop volgende data-analyse. Bart, als collega bedankt voor je hulp en meedenken bij de data analyses. Later, als partner, heb je nog veel meer bijgedragen aan de totstandkoming van dit proefschrift, teveel om hier allemaal te beschrijven, maar bedankt voor alles! Thomas, wij hebben minder nauw samengewerkt, maar ik heb je positieve aanwezigheid in het kantoor altijd als prettig ervaren en ik wens je veel succes met het afronden van je proefschrift. Gert-Jan, zonder jou had ik überhaupt geen fluorescente eiwitten gehad om de focale adhesies te visualiseren en natuurlijk bedankt voor al je troubleshooting van de microscopen. Martin, onze onderwerpen lagen verder uit elkaar, maar toch was je altijd bereid mee te denken en ik heb veel aan je feedback gehad. Alex, jouw Gaussian blur Fiji plugin heeft mij vele uren van met de hand focale adhesies segmenteren bespaard, daarnaast stond je aanwezigheid bij labuitjes sowieso garant voor extra gezelligheid. Jo-Janneke, ik heb jouw eind-stage begeleid. Je was leergierig en hebt geholpen bij het kloneren van veel constructs. Onze wekelijkse besprekingen bij de Doppio waren altijd gezellig. Selçuk, toen jij bij de groep kwam was ik al thuis aan het schrijven, maar ik heb je leren kennen als iemand die positief in het leven staat en ik wens je veel succes met je promotietraject.

Ook buiten de Houtsmullergroep en het OIC was het JNI een fijne werkomgeving. Ik wil specifiek Angelique en Hetty noemen als mede 'vroege vogels' bij wie ik 's morgens vroeg altijd terecht kon en Joke en Mirella die ervoor zorgden dat, wanneer het kloneren minder soepel ging dan gehoopt, de extra tijd in het bacterielab in elk geval gezellig was.

Buiten het Erasmus MC wil ik van het Hubrecht instituut Johan de Rooij en Emma bedanken voor de prettige samenwerking en voor alle praktische tips bij HGF-stimulatie. Verder heb ik bij de TU Delft nauw mogen samenwerken met Jacob Hoogenboom, Nalan en Jason, dat heeft tot een mooi hoofdstuk geleid.

Daarnaast natuurlijk mijn (schoon)familie, vrienden en medebewoners van de flat, jullie weten wie jullie zijn, bedankt voor al jullie steun. Eileen, formeel mogen we dan verre familie zijn, het voelt als naaste familie en ik ben blij dat jij er vandaag bij bent als paranimf. Mijn ouders, bedankt voor alle kansen die jullie me gegeven hebben. Anne-Marie, ik heb geregeld bij jou in Capelle gelogeerd, dat was gezellig en scheelde mij ook veel reistijd. Gelukkig zorgde de, toen nog vaste, gezellige buschauffeurs van lijn 195 ervoor dat die reistijd voorbij vloog. Emma, jouw bijles op maandagavond was voor mij even iets heel anders om op te focussen en sowieso een gezellige start van de werkweek. Opa Jan Legerstee, u was altijd zo trots op mijn wetenschappelijke opleiding, ik vind het bijzonder dat u nu vanaf een afstand nog meemaakt dat ik ga promoveren.

A